DOCTORATE DISSERTATION NO. 2022:8
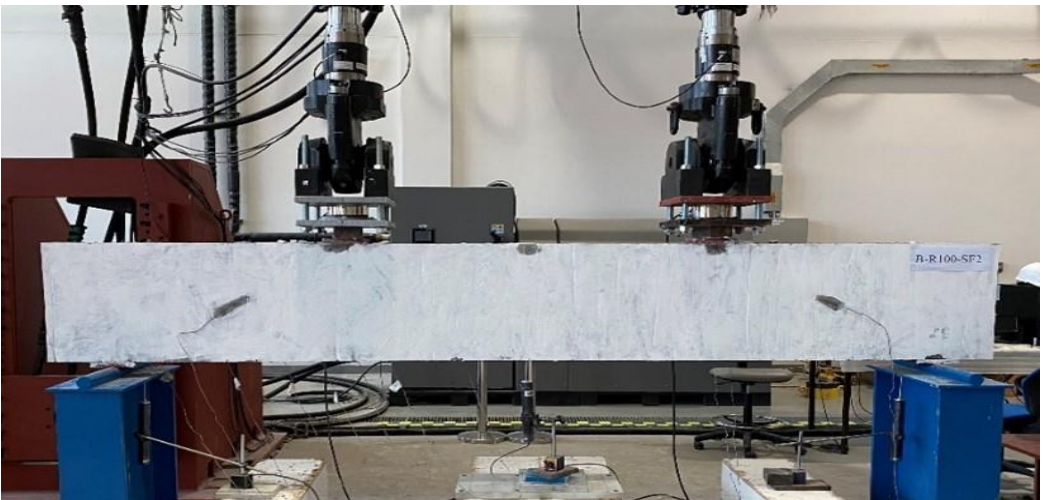
College of Engineering

BEHAVIOR OF STEEL FIBER REINFORCED CONCRETE MADE WITH RECYCLED CONCRETE AGGREGATES: MATERIAL CHARACTERIZATION AND DEEP BEAM SHEAR RESPONSE

Nancy Kachouh

April 2022

United Arab Emirates University

College of Engineering

Department of Civil and Environmental Engineering

BEHAVIOR OF STEEL FIBER REINFORCED
CONCRETE MADE WITH RECYCLED CONCRETE
AGGREGATES: MATERIAL CHARACTERIZATION
AND DEEP BEAM SHEAR RESPONSE

Nancy Kachouh

This dissertation is submitted in partial fulfilment of the requirements for
the degree of Doctor of Philosophy in Civil Engineering

April 2022

Declaration of Original Work

I, Nancy Kachouh, the undersigned, a graduate student at the United Arab Emirates University (UAEU), and the author of this dissertation entitled *"Behavior of Steel Fiber Reinforced Concrete Made with Recycled Concrete Aggregates: Material Characterization and Deep Beam Shear Response"*, hereby, solemnly declare that this dissertation is my own original research work that has been done and prepared by me under the supervision of Professor Tamer El Maaddawy, in the College of Engineering at UAEU. This work has not previously formed the basis for the award of any academic degree, diploma or a similar title at this or any other university. Any materials borrowed from other sources (whether published or unpublished) and relied upon or included in my dissertation have been properly cited and acknowledged in accordance with appropriate academic conventions. I further declare that there is no potential conflict of interest with respect to the research, data collection, authorship, presentation and/or publication of this dissertation.

Student's Signature:

Date: 14/04/2022

Advisory Committee

1) Advisor: Tamer El Maaddawy

Title: Professor

Department of Civil and Environmental Engineering

College of Engineering

2) Member: Hilal El Hassan

Title: Associate Professor

Department of Civil and Environmental Engineering

College of Engineering

3) Member: Bilal El Ariss

Title: Associate Professor

Department of Civil and Environmental Engineering

College of Engineering

Approval of the Doctorate Dissertation

This Doctorate Dissertation is approved by the following Examining Committee Members:

1) Advisor (Committee Chair): Tamer El Maaddawy

   Title: Professor

   Department of Civil and Environmental Engineering

   College of Engineering

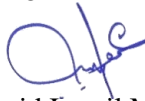   Signature ~~~~~~~~ Date 14/4/2022

2) Member: Amr El Dieb

   Title: Professor

   Department of Civil and Environmental Engineering

   College of Engineering

   Signature ~~~~~~~~ Date 14/4/2022

3) Member: Abdel-Hamid Ismail Mourad

   Title: Professor

   Department of Mechanical and Aerospace Engineering

   College of Engineering

   Signature ~~~~~~~~ Date 14/4/2022

4) Member (External Examiner): Shamim Sheikh

   Title: Professor

   Department of Civil and Mineral Engineering

   College of Engineering, University of Toronto, Canada

   On behalf of external examiner

   Signature ~~~~~~~~ Date 14/4/2022

v

This Doctorate Dissertation is accepted by:

Acting dean of the College of Engineering: Professor Mohamed Al-Marzouqi

Signature _Mohamed AlMarzouqi_

Date __July 01, 2022__

Dean of the College of Graduate Studies: Professor Ali Al-Marzouqi

Signature __Ali Hassan__

Date ___July 01, 2022___

Abstract

This research aims to examine the performance of concrete made with recycled concrete aggregates (RCAs) and steel fibers. It comprises material characterization tests, large-scale reinforced concrete (RC) deep beam tests, and numerical modeling. Material characterization test parameters included the RCA replacement percentage (30, 70, and 100%) and the steel fiber volume fraction ($v_f = 1, 2,$ and 3%). Fourteen large-scale deep beam numerical models with and without web openings made with 100% RCAs and steel fibers were developed and validated through a comparative analysis with test results. A numerical parametric study was conducted to investigate the effect of varying key parameters on the shear response.

Plain concrete mixtures with RCAs exhibited inferior properties relative to those of a baseline mixture made with natural aggregates (NAs). The addition of steel fibers improved the hardened properties of the concrete mixtures with RCAs to an extent that exceeded the original value of some properties of their NA-based counterparts. A bilinear tensile softening law that can describe the post-cracking behavior of concrete made with RCAs and steel fibers was developed based on an inverse analysis of characterization test data. Experimental tests revealed that the addition of steel fibers in solid RC deep beams made with RCAs at v_f of 1 and 2% restored 80 and 90% of the shear capacity, respectively, of a similar beam with minimum steel stirrups. The response of the RCA solid beam having v_f of 3% outperformed that of the NA-based control beam with minimum steel stirrups. The shear strength gain of the RCA-based deep beams with openings due to the inclusion of steel fibers was in the range of 39 to 84%, whereas the use of conventional steel stirrups resulted in an 18% strength gain. The use of steel fibers at v_f of 1% in the RCA-based beam with openings without steel stirrups

was sufficient to restore 96% of the original shear capacity of the NA-based beam with minimum steel stirrups.

Results of the numerical parametric study indicated that the shear strength gain caused by the addition of steel fibers at v_f of 1 and 2% was higher in the deep beam models with the lower shear span-to-depth ratio (a/h) of 0.8, relative to that of their counterparts with a/h of 1.6. The effect of a/h on the shear strength gain of the solid deep beam models diminished at the higher v_f of 3%. The solid deep beam models with a/h of 0.8 exhibited a shear strength gain of 78 to 108% due to the addition of steel fibers, whereas their counterparts with web openings experienced a reduced shear strength gain of 45 to 70%.

Keywords: Steel fibers, recycled concrete aggregates, deep beams, concrete properties, shear behavior, web openings, numerical modeling.

Title and Abstract (in Arabic)

سلوك الخرسانة المسلحة بالألياف الفولاذية المصنوعة من الركام الخرساني المعاد تدويره:
توصيف المواد واستجابة الجسور العميقة لقوى القص

الملخص

يهدف هذا البحث إلى اختبار أداء الخرسانة المصنوعة من الركام الخرساني المعاد تدويره
(RCAs)والألياف الفولاذية. ويشتمل على اختبارات لخصائص المواد المستخدمة، واختبارات
لعينات ذات احجام كبيرة للجسور الخرسانية العميقة المسلحة، وابتكار نماذج عددية لمحاكاة سلوك
الجسور المختبرة. تضمنت اختبارات خصائص المواد فحص تأثير استخدام RCAs بنسب 30 و70
و100% وإضافة الألياف الفولاذية بنسب 1 و2 و3%. تم ابتكار أربعة عشر نموذجًا للمحاكاة العديدة
لعينات ذات احجام كبيرة للجسور العميقة مع وبدون فتحات عرضية والمصنوعة من RCAs بنسبة
100٪ والألياف الفولاذية والتحقق من دقتها من خلال مقارنات مع نتائج الاختبارات المعملية. تم
إجراء دراسة باستخدام نماذج المحاكاة العددية لاكتشاف تأثير بعض المتغيرات الرئيسية على استجابة
الجسور العميقة لقوى القص.

خواص الخرسانة المصنوعة من RCAs كانت أدني مقارنة بخصائص الخرسانة
المصنوعة من الركام الطبيعي (NAs). أدت إضافة الألياف الفولاذية إلى تحسين الخصائص الصلبة
للخرسانة المصنوعة من RCAs لتتخطى أحيانا خصائص نظيرتها المصنوعة من الركام الطبيعي.
تم استنتاج قانون ليصف سلوك قوى الشد في مرحلة ما بعد حدوث الشرخ للخرسانة المصنوعة
من RCAs والألياف الفولاذية بناءً على التحليل العكسي لبيانات اختبار توصيف المواد. كشفت
الاختبارات التجريبية أن إضافة الألياف الفولاذية كان لها تأثير إيجابي على قدرة الجسور الخرسانية
لمقاومة قوى القص حيث أدت إضافة 1 و2% منها إلى استعادة 80 و90%، على التوالي، من هذه
القدرة. مقاومة الجسور التي تحتوي على 3% من الألياف الفولاذية لقوى القص كانت أعلى من
نظيراتها المصنوعة من الركام الطبيعي التي تحتوي على الحد الأدنى من حديد تسليح قوى القص
التقليدي. اكتسبت الجسور العميقة التي تحتوي على فتحات عرضية والمصنوعة من RCAs بالإضافة
إلى الألياف الفولاذية زيادة في مقاومة قوى القص بنسبة 39-84% في حين كانت الزيادة المكتسبة
للجسور التي تحتوي على حديد تسليح القص التقليدي 18%. استخدام 1% من الألياف الفولاذية في
الجسور العميقة التي تحتوي على فتحات عرضية بدون حديد تسليح القص التقليدي كان كافيا لاستعادة

96% من قدرة مقاومة قوى القص للجسور المصنوعة من الركام الطبيعي والتي تحتوي على الحد الأدنى من حديد تسليح القص التقليدي.

أظهرت نتائج دراسة تأثير المتغيرات أن قوى القص الناتجة عن اضافة الألياف الفولاذية بنسب 1 و2% كانت أعلى في الجسور العميقة و التي لها نسبة مسافة القص إلى العمق (a/h) تساوي 0.8، بالنسبة إلى الجسور الاخرى ذات $a/h = 1.6$ تضاءل تأثير a/h على مقدار الزيادة في قدرة مقاومة قوى القص لنماذج الجسور العميقة و التي لا تحتوي على فتحات عرضية عند زيادة الألياف الفولاذية بنسبة 3٪. أظهرت نماذج المحاكاة العددية للجسور العميقة التي لا تحتوي على فتحات عرضية ذات $a/h = 0.8$ زيادة لقدرة مقاومة القص من 78 إلى 108٪ بسبب إضافة الألياف الفولاذية، في حين أن نظيراتها ذات الفتحات العرضية شهدت زيادة منخفضة للقدرة على مقاومة قوى القص بنسبة 45 إلى 70٪.

مفاهيم البحث الرئيسية: الألياف الفولاذية، الركام الخرساني المعاد تدويره، الجسور العميقة، خصائص الخرسانة، سلوك مقاومة قوى القص، الفتحات العرضية، نماذج عددية.

List of Publications

This dissertation is based on the work presented in the following papers, referred to by Roman numerals.

I. Kachouh, N., El-Hassan, H., El-Maaddawy, T. (2019). Effect of steel fibers on the performance of concrete made with recycled concrete aggregates and dune sand. Construction and Building Materials, 213: 348-359. doi: 10.1016/j.conbuildmat.2019.04.087.

II. Kachouh, N., El-Hassan, H., El-Maaddawy, T. (2020). Influence of steel fibers on the flexural performance of concrete incorporating recycled concrete aggregates and dune sand. Journal of Sustainable Cement-Based Materials, 10(1):1-28. doi: 10.1080/21650373.2020.1809546.

III. Kachouh, N., El-Maaddawy, T., El-Hassan, H., El-Ariss, B. (2021). Shear Behavior of Steel-Fiber-Reinforced Recycled Aggregate Concrete Deep Beams. Buildings, 11(9), 423. doi: https://doi.org/10.3390/buildings11090423.

IV. Kachouh, N., El-Maaddawy, T., El-Hassan, H., El-Ariss, B. (2022). Shear Response of Recycled Aggregates Concrete Deep Beams Containing Steel Fibers and Web Openings. Sustainability, 14(2):945 doi: 10.3390/su14020945.

Author's Contribution

The contribution of Nancy Kachouh to the papers included in this dissertation was as follows:

I. Participated in planning of the work, had main responsibility for the experimental work, data collection and processing, evaluation of results and manuscript writing.

II. Participated in planning of the work, had main responsibility for the experimental work, data collection and processing, evaluation of results and manuscript writing.

III. Participated in planning of the work, had main responsibility for the experimental work, data collection and processing, evaluation of results and manuscript writing.

IV. Participated in planning of the work, had main responsibility for the experimental work, data collection and processing, evaluation of results and manuscript writing.

Author Profile

Nancy Kachouh is currently a Research Associate at the United Arab Emirates University, UAE. She has published her research work in top Q1 journals as the first author. Nancy is the winner of the first American Concrete Institute (ACI) Middle East Award for 2019-2020 for having the strongest combination of interest and potential for professional success in the concrete industry. She is the founder of the ACI Student Chapter at the United Arab Emirates University, UAE. She attended ACI conventions in Canada and USA and participated as volunteer in the ACI international Student competition in Cincinnati, USA. She was invited as a speaker to the Big 5 event held in Dubai in 2019. She also attended many international conferences and presented her research work. She received the best presentation Award in ISEC-11 conference in 2021 in Cairo, Egypt. Nancy lives in Dubai with her husband. She holds a bachelor's degree in Mathematics from the Lebanese University in Lebanon. She received her bachelor's degree in Civil Engineering and her Master of Science in Civil Engineering with distinction from the University of Balamand in Lebanon. She also received her Master of Engineering from the American University of Beirut in Lebanon. She ranked among the top 10% of graduate students in the Civil and Environmental Engineering Department in the American University of Beirut in Lebanon.

Acknowledgements

First and foremost, I would like to thank God for giving me the faith, strength, and ability to complete my PhD work.

I would like to express my sincere gratitude to my advisor and mentor Professor Tamer El Maaddawy for the continuous support, patience, motivation, inspiration, and immense knowledge.

In addition, I would like to thank my co-advisors: Dr. Hilal El Hassan and Dr. Bilal El Ariss for their insightful comments, suggestions and encouragements which incented me to widen my research from various perspectives.

I would like also to express my keen appreciation to the concrete and structural engineering laboratory specialists at the United Arab Emirates University for their help throughout testing.

My gratitude is also extended to my friends and colleagues at the United Arab Emirates University for a cherished time spent together during the past four years.

My appreciation also goes out to my mother, brother and sister for their prayers, encouragement, and unconditional support.

Last but not least, I would like to thank my husband Elias Bassil for his love, unwavering support, and belief in me, whom without, this would have not been possible.

Dedication

To the soul of my father

Table of Contents

List of Tables

List of Figures

List of Abbreviations and Symbols

a_1 and a_2	Coefficients defining the opening size
a_x	Width of the opening
a_y	Height of the opening
A_w	Area of an individual web steel bar
A_b	Area of an individual steel reinforcing bar
A_s	Area of tension steel
α	Angle of intersection between web steel bar and the potential shear crack
α_1	Angle of inclination between a typical bar and a potential diagonal crack
a/d	Shear span-to-effective depth ratio
a/h	Shear span-to-depth ratio
b	Beam width
β	Angle of inclination of the natural load path
C_1	Coefficient equal to 1.4 for normal weight concrete
C_2	Coefficient equal to 130 N/mm^2 for plain round bards and 300 N/mm^2 for deformed bars
C_{sf}	Coefficient determined from inverse analysis
CDW	Construction and demolition waste
CMOD	Crack mouth opening displacement
d	Effective depth of the beam
D_f	Mean diameter of steel fibers

d_f	Bond factor
$D_{BZ,2}$ and $D_{BZ,3}$	Energy absorption capacity
δ_p	Deflection at peak load
δ_L	Deflection corresponding to f_L
Δ_{cr}	Deflection corresponding to shear cracking load
Δ_{max}	Deflection corresponding to shear capacity
Δ_{EXP}	Deflection corresponding to experimental shear capacity
Δ_{FE}	Deflection corresponding to numerical shear capacity
E_c	Concrete modulus of elasticity
E_s	Steel modulus of elasticity
E_{sp}	Post-yield modulus of steel
e_x and e_y	Eccentricities of the opening
ε_d	Plastic concrete strain at zero stress
ε_{cp}	Plastic concrete strain at compressive strength
ε_{cfmax}	Maximum plastic fracture strain
ε_y	Yield strain of steel
f_1	Reduction factor to account for the size of openings
f_2	Reduction factor to account for the degree of interruption of the opening
f'_c	Concrete cylindrical compressive strength

$f'_{c,3D}$	Concrete compressive strength at the age of 3 days
$f'_{c,7D}$	Concrete compressive strength at the age of 7 days
f_{cu}	Concrete cube compressive strength
f_t	Concrete uniaxial tensile strength
f_r	Modulus of rupture
f_{sp}	Concrete splitting tensile strength
f_y	Yield strength of reinforcing steel bar
f_u	Ultimate strength of reinforcing steel bar
f_L	Limit of proportionality strength
$f_{R1}, f_{R2}, f_{R3},$ and f_{R4}	Residual flexural tensile strengths in the three-point bending test
f_{eq2} and f_{eq3}	Equivalent flexural strengths in the three-point bending test
f_{150}^{100}	Residual flexural strength at a deflection of $l/150$ in the four-point bending test
FE	Finite element
G_F	Fracture energy
h	Beam depth
h_0/h	Opening height-to-depth ratio
I	Rate of water absorption
ITZ	Interfacial transition zone
k	Distance of the center of opening from the beam axis

K_1, K_2 and K_3	Coefficients defining the position of opening
λ	Empirical coefficient, equal to 1.5 for web bars and 1 for main bars
λ_1, λ_2, and λ_3	Factors that account for the opening size and location
l	Prism span length
LVDT	Linear variable displacement transducer
l_f	Mean length of steel fibers
l_f/D_f	Aspect ratio of steel fibers
m	Ratio of path length intercepted to total path length along the natural load path
NAs	Natural aggregates
NMS	Nominal maximum particle size
OPC	Ordinary Portland cement
r	Factor depending on the location of the center of opening
RC	Reinforced concrete
RCAs	Recycled concrete aggregates
ρ_f	Concrete fresh density
ρ_h	Concrete hardened density
SG	Strain gauge
SSD	Saturated surface dry condition
T_{150}^{100}	Flexural toughness
τ	Average fiber matrix interfacial bond stress

3D	Three-dimensional
UPV	Ultrasonic pulse velocity
v_f	Steel fiber volume fraction
V_n	Nominal shear capacity of RC deep beams
V_w	Web shear reinforcement contribution to shear capacity
V_{cd}	Concrete contribution to shear capacity including the influence of dowel action
V_c	Concrete contribution to shear capacity
V_s	Contribution of steel bars to the shear resistance, including web reinforcement and dowel action
V_d	Contribution of the dowel action to the shear resistance
v_u	Ultimate shear stress
V_{cr}	Shear cracking load
V_{max}	Shear capacity
V_{EXP}	Experimental shear capacity
V_{FE}	Numerical shear capacity
V_n	Analytical shear capacity
W_0	Area under the load-deflection curve
w_0/a	Opening width-to-shear span ratio
w/cm	Water-to-cementitious material ratio
w/c	Water-to-cement ratio
X	Clear shear span

X_N Nominal shear span

y Depth of the intersection between the web steel bar and a potential shear crack measured from the compression face of the beam

y_1 Depth at which a typical bar intersects a potential critical diagonal crack

Chapter 1

Chapter 1: Introduction

1.1 Overview

At the end of their service lives, aged concrete structures are demolished creating massive amounts of construction and demolition waste (CDW). This CDW is mostly disposed of in stockpiles or landfills, causing serious environmental hazards (Radonjanin et al., 2013). A sustainable solution to the problem of CDW and the scarcity of natural resources for natural aggregates (NAs), is the concept of recycling this waste in the form of recycled concrete aggregates (RCAs). The potential substitute of NAs by RCAs is considered a promising approach to promote the use of sustainable materials in construction. The use of RCAs in concrete mixtures has been accompanied by a decrease in its mechanical performance compared to its conventional counterpart (Debieb et al., 2010; Guo et al., 2020; Wagih et al., 2013). Nevertheless, its positive environmental impact has driven researchers to investigate the effect of its usage in structural applications such as reinforced concrete (RC) beams. The shear behavior of RC beams with RCAs is an important aspect that requires investigations and experimental evidence prior to using RCAs routinely in structural applications.

Although the properties of RCAs are inferior to those of NAs, its ability to reduce the environmental impact of concrete production has driven research into investigating more ways to properly utilize it. To counteract the strength reduction when RCAs are used in concrete, different measures were proposed such as increasing the cement content, reducing water-to-cementitious material (*w/cm*) ratio, adding fly ash, removing the old adhered mortar by using a mechanical grinder or by presoaking in water or in acid, strengthening the old adhered mortar attached to the RCAs by using pozzolanic solutions or calcium carbonate deposition that can fill the micro cracks inside the adhered mortar, and adding steel fibers (Shi et al., 2016).

Previous research studies investigated the effect of adding up to 2% steel fibers, by volume, on the properties of RCA concrete mixtures. Results of steel fiber-reinforced RCA concrete showed that the compressive strength, elastic modulus, tensile strength, toughness, and impact resistance increased (Bencardino et al., 2008; Meddah & Bencheikh, 2009). The main advantage of adding steel fibers to concrete is their capacity to increase the tensile strength, post-cracking residual tensile strength, toughness, and fracture energy. This is mainly due to the bridging effect of steel fibers that can reduce the initiation and propagation of cracks, resulting in an increase in the energy absorption capacity of the material (Bencardino et al., 2010). Figure 1.1 shows the common types of steel fibers. The straight fibers are rarely used in practice and most of the commercially available fibers have a pre-deformed geometry (Cunha, 2010). The primary reason for the pre-deformation to fibers is to introduce mechanical anchorage contribution to the bond with the concrete matrix. The use of steel fiber-reinforced recycled aggregate concrete in structural application is limited, even though significant potential exists for full or partial replacement of costly, manually placed, steel bar reinforcement. One of the reasons for the limited utilization of steel fiber-reinforced recycled aggregate concrete in structural applications is the lack of standardized design procedures and information on properties of such a composite material. The accurate determination of material properties and tensile softening laws through material characterization will promote its application into structural elements.
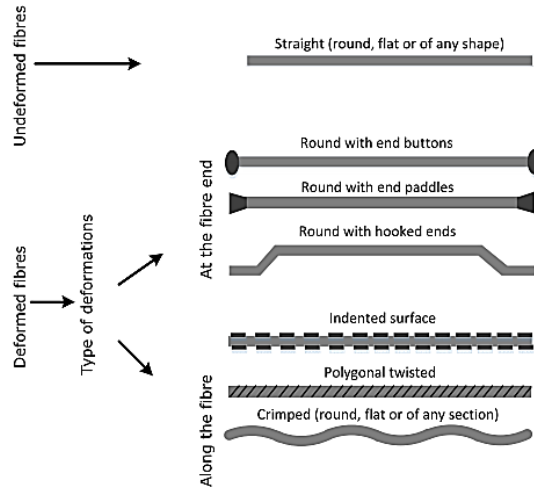
Figure 1.1: Different types of steel fibers categorized according to their geometric shape (Cunha, 2010)

The structural member of interest in this research is the reinforced concrete deep beam. Reinforced concrete deep beams are important structural members generally used as load-transferring elements, such as transfer girders in high rise buildings, pile caps, tanks, folded plates, and foundation walls. A deep beam is defined by the ACI 318-14 (2014) as a structural element in which either the clear span is equal to or less than four times the overall depth, or the concentrated loads are applied within a distance equal to or less than two times the depth from the face of the support. The inclusion of web openings in RC deep beams is frequently required to provide passage for electrical and mechanical ducts. Web openings produce discontinuity in the normal flow of stresses which reduces the beam shear capacity and stiffness (Campione & Minafò, 2012; El Maaddawy & Sherif, 2009; Hu et al., 2007; Yang et al., 2006; Yang & Ashour, 2008). Reinforced concrete deep beams transfer the loads directly to the supports through the arch action and are typically classified as shear-critical RC elements (ACI 318-14, 2014). The potential use of steel fibers to fully or partially replace traditional shear

reinforcement in recycled aggregate RC deep beams with and without web openings have not been fully exploited yet.

1.2 Statement of the Problem

Concrete is one of the most consumed construction materials. It uses significant amount of non-renewable natural resources in the production of its components, aggregates, and cement. To sustain the continuous population growth and construction development, more concrete will be required. Consequently, the increasing demand for aggregates raises concerns of the depletion of their current sources and the availability of new sources. Massive amounts of CDW are mostly disposed of in landfills, instigating serious environmental hazards. The limited space for landfills to contain CDW and the scarcity of NAs promote the concept of reusing this waste by manufacturing RCAs as a potential substitute to NAs. However, concrete mixtures made with RCAs possess inferior mechanical properties compared to those of conventional concrete made with NAs (Etxeberria et al., 2007; Meyer, 2009). The inferior performance of concrete made with RCAs hinders its widespread use in structural application. Steel fibers have a potential to upgrade the performance of conventional concrete. There is, however, a lack of information on the behavior of concrete made with RCAs and steel fibers.

1.3 Insight into the Benefits of Recycled Aggregates and Steel Fibers

Despite the substantial environmental benefits that can be obtained by using RCAs in the construction industry as an alternative to NAs, they are not commonly accepted by the engineering community or code provisions to produce structural concrete elements due to the inferior properties of RCA-based concrete mixtures. The uncertainty in satisfying structural performance requirements of a structural concrete beam made with RCAs and steel fibers increases in the presence of openings and/or discontinuity regions. The addition of steel fibers has great potential to improve the properties of

concrete mixtures made with RCAs. Although the addition of steel fibers would result in a direct cost increase, there is a potential of reducing or eliminating the use of conventional shear reinforcement in large-scale RC beams, which would result in a direct and indirect cost savings. Practitioners should consider a balance between structural performance requirements, environmental benefits, and associated costs. Such an analysis requires identification of quantifiable measures and criteria for performance evaluation.

Although the financial and environmental aspects are beyond the scope of the current study, Table 1.1 shows typical quantifiable measures that could help practitioners and researchers to evaluate environmental benefits and associated costs of RC structures made with RCAs and steel fibers. The environmental impact of the alternative materials can be quantified by evaluating their global warming potential (GWP) values published in the literature (Alzard et al., 2021; Braga Maia et al., 2017; Polat et al., 2006; bre, 2015; Madar Emirates for Buildings Materials, 2022; Sinopro Industrial Products, 2022). From Table 1.1, it is evident that the use of RCAs along with steel fibers in replacement of NAs and conventional steel stirrups results in a significant reduction in GWP. The direct cost of RCAs is approximately 20% lower than that of NAs whereas the unit price of steel fibers is approximately 35% higher than that of conventional steel including the cost of steel fabrication. The economic analysis should, however, include other factors that would affect the cost benefit analysis such as the landfill space saved, reduction in construction time, lifting of reinforcing bars to upper floors, service life of the structure, and other labor- and indirect-related costs. The total cost saving in construction due to the use of steel fibers in replacement of conventional steel reinforcing bars can be as high as 30% (ACI Committee 544, 2015). Previous studies have also verified that the extra cost caused by the inclusion of steel fibers could be counteracted significantly by quantified

sustainable benefits of RCAs in an optimum concrete mixture (Awchat, 2021; Tam et al., 2013; Senaratne et al., 2016).

Table 1.1: Cost and GWP values of the alternate materials used in the beams (Alzard et al., 2021; Braga Maia et al., 2017; Polat et al., 2006; bre, 2015; Madar Emirates for Buildings Materials, 2022; Sinopro Industrial Products, 2022)

Material	Cost (USD/kg)	GWP (kg CO_2eq)/kg
Natural aggregates (NAs)	0.00675–0.00953	0.0052–0.0314
Recycled concrete aggregates (RCAs)	0.0054–0.0081	6.67×10^{-4}–7.44×10^{-3}
Conventional steel reinforcement	0.72–0.84	0.9052
Fabrication of steel cages	0.22–0.576	0.102
Steel fibers	1.62	0.771

1.4 Research Objectives

This research aims to characterize and examine the structural behavior of concrete made with RCAs and steel fibers. The major objectives of this study are:

- Examine fresh and hardened properties of concrete mixtures made with RCAs and steel fibers.

- Develop tensile constitutive laws that can accurately describe the post-cracking behavior of concrete made with RCAs and steel fibers.

- Examine the structural shear behavior of RC deep beams with and without web openings made with RCAs and steel fibers.

- Examine the accuracy and validity of published analytical models to predict the shear capacity of steel fiber-reinforced recycled aggregate RC deep beams with and without web openings.

- Develop three-dimensional (3D) finite element (FE) models capable of simulating the shear behavior of steel fiber-reinforced recycled aggregate RC deep beams with and without web openings.

1.5 Relevant Literature

1.5.1 Characteristics of Concrete with Recycled Aggregates and Steel Fibers

1.5.1.1 Concrete Mixtures with Recycled Aggregates

The concrete fresh properties, primarily the workability and wet density, depend on many factors such as the size of aggregates, the moisture content of aggregates, the water absorption and the shape and texture of the aggregates. The RCAs have higher porosity compared to that of the NAs, therefore the workability of RCA-based concrete mixes is lower for the same *w/c* ratio than that of NA-based concrete mixes (Rao et al.,2007). The wet concrete density decreased with an increase in the content of RCAs (Malešev et al., 2010). The reason for such a decrease is the lower specific gravity of RCAs due to the old, adhered mortar attached to the surface of the RCAs.

The mechanical properties of concrete made with RCAs include the compressive strength, tensile strength, modulus of elasticity, and modulus of rupture. Such properties depend on many factors such as *w/c* ratio, properties of RCAs, properties of adhered mortar, mixing approach and the use of admixtures. The increase in the amount of RCAs at the same *w/c* ratio resulted in a decrease in the compressive strength (Nixon, 1978). However, other researchers reported that the compressive strength of concrete remained unaffected for replacement of NAs by RCAs up to 25% (El Hakam et al., 2012; Fonseca et al., 2011). This contradicting behavior may be attributed to a large extent to the heterogeneity and the quality of RCAs (Etxeberria et al., 2007). The splitting tensile strength and modulus of rupture of concrete made with RCAs decreased with an increase in RCA replacement percentage (Kou et al., 2013; Malešev et al., 2010). The modulus of rupture of concrete made with 25% and 50% RCAs was 6-13% lower than that of NA-based concrete. When 100% RCAs were used, the reduction in the modulus of rupture was

26% compared to that of the NA-counterpart. This reduction can be attributed to the poor quality of the interfacial zone between the old, adhered mortar and the new cement paste covering the RCAs. The modulus of elasticity was also reduced due to the incorporation of RCAs (Kou et al., 2013).

Concrete made with RCAs possesses inferior durability properties relative to those made with NAs. The depth of carbonation of RCA-based concrete increased with an increase in the RCA replacement percentage. Full replacement of NAs with RCAs resulted in a 100% increase in the depth of carbonation (Debieb et al., 2010; Kou et al., 2013). The permeability of concrete made with RCAs was typically higher than that of NA-based concrete (Kwan et al., 2012). This is because RCAs have higher porosity and contain more cracks on the adhered mortar, formed in the RCAs during the crushing and production process. The water permeability in RCA-based concrete increased with an increase in the content of RCAs and *w/c* ratio due to an increase in the porosity of the interfacial transition zone (ITZ). Increasing the amount of RCAs also increased the chloride penetration into the concrete (Kou et al., 2013).

Çakır (2014) examined the properties of concrete made with different RCA replacement percentages in the range of 25 to 100%. The RCAs were acquired from Istanbul environmental protection and waste processing corporation, while the NAs were crushed limestone. The percentages of water absorption for sand, NAs and RCAs were 1.7, 2.2, and 7.4%, respectively. The percentages of loss in the Los Angeles abrasion test were 23% for NAs and 47% for RCAs. It was concluded that the compressive strength of concrete made with 100% RCAs decreased by approximately 24% compared to that of concrete made of NAs. The splitting tensile strength of concrete made with 25, 50, 75 and 100% RCAs decreased by 3, 3, 21, and 9%, respectively, compared to that of the NA-based concrete. The hardened

concrete density of concrete mixture made with 25, 50, 75 and 100% RCAs decreased by 8, 10, 16, and 20%, respectively, compared to that of the NA-based concrete. The water absorption of concrete mixture made with 25, 50, 75 and 100% RCAs increased by 29, 88, 143, and 205%, respectively, compared to that of the NA-based concrete.

Corinaldesi (2010) investigated the mechanical behavior of concrete made of RCAs. Concretes mixtures were prepared by alternatively using two different RCAs (coarse and finer coarse) obtained from a recycling plant in which rubble from demolition was collected after conducting a proper quality check in order to avoid hazardous materials such as asbestos or chalk, then ground, cleaned and sieved. The RCA replacement percentage was 30% with coarse RCAs (11 to 22 mm), or finer coarse RCAs. Five different *w/c* were adopted as: 0.40, 0.45, 0.50, 0.55 and 0.60. The slump was in the range of 190 to 200 mm. All concrete mixtures had the same proportions. The specific gravity of RCAs was lower than that of NAs. The water absorption of RCAs was higher than that of the NAs. The compressive strength of coarse RCA-based concrete was higher than that of finer coarse RCA-concrete by 8%. Shrinkage strains of finer coarse RCAs were lower than that of the coarse RCAs. The target compressive strength was attainable with up to a 30% replacement of RCA. However, with this RCA replacement percentage, the elastic modulus decreased by 15% compared to that of a NA-based concrete.

Malešev et al. (2010) studied fresh and hardened properties of concrete made with different replacement percentages of RCAs (50 and 100%). Fine and coarse NAs with NMS of 4 mm and 31.5 mm, respectively, were obtained from River Sava in Serbia. The RCAs were collected from the concrete laboratory of University of Belgrade. Additional water was used to achieve the required workability of RCA-based concrete. The researchers reported that the use of 100% RCA replacement percentage increased the

water absorption increased by 43% compared to that of the NA counterpart. The bulk density of fresh concrete, wear resistance, and modulus of elasticity decreased while increasing the quantity of RCAs. Furthermore, when the RCAs were obtained by crushing a high-strength concrete, the compressive strength was not reduced compared to that of concrete made with NAs. The modulus of rupture, splitting tensile strength and modulus of elasticity of RCA-based concrete were comparable to those of the NA-based concrete. According to the researchers, this result was due to the quality of RCAs which were not exposed to any chemicals and/or regressive environment.

Tabsh & Abdelfattah (2009) investigated the effect of full replacement of NAs by RCAs on properties of concrete. The test variables included the source of the recycled concrete (crushed old concrete of unknown compressive strength, crushed old concrete of compressive strength of 30 and 50 MPa) and the target concrete compressive strength (30 and 50 MPa). Results of the toughness and soundness test on the RCAs showed higher percentage loss than NAs but remained within the acceptable limits. Test results showed that the loss of compressive or tensile strength due to the use of RCAs was more significant for concrete mixtures with a target strength of 30 MPa. Concrete made of RCAs obtained from an unknown source had lower compressive and tensile strengths than those of concrete made of RCAs obtained by crushing of concrete structures with known compressive strengths of 30 and 50 MPa. It was concluded that, the strength of RCA-based concrete can be 10 to 25% lower than that of conventional concrete made with NAs.

Shaikh & Nguyen (2013) investigated the effect of RCAs on the mechanical and durability properties of concrete. The RCA replacement percentages were 25 and 50%. Concrete made with RCAs exhibited about 10% average reduction in the compressive strength compared to that of its

NA-based counterpart. The splitting tensile strength and modulus of rupture of concrete containing 25% RCAs were comparable to those of the NA-based concrete. A higher RCA replacement percentage of 50% reduced the splitting tensile strength by 10% and the modulus of rupture by 14 to 24%. The drying shrinkage of RCA-based concretes also increased with an increase in the content of RCAs. Concrete made with RCAs exhibited higher sorptivity and water absorption compared to those of their counterparts made with NAs. The concrete containing 25% RCAs exhibited comparable resistance against chloride ion permeability to that of concrete containing NAs. However, the concrete containing 50% RCAs exhibited about 40% increase in chloride permeability values than that of concrete containing NAs.

Rao et al. (2007) studied the effect of RCAs on fresh and hardened properties of concrete. The water absorption of RCAs used in this study ranged from 3 to 12% for the coarse and the fine fractions, depending on the type of concrete used for producing the RCAs. The workability of the mixes made with RCAs was lower especially when the RCA replacement percentage exceeded 50%. The air content of the RCA-based concrete was 4 to 5% higher than concrete made with NAs at 100% replacement percentage. A reduction in the modulus of rupture and the splitting strength of 15 to 20% was reported at 100% RCA replacement percentage. It was reported that the direct tensile strength of concrete made with RCAs was 10% lower than that of the NA-based counterpart. The modulus of elasticity of the concrete made with RCAs was in the range of 50 to 70% of that of concrete made with NAs. The carbonation depth of the RCA-based concrete was 1.3 to 2.5 times that of the reference concrete made with NAs.

Etxeberria at al. (2007) studied the influence of RCAs, obtained from crushed concrete, on properties of concrete. The RCA replacement percentages were 25, 50 and 100%. All concrete mixtures were designed in a

way to achieve the same compressive strength. The RCAs were used in a wet unsaturated condition. Test results showed that concrete made with 100% of RCAs had 20 to 25% less compressive strength than that of a conventional concrete made with NAs at the same *w/c* ratio and cement quantity. Concrete made with 25% of RCAs had mechanical properties comparable to those of the conventional concrete employing the same quantity of cement and the equal effective *w/c* ratio. Concrete made with 50 or 100% of RCAs needed 4 to 10% lower effective *w/c* ratio and 5 to 10% more cement content than conventional concrete to achieve the same compression strength at 28 days. The modulus of elasticity of the concrete made with RCAs was lower than that of the conventional concrete. Standard deviation of compressive strength increased by up to 50% when 100% RCAs was used compared to the standard deviation of the conventional concrete, possibly due to the heterogeneity of RCAs.

Yehia et al. (2015) studied the durability and strength properties of concrete produced with 100% of RCAs. Concrete mixes had different grading of RCAs and one control mix consisted of NAs with a maximum size of 25 mm blended with crushed stone sand. The NAs were crushed limestone, while the RCAs were obtained from a recycling facility in the UAE. The recycling process involved crushing, separation of metals by a magnet, manual removal of other impurities (plastic, wood, etc..), and classification of RCAs to different grades based on particle size. The absorption, abrasion loss and the crushing value of RCAs were higher than those of NAs. The target compressive strength was 50 MPa. A microstructure evaluation was conducted using scanning electron microscopy (SEM) scans. Examination of the SEM micrographs showed cracks at the interface between the RCAs and mortar. Due to the high absorption and low specific gravity of the RCAs, a 7 to 15% reduction in the concrete compressive strength of the mixes with RCAs was reported compared to the target strength. Flexural and splitting

strength did not show a clear trend resulting from the use of 100% of RCAs. The use of 100% of RCAs resulted in 10 to 15 % reductions in the modulus of elasticity compared to that of the NA-counterparts. The use of two different coarse RCA distributions along with the fine aggregates led to a denser mix with less voids and better resistance to the chloride ion penetration.

Thomas et al. (2013) carried out an experimental study to examine the physical, mechanical and durability properties of concrete made with RCAs. Test variables included different replacement percentages of RCAs (20, 50 and 100%) and various *w/c* ratios (0.65, 0.55, 0.50, and 0.45). Limestone aggregates were used as NAs. The absorption and abrasion loss of RCAs were higher than those of the NAs by 66 and 27%, respectively. The density of the RCAs was lower than that of the NAs by 9%. All aggregates had a NMS of 20 mm. It was reported that the accessible porosity of the RCA-based concrete, compared with the control concrete, increased with the *w/c* ratio and the degree of substitution of NAs by RCAs. The incorporation of RCAs increased the porosity of concrete. The use of 20% RCAs did not result in a significant change in properties of concrete. In contrast, the use of 100% of RCAs significantly reduced the compressive strength. it was necessary to reduce the *w/c* ratio to achieve the target strength. The splitting tensile strength of the concrete made with 20, 50, and 100% RCAs were 90, 85 and 80% of that of the concrete made with NAs. The reduction in the elastic modulus due to the use of RCAs was more significant than that of the compressive strength. There was a significant increase in the rate of carbonation with the incorporation of RCAs due to the higher permeability and alkalinity of the so-produced concrete. Water permeability increased with increasing the *w/c* ratio and the percentage of RCAs.

Evangelista & de Brito (2010) studied the durability performance of concrete made with fine RCAs. Water absorption by immersion and capillary,

chloride penetration, and carbonation were the investigated properties. The fine RCAs used in the study were obtained by crushing a 30 MPa concrete produced in the laboratory by an impact crusher. The RCAs used had sizes of up to 1.19 mm. The RCA replacement percentages considered were 30 and 100%. Water absorption by immersion increased by 46% when the fine NAs where fully replaced by fine RCAs. The sorptivity coefficient had a relative increase of 70% for concrete made with 100% fine RCAs compared with that of the reference concrete made with fine NAs. The chloride migration coefficient increased linearly with the replacement ratio of the fine RCAs, reaching an increase of 34% at fine RCA replacement percentage of 100%. The carbonation resistance decreased with the addition of fine RCAs to the concrete; where CO_2 penetration depth increased about 110% for the concrete made with 100% fine RCAs.

Kou et al. (2013) studied the long-term mechanical and durability properties of concrete made with different coarse RCA replacement percentages of 50 and 100%. In this study, crushed granite was used as NAs. The RCAs were crushed concrete rubbles obtained mainly from building demolition projects. The nominal sizes of the NAs and RCAs were 20 and 10 mm. Concrete mixtures with a target initial slump of 120 mm were prepared in the laboratory. At 28 days, the compressive strength of the concrete made with 50 and 100% RCAs decreased by 13 and 22%, respectively, in comparison to the strength of the control concrete. However, the impact of RCAs on the compressive strength decreased with increasing the curing age. After 10 years, the compressive strength of the concrete made with 50 and 100% RCAs decreased by 4 and 8%, respectively, in comparison to the strength of the control concrete. At 28 days, the splitting tensile strength of the control mixture was higher than that of the concrete mixture made with 50 and 100% RCAs by 5 and 7.5%, respectively. However, comparing the results at 1 and 10 years of concrete age showed that there was continuous

and significant improvement in the splitting tensile strength of RCA-based concrete. The splitting tensile strength of the concrete mixtures with 100% RCAs was comparable to that of the control mixtures at 1 and 10 years. At 28 days, the modulus of elasticity values of concrete mixtures with 50 and 100% RCAs decreased by 13 and 25%, respectively, compared to that of the control mixture. Approximately a similar reduction in the modulus of elasticity was observed after 10 years. At 28 days, the resistance to chloride ion penetration of the mix made with 100% RCAs was 11% lower than that of the control mixture. After 10 years of outdoor exposure, the resistance to chloride ion penetration of RCA-based concrete was still lower than that of the NA-based concrete. At 28 days, the carbonation depth of the concrete made with 100% RCAs was 8% higher than that of the NA-based concrete. The increase in carbonation depth became 11% after 10 years of outdoor exposure.

1.5.1.2 Concrete Mixtures with Steel Fibers

Sharma et al. (2018) studied the mechanical and durability properties of high-strength steel fiber-reinforced concrete. The concrete compressive strength was 90 MPa. The steel fibers used at v_f of 1, 1.25, and 1.5%. The steel fibers were hooked-end with a diameter of 0.55 mm and an aspect ratio of 63. Substantial improvement in the toughness, and energy absorption capacity of steel fiber-reinforced concrete was reported at $v_f \geq 1.25\%$. The slump of the control concrete was 150 mm. The addition of steel fibers into the mixture reduced the slump and affected the workability. A high-range water-reducing admixture was used to maintain the required slump of 130 to 150 mm. The compressive strength of the steel fiber-reinforced concrete increased by 12 and 14% at v_f of 1.25% and 1.5%, respectively, compared to that of the control mix without steel fibers. The modulus of rupture increased by 22, 37 and 44% at v_f of 1, 1.25 and 1.5%, respectively, compared to that

of the control mix without steel fibers. The specimens with steel fibers tested in flexure exhibited a post-peak ductile response. The flexural toughness increased by 59 and 119% at v_f of 1.25 and 1.5%, respectively, compared to that of the concrete mix with 1% steel fibers. The splitting tensile strength of steel fiber-reinforced concrete increased by 40 to 75% compared to that of the control mixture. The abrasion wear value decreased by 58, 64 and 39% due to the addition of steel fibers at v_f of 1, 1.25 and 1.5%, respectively, compared to that of the control mix without steel fibers. The drying shrinkage of steel fiber-reinforced concrete decreased compared to that of the control mix without steel fibers. The water permeability decreased significantly with increasing the steel fiber content. The water penetration decreased by 17, 50, and 58% due to the addition of steel fibers at v_f of 1, 1.25, and 1.5%, respectively, compared to that of the control mix without steel fibers. Air permeability coefficient values of the steel fiber-reinforced concrete specimens were less than that of control concrete by 80 to 91%. The researchers concluded that the low permeability of the hardened concrete was mainly attributed to the breaking of connectivity of porous channels by impermeable steel fibers.

Ramadoss & Nagamani (2008) investigated the effect of inclusion of steel fibers on tensile and durability properties of high-performance concrete. Flexural and splitting tensile strengths were determined at 28 days. The variables investigated were the steel fiber volume fraction (0.5, 1, and 1.5%) silica fume replacement ratio (5 and 10%) and matrix composition (*w/cm* ratios ranging from 0.25 to 0.40). The steel fibers had an aspect ratio of 80. A superplasticizer was used to maintain the adequate workability of plain and fiber reinforced concrete. The slump was 75 ± 25 mm for the steel fiber concrete mixes, whereas their VeBe value was 12 ± 3. Test results showed that at *w/cm* of 0.4 and a silica fume replacement ratio of 5%, the addition of steel fibers at v_f of 0.5, 1 and 1.5% resulted in an increase in the compressive

strength by 4, 11, and 12%, respectively, compared to that of the control mix without steel fibers. At these same conditions, the modulus of rupture increased by 19, 28, and 33%, respectively, whereas the splitting tensile strength increased by 28, 44, and 56%, respectively. At *w/cm* of 0.25 and a silica fume replacement ratio of 5%, the addition of steel fibers at v_f of 0.5, 1 and 1.5% resulted in an increase in the compressive strength by 4, 6, and 6%, respectively, compared to that of the control mix without steel fibers. At same conditions, the modulus of rupture increased by 17, 23, and 30%, respectively, while the splitting tensile strength increased by 28, 46, and 54%, respectively. At *w/cm* of 0.4 and 0.25, and a silica fume replacement ratio of 5%, the addition of steel fibers at v_f of 0.5, 1 and 1.5% resulted in an increase in the hardened concrete density by 1, 2, and 3%, respectively, compared to that of the control mix. At *w/cm* of 0.4 and a silica fume replacement ratio of 5%, the addition of steel fibers at v_f of 0.5, 1 and 1.5% resulted in a decrease in water absorption by 1, 3, and 2%, respectively, compared to that of the control mix. At *w/cm* of 0.25 and a silica fume replacement ratio of 5%, the addition of steel fibers at v_f of 0.5, 1 and 1.5% resulted in an increase in the air content by 1, 4, and 3%, respectively, compared to that of the control mix. The addition of 1.5% of steel fibers resulted in a decrease in the sorptivity by 2% compared to that of the control mix, at *w/cm* of 0.4 and a silica fume replacement ratio of 5%.

Shi et al. (2020) studied the behavior of steel fiber reinforced concrete under uniaxial compression and tension. Two types of steel fibers (straight and hooked fibers) with various fiber volume fractions (0.5, 1, 1.5, 2, and 3%) were investigated. The hooked fibers had an aspect ratio of 60 and the straight fiber had an aspect ratio of 65. The straight fibers were coated with copper by the manufacturer to prevent corrosion. The target concrete compressive strength was 28 MPa. The *w/cm* ratio was 0.43% and 25% of the required weight of cement was replaced by fly ash. A water reducer was used

in the concrete mixes. Test results showed that adding steel fiber significantly decreased the concrete slump. The concrete mix with straight steel fibers at v_f of 3% had the highest compressive modulus of elasticity while the concrete mix with hooked steel fibers at v_f of 1.5% had the highest compressive strength among all tested mixtures. No clear trend was found for the effect of steel fibers on the concrete compressive modulus of elasticity and compressive strength. Unlike the compressive strength and modulus of elasticity, the strain at the peak load, residual strength, and toughness obtained from the uniaxial tensile test showed clear trends. It is worth noting that the residual strength was taken as the stress value associated with the strain of 0.015 on the stress-strain curve, and the toughness was calculated using the area under the stress-strain curve (up to the strain of 0.015). Generally, the higher the steel fiber volume fraction, the higher those three parameters were. Mixing and consolidation problems were reported for the tension test specimens having v_f of 3%. Concrete mixes with 1% straight steel fibers had the highest average values in both tensile modulus and tensile strength among the mixes with straight steel fibers. The mixes with hooked steel fibers at v_f of 0.5% had the highest average tensile modulus of elasticity and tensile strength among the mixtures with hooked steel fiber mixtures. The tensile strain at peak increased with the increase in the value of v_f with the highest increase was 50% in the mix with 2% of straight steel fiber and 25% for the mix with 2% of hooked steel fibers. The flexural toughness increased by 5 and 8 folds due to the addition of straight and hooked steel fibers at v_f of 2%, respectively, compared to that of their plain counterparts. Steel fibers remarkably enhanced the concrete post-cracking behavior in terms of achieving a higher residual strength and toughness under compression and tension.

1.5.1.3 Concrete Mixtures with Recycled Aggregates and Steel Fibers

The main advantage of adding steel fibers to concrete is their capacity to increase the tensile strength, post-cracking residual tensile strength, toughness, and fracture energy. This is mainly due to the bridging effect of steel fibers that can reduce the initiation and propagation of cracks, resulting in an increase in the energy absorption capacity of the concrete. Results of steel fiber-reinforced RCA concrete showed that the elastic modulus, tensile strength, toughness and impact resistance increased, while the compressive strength was not significantly affected by the inclusion of steel fibers, compared with those of the NA-based concrete. The inclusion of steel fibers improved the quality of concrete made of RCAs by reducing the development of micro-cracks (Bencardino et al., 2008; Marco et la., 2013; Kachouh et al., 2021).

Carneiro et al. (2014) conducted an experimental work to investigate the influence of steel fibers on the compressive strength, flexural strength and splitting tensile strength of concrete made with RCAs. Natural coarse and fine aggregates were replaced by RCAs and recycled fine aggregate at a replacement percentage of 25%. Hooked end steel fibers with 35 mm of length and aspect ratio of 65 were used at v_f of 0.75%. The compressive strength of the concrete made with RCAs increased by about 10 to 19% with the addition of the steel fiber to the mixtures. The use of RCAs had no significant effect on the elastic modulus, splitting strength and modulus of rupture of concrete. The splitting and flexural strength of the RCA-based concrete with steel fibers increased by about 20 to 26% and 8 to 36%, respectively, relative to those of their counterparts without steel fibers.

Gao et al. (2017) studied the combined effect of steel fibers and RCAs on the compressive strength, Young's modulus and compressive stress-strain curves. Compared to NAs, RCAs had lower specific gravity,

higher water absorption and higher porosity. A water reducing agent was used to obtain a slump of 50 mm for all mixes. All aggregates were used in the air-dry condition. The steel fibers were hooked at both ends, and had a mean diameter of 0.6 mm, mean length of 30.5 mm, and aspect ratio of 54.6. The RCA replacement percentages, by mass, were 30, 50, and 100%. The steel fibers were used at v_f of 0.5, 1, 1.5, 2%. Eight groups of concrete were designed to achieve the same target compressive strength (f_{cu} of 45 MPa) by slight modifications in the design. The Young's modulus and stress-strain curves of the steel fiber-reinforced RCA concrete were similar to those made with NAs, but the critical strain corresponding to the peak stress significantly increased with the increase of steel fiber content and RCA replacement percentage with a greatest increase ratio of 40%. For concrete mixes made with 50% RCAs, the addition of steel fibers at v_f of 2% increased f_{cu} and f'_c by 11 and 29%, respectively, compared to those of their plain counterparts. For concrete mixes made with 100% RCAs, the addition of steel fibers at v_f of 1% increased f_{cu} and f'_c by 6 and 16%, respectively, compared to those of their plain counterparts. At v_f of 1%, the Young's modulus increased by 15% by increasing the RCA replacement percentage from 0 to 100%. For concrete made with 50% RCAs, with the increase of v_f from 0 to 2%, the Young's modulus increased by 44%.

Younis et al. (2019) conducted a study to examine the feasibility of using recycled tyres steel fibres in RCA-based concrete for structural applications. Natural sand was used as fine aggregates and two types of coarse aggregates were used; a natural (gravel) river aggregates and RCAs obtained from crushing a mix of CDW containing crushed concrete, masonry (brick) and asphalt. Silica fume (2% by cement mass) in liquid form was used to coat the RCAs to improve their properties. Industrial fibers from a cold-drawn process were used and they had a length of 50 mm, and a diameter was 1 mm. Six different mixes were prepared with the same w/c ratio of 0.4. The

RCA replacement percentage was 100%. Fiber reinforced concrete mixes contained v_f of 2% of tyres steel fibers. Superplasticizers were used to achieve concrete with a slump between 70 and 110 mm. The use of RCAs reduced the compressive strength by 27% in comparison to that of the NA-based concrete. The addition of the steel fibers to the mixes with RCAs at v_f of 2% and the increased the compressive strength of by 25% and the flexural strength by 15%. The post-cracking performance of the RCA-based concrete with steel fibers was improved compared to that of a counterpart mix without steel fibers.

Gao & Zhang (2018) examined the flexural performance of steel fiber-reinforced RCA concrete prisms following the ASTM C1609 (2012) and the Chinese Standard JG/T 472-2015 (2015). Test parameters included the RCA replacement percentage of 30, 50, and 100%, and steel fiber volume fraction of 0.5, 1, 1.5, and 2%. The NAs were crushed limestone, and RCAs were crushed waste ready-mix concrete sourced from a concrete testing station. All aggregates were used in the air-dry condition. The steel fibers were hooked at both ends with a mean diameter of 0.6 mm, mean length of 30.5 mm, and an aspect ratio of 54.6. Replacing the NAs by RCAs by 30 and 100% in mixes with 1% steel fibers had a negligeable effect on the cube compressive strength and the Young's modulus of the concrete. For mixes made with 50% RCAs, the addition of steel fibers at v_f of 0.5, 1, and 2% increased the cube compressive strength by 2, 7, and 11%, respectively, compared to that of the plain mix with 50% RCAs. For mixes made with 50% RCAs, the addition of steel fibers at v_f of 0.5, 1, and 2% increased the Young's modulus by 23, 51, and 55%, respectively, compared to that of the plain mix with 50% RCAs. Increasing the steel fiber v_f resulted in an increase in the flexural strength, flexural toughness, and deflection at peak noting that the mixture proportions in this study were modified to maintain mechanical properties similar to those of the NA-based control concrete mix.

Afroughsabet at al. (2017) studied the influence of steel fibers on mechanical and durability properties of high-performance concrete, made with RCAs. Natural coarse aggregates were replaced by RCAs derived from parent concretes with compressive strengths of 40 and 80 MPa at replacement percentages of 50 and 100%. Double hooked-end steel fibers were added at v_f of 1%. Steel fibers used in study had a length of 60 mm, a diameter of 0.9 mm, an aspect ratio of 65. The replacement of NAs with RCAs derived from 40 MPa concrete reduced the compressive strength of concrete. The compressive strength of the mixes made with 100% RCAs was slightly lower than that of the corresponding mixes with 50% RCAs. The compressive strength of the RCA-based concrete containing steel fibers increased by 3 to 14% compared to that of their NA-based counterparts. The splitting tensile strength of the concrete incorporating 50 and 100% RCAs derived from 40 MPa concrete was 4 and 11% lower than that of the NA-based counterpart, respectively. The increase in the splitting tensile strength of RCA concretes containing steel fibers ranged from 37 to 60%, while an increase of up to 88% was attained in the flexural strength. Full replacement of NAs with RCAs derived from 40 and 80 MPa concrete resulted in an increase of up to 57 and 27% in the water absorption, respectively. The water absorption of RCA-based concrete containing steel fibers was up to 23% lower than that of the corresponding mixes without fibers. These results suggested that the inclusion of steel fibers restricted the formation and propagation of cracks in the body of concrete leading to a reduced permeability. The results indicated that irrespective of the content and type of the RCAs, the replacement of NAs with RCAs led to a reduction in the electrical resistivity of concrete. The reduction in the electrical resistivity of the recycled aggregate concretes varied from 11 to 49%, depending on the content and type of RCAs, and testing age. The mix made with 100% RCAs and 1% steel fibers had an electrical resistivity 80% lower than that of the NA plain concrete mix. The

incorporation of steel fibers in RCA-based concrete led to a reduction in the shrinkage strain of up to 15%.

Koushkbaghi et al. (2019) studied the mechanical properties, acid resistance and durability properties of steel fiber-reinforced concrete incorporating rice husk ash and recycled aggregate. The steel fibers were hooked at both ends and had an aspect ratio of 67. The aggregates were pre-wetted before mixing the concrete. All the aggregates were in saturated surface dried (SSD) condition prior to concrete mixing. Twelve mix designs with varying RCA replacement percentages of 50 and 100% were made. Steel fibers with v_f of 1.5% were used. The use of 100% of RCAs, caused a decrease of 22 to 29% in compressive strength compared to that of the NA-concrete mix without steel fibers. The splitting tensile strength was found to decrease as the RCAs content increased. At 100% RCAs replacement, a decrease of 22 and 15% was reported for non-fibrous and fibrous specimens, respectively, compared to that of the NA-concrete. Steel fibers significantly increased the splitting tensile strength at the early age of the concrete comparing to the corresponding non-fibrous concrete. The increase in the splitting tensile strength was 35 and 17% at ages of 28 and 90 days, respectively, comparing to that of the non-fibrous concrete. At 100% RCAs, the average increase in the diffusion coefficient among all mixtures was 11 and 15% for non-fibrous and fibrous concrete, respectively, relative to that of the concrete made with NAs. The increase in RCA content from 0 to 100% for non-fibrous and fibrous concrete increased the water absorption by 4 and 33%, respectively. Incorporating steel fibers increased the water absorption by 9% compared to that of the corresponding samples with no fibers. The steel fibers increased the connectivity between the pores and micro-channels which resulted in higher absorption. The increase in the RCA content decreased the resistance to acid. The steel fibers improved the resistance of concrete in all the mixtures exposed to acid. The important factor affecting

the acid attack was the permeability of the concrete which was influenced by connectivity, size, and distribution of the pores in the concrete.

Gao et al. (2020) studied the durability of steel fiber-reinforced recycled coarse aggregate concrete. Carbonation resistance and chloride ion penetration experiments were performed to evaluate the effects of the RCAs and the steel fibers on the durability of steel fiber reinforced recycled aggregate concrete. All aggregates were used in the air-dry condition. The steel fibers were hooked at both ends with a mean diameter of 0.6 mm, mean length of 30.5 mm, and an aspect ratio of 54.6. The RCA replacement percentages were 30, 50, 100%. The steel fibers used at v_f of 0.5, 1, 1.5, and 2%. Test results indicated that at the same v_f, the RCA replacement percentage had little effect on the carbonation resistance and anti-chloride permeability of steel fiber-reinforced RCA concrete. At 50% RCAs, the addition of steel fibers at v_f of 0.5, 1.5, and 2% decreased the chloride penetration at depth of 10 to 15 mm by 6, 30, and 15%, respectively, compared to that of their plain counterparts. At the same RCA replacement percentage of 50%, the addition of 0.5, 1.5, and 2% steel fibers decreased the chloride penetration at depth of 15 to 20 mm by 31, 35, and 33%, respectively, compared to that of their plain counterparts. At RCA replacement percentage of 50%, the addition of 0.5, 1.5, and 2% of steel fibers decreased the carbonation depth at 28 days by 3, 17, and 13%, respectively, compared to that of their plain counterparts.

1.5.2 Shear Behavior of RC Beams

This section includes a review of the available literature on the shear behavior of RC beams made with RCAs and steel fibers. As demonstrated in Table 1.2, the shear behavior of RC beams made with RCAs and steel fibers has received little attention. Furthermore, no information is available in the literature on the shear behavior of RC deep beams with and without web

openings made with RCAs and steel fibers. The section is divided into three sub-sections. The first one discusses the effect of RCAs on the shear behavior of RC beams without steel fibers. The second one focuses on the shear behavior of steel fiber-reinforced RC beams made with NAs. The third sub-section reviews studies on shear response of -RC beams with RCAs and steel fibers.

Table 1.2: Summary of previous studies on the shear behavior of RC beams

Researchers	Type of beam				Type of aggregates		Concrete and steel			
	Slender ($a/h \geq 2$)	Deep ($a/h < 2$)	Solid	With openings	NAs	RCAs	Concrete strength	Longitudinal steel	Internal stirrups	Steel fibers
Arezoumandi et al. (2013)	■		■		■	■		■		
Rahal & Al Refaei (2017)	■		■		■	■				
Rahal & Al Refaei (2018)	■		■		■	■			■	
Wardeh & Ghorbel (2019)	■	■	■		■	■				
Al Mahmoud et al. (2020)	■		■		■	■				
Gonzalez-Fonteboa & Martinez-Abella (2021)	■		■		■	■				
FAthifazl et al. (2009)	■	■	■		■	■				
Khergamwala (2016)	■	■	■		■	■				
Ignjatovic et al. (2017)	■		■		■	■			■	
Elmatty el al. (2020)	■			■	■	■				
Aly at al. (2015)		■		■	■	■				
Dinh et al. (2010)	■		■		■			■		■
Sahoo & Sharma (2014)	■		■		■		■	■	■	■
Amin & Foster (2016)	■		■		■				■	■
Cucchirra et al. (2004)	■	■	■		■				■	■

Table 1.2: Summary of previous studies on the shear behavior of RC beams (continued)

Researchers	Properties and Parameters									
	Type of beam				Type of aggregates		Concrete and steel			
	Slender (a/h ≥ 2)	Deep (a/h < 2)	Solid	With openings	NAs	RCAs	Concrete strength	Longitudinal steel	Internal stirrups	Steel fibers
Juárez et al. (2007)		■	■		■		■			■
Kang et al. (2011)	■	■	■		■				■	■
Ma et al. (2018)		■	■		■					■
Garcia et al. (2021)		■	■		■					■
Do-Dai et al. (2021)		■	■		■				■	■
Mansur & Alwist (1984)		■		■	■				■	■
Swaddiwudhipong & Shanmugam (1988)		■		■	■					■
Al-Sarraf & Diab (2011)		■	■	■	■					■
Sahoo et al. (2012)		■		■	■				■	■
Zewair et al. (2021)		■		■	■					■
Chaboki et al. (2019)	■		■		■	■			■	■

1.5.2.1 Shear Behavior of RC beams with Recycled Aggregates

The shape and surface texture of the aggregates influence the aggregate interlock which is one of the main contributors to the concrete shear strength. The RCAs have a rough surface resulting from the crushing process which might positively contribute to the concrete shear strength. However, the old mortar adhered to the RCAs creates a weak interfacial transition zone (ITZ) that might weaken the aggregate interlock and reduce the concrete shear strength. The effect of RCA replacement on the shear response of RC

beams is uncertain. Some researchers reported an inferior shear behavior for RCA-based beams relative to that of NA-based counterparts (Arezoumandi et al., 2013; Rahal & Al Refaei, 2017; Rahal & Al Refaei, 2018; Wardeh et al., 2019; Al Mahmoud et al., 2020) while others reported an insignificant variation in the shear response of NA- and RCA-based beams (Gonzalez-Fonteboa & Martinez-Abella, 2021; Fathifazl et al., 2009; Khergamwala, 2016; Ignjatovic et al., 2017).

Arezoumandi et al. (2013) conducted an experimental investigation to study the shear strength of full-scale beams constructed with 100% RCAs obtained from crushing of concrete laboratory specimens at the age of 28 days. The concrete mixtures had a target concrete compressive strength of 35 MPa. The experimental program consisted of twelve beams having a shear span-to-effective depth ratio (a/d) of 3. The longitudinal reinforcing bars had a diameter of 22 mm. The number of bars in the tension zone varied between 4, 6 and 8. The researchers reported a 12% reduction in the shear strength of beams with a 100% RCA replacement percentage compared to that of their NA-based counterparts. The reduction in shear strength resulting from the use of RCAs was higher in the beams with the higher longitudinal reinforcement ratio. No difference was observed in the crack morphology, crack progression, and stiffness of NA- and RCA-based concrete beams.

Rahal & Al Refaei (2017) studied the effects of using RCAs on the shear strength of RC beams with a/d of 3. The target compressive strength of the concrete was 35 MPa. The RCA replacement percentages were in the range of 10 to 100%. The RCAs were obtained from a local plant that demolished thirty- to forty-year-old concrete structures constructed from concrete having 15 to 25 MPa compressive strength. The test region was pre-selected by reinforcing the opposite side of the beam with double-legged 6-mm stirrups spaced at 160 mm. The reduction in strength ranged from 13 to

18%, with an average of 15%. All the beams failed similarly in shear along a crack which started as a flexural crack at the bottom side of the beam and extended diagonally toward the loading plate. At ultimate, the lower tip of the failure crack extended horizontally along the level of the longitudinal bars toward the support plate, causing a splitting bond failure. The load-deflection curves did not follow a clear trend. The deflections were larger in the NA-based beams relative to those of the RCA-based beams at the earlier stages of loading but became smaller at relatively higher loads.

Rahal & Al Refaei (2018) investigated the effect of RCA replacement percentage (20 and 100%) on the shear behavior of RC beams having *a/d* of 3. The RCAs were crushed waste concrete that were produced by a local plant. The researchers reported average reductions of 5 and 9% in the shear strength of RC beams at RCA replacement percentages of 20 and 100%, respectively. A shear tension mode of failure was observed in all beams. The beams with a 100% RCA exhibited higher deflections than those of the NA beams at service and ultimate loads. This behavior was not evident for the beams with a 20% RCA replacement percentage.

Wardeh & Ghorbel (2019) reported that the shear strength of RC beams with a 100% RCA replacement percentage and *a/d* of 3 was 23% lower than that of their NA counterparts, while for those with *a/d* of 1.5, the reduction was more than 10%, noting that the full shear capacity of the NA-based beams with *a/d* of 1.5 was not reached due to the limited capacity of the loading actuator used in the test. The RCAs were obtained from a concrete recycling platform. The target compressive strength was 35 MPa. Beams with *a/d* of 1.5 tended to exhibit a shear compression mode of failure, whereas a diagonal tension mode of failure was recorded for the beams with *a/d* of 3. The RCA-based beams showed flatter slopes in the post-cracking phase compared with those of the NA-based counterparts. The reduction in stiffness

of the RCA beams was attributed to the reduced elastic modulus and tensile strength of the RCA-based concrete mixtures.

Al Mahmoud et al. (2020) investigated the effect of using fine and coarse RCAs on the structural behavior of RC beams. The target compressive strength was 25 MPa. The beams had *a/d* of 2.6. The researchers reported a shear strength reduction of 11% due to a full replacement of coarse NAs by RCAs and a shear strength reduction of 29% due to the full replacement of fine and coarse NAs by RCAs. The stiffness of the RCA-based beams was, however, comparable to that of the NA-based beams, and no change was reported in the failure mode.

Gonzalez-Fonteboa & Martinez-Abella (2021) studied the shear behavior of beams with *a/d* of 3 made with 50% RCAs. Coarse RCAs were obtained from demolition debris and used after being washed and screened. Natural fine aggregates were used in all concrete mixes. To achieve the same level of workability for both NA- and RCA-based concrete, the water content of the RCA-based concrete was increased. The cement content was correspondingly increased to maintain the required *w/c* ratio and the percentage of superplastizer. The researchers reported no significant difference between the shear strength of NA- and RCA-based RC beams. Nevertheless, premature cracking and notable splitting cracks along the tension reinforcement were observed in the RCA-based beams. The RCA-based beams exhibited shear cracks at earlier load stages than those of the conventional concrete beams made with NAs.

Fathifazl et al. (2009) investigated the shear performance of RC beams made with coarse RCAs without shear reinforcement. Test parameters were the RCA replacement percentage (64, and 74%), *a/d* (1.5, 2.0, 2.7, and 4.0), and the beam size. In this study, RCAs were acquired from two different sources. The original virgin aggregates in one of the RCA sources was

limestone whereas the other one was river-bed gravel. Natural fine aggregates were used in all concrete mixes. Concrete mixes were proportioned by the equivalent mortar volume (EMV) method. In this mixing method, the residual mortar in RCAs is treated as part of the total mortar volume of concrete. The total mortar volume is considered as the sum of the residual and fresh mortar volumes in RCA-concrete. Concrete proportioned based on EMV method was found to have fresh and hardened properties comparable to that of the NA-based concrete. The researchers reported that for the same *a/d* ratio, concrete compressive strength and beam depth, varying aggregate type (RCAs against NAs) had a negligeable effect on the shear strength of the tested beams. No major differences between the failure mode and cracking pattern of RCA- and NA-based beams. The crack width in the RCA-beams was below the maximum crack width limit, despite being slightly larger than that of their NA-based counterparts.

Khergamwala (2016) studied the shear behavior of RC beams without shear reinforcement made with RCAs at replacement percentages of (25 and 50%). The RACs were obtained from laboratory tested concrete cubes that contained well-graded crushed granite stones. The beams had *a/d* of 1.5, 2.5, and 3.5. The target concrete compressive strength was 20 MPa. A constant *w/c* ratio of 0.5 was used. All aggregates were used in SSD condition. The researchers reported comparable shear behavior for NA- and RCA-based concrete beams with 25 and 50% RCA replacement percentages irrespective of the *a/d* value. Short beams with *a/d* < 2.5 failed in a shear compression mode of failure, whereases slender beams with *a/d* ≥ 2.5 failed in a diagonal tension mode of failure.

Ignjatovic et al. (2017) studied the shear behavior of RCA-based beams with *a/d* of 4.2. Test parameters included the RCA replacement percentage (50 and 100%) and shear reinforcement ratio (0, 0.14, and 0.19%).

The origin of RCAs used in this study was from a demolished 40-year-old reinforced concrete frame structure and from laboratory waste concrete samples. In both cases, the properties of the original concrete were unknown. River gravel was used as NAs. Natural sand was used as fine aggregates in all mixes. The design target concrete compressive strength and slump were 40 MPa and 8 mm, respectively. The shear behavior of RCA-based beams with 50 and 100% replacement percentages was similar to that of their NA-based counterparts. The difference between the service load deflection of the beams with and without RCAs was within 10%. First shear cracks in NA- and RCA- based beams without shear reinforcement initiated at the same load. Shear failure modes of RCA-beams without shear reinforcement did not differ from that of the NA-beams. Shear failure modes of beams with shear reinforcement did not depend on the replacement percentage of RCAs. Crack patterns were also similar although in RCA-beams, the formation of series of thinner and shorter cracks between dominant inclined cracks was observed. In the absence of shear reinforcement, the beams made with RACs exhibited a shear strength reduction of 15% relative to that of the beams with NAs. At the same amount of shear reinforcement, the difference in normalized shear strength of the NA- and RCA-based beams was within 5%.

Very limited number of studies focused on examining the behavior of RC beams made of RCAs with web openings. Elmatty et al. (2020) conducted an experimental and numerical investigations to study the shear behavior of simply supported concrete beams made of NAs and RCAs. A total of eight beams with a/h of 2.4 using were tested. Four beams were solid and four beams had a rectangular opening in the center of each shear span. The opening height-to-depth ratio (h_o/h) was 0.4 and the opening width-to-shear span ratio (w_o/a) was 0.33. The RCA replacement percentages were 25, 50, and 100%. No additional reinforcement was used around the openings. Test results showed that the full replacement of NAs by RCAs in the solid

beams reduced the shear capacity by 5% with insignificant change in the deflection capacity. For beams with openings, the full replacement of NAs by RCAs decreased the shear capacity by 13%. The shear strength of RC beams with openings were 22 to 30% lower than those of the solid beams. Three-dimensional non-linear finite element models using ANSYS 1 software were developed. Measured properties of the NA- and RCA-based mixes were used as input data in the analysis. The numerical results were in good agreement with those obtained from the experiments.

Aly et al. (2015) studied the effect of RCA replacement percentage, a/d, and web opening location on the shear behavior of RC deep beams. The RCA replacement percentages considered were 25, 50 and 75%. The a/d considered were 1, 1.5 and 2. The h_0/h was 0.29 and the w_0/a were 0.22, 0.3, and 0.44. Additional horizontal reinforcements were provided above and below the openings. The shear response of the beams with up to 50% of RCAs was comparable or better than that of the beams with NAs. An 8% reduction in the shear capacity was, however, noted for the beams with RCA replacement percentage of 75%. The increase of a/d led to reduction in shear strength. The beam with a web opening far from support recorded higher shear capacity compared to that of the beam in which the opening was in the middle of the shear span.

1.5.2.2 Shear Behavior of RC beams with Steel Fibers

The aim toward wider use of RCAs in construction to promote the concept of sustainability and circular economy led researchers to investigate different methods to improve the performance of RCA-based concrete (Shi et., 2016). The inclusion of steel fibers in RCA-based concrete reduces the development of microcracks and improves different tensile properties of concrete mixtures (Gao et al., 2017; Kachouh et al., 2021). Previous studies provided interesting findings on the shear behavior of steel-fiber-reinforced

NA-based slender and deep RC beams (Dinh et al., 2010; Sahoo & Sharma, 2014; Amin & Foster, 2016; Cucchiara et al., 2004). Steel fibers have a potential to substitute the minimum steel stirrups, partially or fully, which can potentially reduce the congestion of reinforcing bars and operational costs (Cucchiara et al., 2004).

Dinh et al. (2010) conducted experimental research aimed at studying the shear behavior of steel fiber-reinforced concrete beams and the possibility of using steel fibers as minimum shear reinforcement. The RC beams considered in this study had *a/d* of 3.5. The target concrete compressive strength was 45 MPa. The test parameters were the beam depth (455 and 685 mm), fiber length (30 and 60 mm), fiber aspect ratio (55 and 80), fiber strength (1100 and 2300 MPa), and fiber volume fraction (0.75 and 1.5%). The three types of steel fibers considered were hooked at both ends. The tensile longitudinal reinforcement ratios considered were 1.6, 2, and 2.7%. It was concluded that the addition of steel fibers at v_f of 0.75% resulted in a significant increase of 160% in the shear capacity of RC beams with *a/d* of 3.5. Further increase in the steel fiber volume fraction to 1 and 1.5% resulted in a marginal additional improvement in the shear capacity. Hooked steel fibers with a length of 60 mm allowed a greater inclined crack opening before failure compared to that observed in beams with 30 mm long fibers. The length and type of the steel fibers had an insignificant effect on the shear response at $v_f \leq 1\%$. In contrast, at v_f of 1.5%, beams with the longer steel fibers of 60 mm exhibited a higher shear strength than those with fibers at a length of 30 mm.

Sahoo & Sharma (2014) studied the effect of steel fibers on the shear behavior of concrete beams. Test parameters included concrete compressive strength (20 and 25 MPa), percentage of longitudinal reinforcement (0.87, 1.15, 1.95%), steel fiber volume fraction (v_f = 0.75, 1, and 1.25%), amount of

transverse stirrups, and *a/d* (2.3 and 3.45). The steel fibers used were hooked at both ends and had a length of 60 mm, a diameter of 0.75 mm, and a tensile strength of 1100 MPa. The addition of steel fibers in RC beams at v_f of 0.75, 1, and 1.25% increased the normalized shear strength by 5, 6, and 28%, respectively, compared to that of a control specimen without steel fibers. A steel fiber volume fraction of 0.75% was sufficient to achieve a shear strength equal to or higher than that of the beam with traditional steel stirrups.

Amin & Foster (2016) conducted an experimental work to examine the effect of steel fibers on the shear strength of concrete beams having *a/d* of 2.8. Test parameters included the steel fiber volume fraction (0, 0.5, and 1%), diameter of stirrups (6 mm and 10 mm) and spacing of stirrups (300 mm and 450 mm). Steel fibers used were hooked at both ends with a diameter and length of 0.9 mm and 60 mm, respectively. The tensile strength of the steel fibers was 2300 MPa. All beams failed in shear. The addition of 0.5% steel fibers to the beam without stirrups resulted in a shear strength equivalent to that of a beam without steel fibers having minimum shear reinforcement. The addition of steel fibers at v_f of 0.5 and 1% increased the shear strength by 42 and 127%, respectively, compared to that of a similar beam without steel fibers. Beams with steel fibers exhibited a smaller crack width than that of the control beam without fibers. The number of shear cracks increased with an increase in the fiber volume fraction.

Cucchirra et al. (2004) studied the effectiveness of using steel fibers as shear reinforcement in beams with and without stirrups. Test parameters included the steel fiber volume fraction (0, 1 and 2%), *a/d* (2 and 2.8), the presence of stirrups and the spacing of stirrups (200 and 60 mm). The steel fibers were hooked at both ends with a length of 30 mm, a diameter of 0.5 mm, an aspect ratio of 60 and a nominal tensile strength of 1115 MPa. It was concluded that for beams with *a/d* of 2.8, the addition of steel fibers at v_f of 1

and 2% resulted in an increase in shear strength of 138 and 155%, respectively. For beams with a/d of 2, the addition of steel fibers at v_f of 1 and 2% resulted in an increase in shear strength of 132 and 133%, respectively. The researchers concluded that the effectiveness of steel fibers as shear reinforcement was more pronounced for the beams with a/d 2.8.

Juárez et al. (2007) studied the shear behavior of 16 steel fiber-reinforced concrete beams having a/d of 2. The variable parameters included the concrete compressive strength (19 and 37 MPa) and v_f (0.5, 1 and 1.5%). All beams had stirrups with a diameter of 6 mm spaced at 100 mm. The addition of steel fibers at v_f of 1.5% in RC deep beams with f'_c of 37 MPa resulted in a 37% increase in the load at first shear crack, whereas similar beams with f'_c of 19 MPa experienced an increase of 59% in the load at the first shear crack. The addition of steel fibers at v_f of 1.5% in RC deep beams with f'_c of 37 MPa resulted in a shear strength gain of 12% whereas similar beams with f'_c of 19 MPa experienced a shear strength gain of 54%.

Kang et al. (2011) investigated the effect of steel fibers on the shear strength of lightweight concrete beams without web reinforcement. The main parameters included the a/d (2, 3, and 4), v_f (0.5 and 0.75%), and concrete density (normal-weight versus light-weight). A total of 12 beams were tested under four-point bending, including six steel fiber-reinforced lightweight concrete beams, three normal-weight steel fiber-reinforced concrete beams and three lightweight concrete beams without steel fibers. It was concluded that, for lightweight concrete deep beams with a/d of 2 the addition of steel fiber at v_f of 0.5 and 0.75% increased the shear capacity by 16 and 18%, respectively. For lightweight concrete beams with a/d of 3, the respective increases in shear capacity were 1 and 9%. For lightweight concrete beams with a/d of 4 the addition of steel fiber at v_f of 0.5 and 0.75% increased the shear capacity by 37 and 63% respectively. The a/d affected the shear

behavior of the lightweight fiber-reinforced beams to a greater extent than did for the steel fiber normal-weight beams. The average shear stresses at diagonal cracking and at peak load reduced as the *a/d* increased. An improvement in the beams' stiffness was also observed due to the addition of steel fibers.

Ma et al. (2018) conducted an experimental investigation to study the shear behavior of RC deep beams with two types of steel fibers with v_f of up to 2%. The first type consisted of steel fibers with a length of 30 mm and a diameter of 0.55 mm and was considered as long steel fibers. The second type consisted of steel fibers with a length of 13 mm and a diameter of 0.2 mm and was considered as short steel fibers. The deep beams had *a/d* of 0.9. The use of hybrid steel fibers (i.e., a combination of steel fibers with different shapes and geometry) can effectively bridge shear cracks in RC deep beams at both the micro- and macro-scale levels, thus improving the shear strength and deformation capacity. The shear capacity of a concrete deep beam with *a/d* of 0.9 and a hybrid v_f of 2% (1.5% long fibers and 0.5% short fibers) was two times that of a similar beam without fibers. The performance of a deep beam with hybrid steel fibers without internal shear reinforcement outperformed that of a similar beam with internal shear reinforcement.

Recently, Garcia et al. (2021) studied the effect of adding steel fibers at v_f of 1% on the shear behavior of RC deep beams made of sand-lightweight concrete. Six deep beams without transversal reinforcement made with sand-lightweight concrete and six deep beams made with sand-lightweight concrete with 1% steel fibers were tested. The results were compared with those of conventional concrete deep beams with and without steel fibers. The deep beams were tested to failure under four-point bending. The deep beams had *a/h* of 0.5, 0.8, and 1. The cross-section heights were 400, 600, and 700 mm. All beams had the same width of 150 mm. For the same load level, the

sand lightweight deep beams with v_f of 1% had less deflection compared with that of its counterpart without steel fibers. Deep beams with *a/h* of 0.8 and 1 had greater deflections at peak load than that of their counterpart with *a/h* of 0.5. Sand lightweight concrete deep beams failed by diagonal compression, whereas sand lightweight steel fiber-reinforced deep beams failed by diagonal tensile rupture. The beam size effect was more significant in sand lightweight concrete deep beams with *a/h* of 0.8 and 1.0 in comparison to that of the deep beams with *a/h* of 0.5. A shear strength gain of approximately 17% was reported for a deep beam with *a/h* of 0.5 due to the inclusion of steel fibers at v_f of 1%. Beams with *a/h* of 0.8 and 1 exhibited an average shear strength gain of 15%.

Do-Dai et al. (2021) studied the interaction between the amount of steel fibers and stirrup ratio on the shear behavior of RC deep beams. The experimental program was carried out on twelve deep beams with different v_f ranging from 0.4 to 0.85% and stirrup ratios of 0.1, 0.15, and 0.25%. All beams had *a/h* was 1.6. The use of steel fibers in the range of 0.4 to 0.85% increased the shear resistance of RC deep beams by up to a 55%. Beams with steel fibers were stiffer than the control beam. The use of steel fibers also reduced the shear crack width by up to 11 times. Failure modes of the beams without steel fibers were brittle and sudden, while the steel fiber-reinforced beams failed in a more ductile mode at a smaller crack width. The stiffness of the steel fiber-reinforced beams was significantly higher than that of the control beams without steel fibers. For beams with a stirrup ratio of 0.25%, the addition of steel fibers at v_f of 0.4% significantly reduced the ultimate deflection by up to 44%. However, a further increase in v_f did not result in a further reduction in the ultimate deflection. It was noted that the effectiveness of the stirrups in reducing the beam's deflection decreased as the steel fiber amount increased. For the deep beams with v_f of 0.4%, an increase in the stirrup ratio from 0.1 to 0.25% reduced the beam's deflection at service load

by approximately 42%. For the beams with the higher value of v_f of 0.85%, the corresponding reduction was on average 22%. The addition of steel fibers increased the shear cracking load of the tested beams by 17 to 30% in comparison with that of the beams without steel fibers. The researchers concluded that increasing the stirrup ratio in a deep beam having a high steel fiber volume fraction reduced the efficacy of the fibers in improving the beam's shear capacity.

Mansur & Alwist (1984) tested twelve steel fiber-reinforced deep beams with rectangular web openings having h_0/h of 0.19. The values of w_0/a were 0.54, 0.67, and 0.9. The major parameters were the value of v_f 0.5, 1, and 1.5, opening location in the shear span, a/h (0.45, 0.55, and 0.65), and the web reinforcement ratios (0.86 and 0.5%). The steel fibers were hook-ended with a length and diameter of 30 mm and 0.4 mm, respectively. The concrete mix was designed for a 28-day cube compressive strength of 40 MPa. The researchers concluded that for beams with a/h of 0.55, a web steel of 0.86%, and an opening placed in the middle of the shear span the addition of steel fibers at v_f of 0.5, 1 and 1.5% increased the shear strength by 12, 41 and 58%, respectively. At v_f of 1%, a/h of 0.55, and web steel ratio of 0.86% the inclusion of opening in middle of shear span resulted in a decrease in shear capacity by 38% compared to that of the counterpart solid beam. By moving the opening from its central position in the shear span to the top left or bottom right of the center of the shear span (i.e. away from the natural load path), the reduction in the shear strength became in the range of 6 to 17% compared to that of their counterpart solid beams. By moving the opening from its central position in the shear span to the top right or bottom left of the center of the shear span (i.e. crossing the natural load path), the shear strength reduction became in the range of 47% to 55% compared to that of their counterpart solid beams. At v_f of 1%, a/h of 0.55 and inclusion of opening in the center of the shear span, a decrease in web steel ratio from 0.86 to 0.5% resulted in

a decrease in shear strength by 15%. For the same material and geometrical properties, the influence of *a/h* ratio was not evident. The researchers concluded that the amount of web reinforcement, either in the form of discrete steel fibers or as continuous reinforcement, delayed the formation and widening of cracks and improved the shear strength of RC deep beams with openings. Deep beams in which the opening was located away from the natural load path failed in the typical shear failure of a solid deep beam by diagonal cracking along a line joining the loading and reaction points.

Swaddiwudhipong & Shanmugam (1988) conducted an experimental investigation to study the shear behavior of steel fiber-reinforced concrete deep beams with openings. Test variables were the value of v_f (0.5, 1, and 1.5%), opening location in the shear span, and *a/h* (0.45, 0.55, and 0.65). The opening had h_0/h of 0.19 and w_0/a of 0.54, 0.67, and 0.9. The steel fibers were made of cold drawn steel wire with hooks at both ends and with a length and diameter of 30 mm and 0.5 mm, respectively. The researchers concluded that for beams with *a/h* of 0.55 and an opening placed in the middle of the shear span, the addition of steel fibers at v_f of 0.5, 1 and 1.5% increased the shear strength by 18, 69 and 100%, respectively. At v_f of 1% and *a/h* of 0.55, the inclusion of an opening in middle of shear span decreased the shear strength by 53% compared to that of the solid beam. By moving the opening from its central position in the shear span to the top left or bottom right of the center of the shear span (i.e. away from the natural load path), the shear strength reduction became in the range of 17 to 29% compared to that of their counterpart solid beams. By moving the opening from its central position in the shear span to the top right or bottom left of the center of the shear span (i.e. crossing the natural load path), the shear strength reduction became in the range of 54 to 73% compared to that of their counterpart solid beams. The beams with openings failed by diagonal tension, causing a clean and sudden fracture that occurred mainly along a line joining the edge of the support or

loading plates to the corner of the opening. For the solid beam, the fracture was along the natural load path.

Al-Sarraf & Diab (2011) studied the effect of steel fibers on the shear behavior of RC deep beams with and without web openings. The experimental program included testing of six solid deep beams and six deep beams with a square opening placed in the middle of the shear span. The w_0/a considered were 0.33 and 0.38 and the h_0/h was 0.2. The a/d considered were 0.7 and 0.6 (corresponding to a/h 0.61 and 0.53). The values of v_f considered were 0.5 and 1%. For beams having a/d of 0.7, the addition of steel fibers at v_f of 0.5 and 1% increased the shear capacity by 19 and 53%, respectively, compared to that of the concrete beam without steel fibers. For beams having a/d of 0.6, the addition of steel fibers at v_f of 0.5 and 1% increased the shear capacity by 22 and 59% respectively, compared to that of the concrete beam without steel fibers. Decreasing a/d from 0.7 to 0.6 resulted in an insignificant increase in the shear strength of beams with openings. For the beams without steel fibers having a/d of 0.7, creating an opening in the shear span decreased the shear strength by 33% compared to that of the solid beam. Creating openings in deep beams having a/d of 0.7 and v_f of 0.5 and 1% decreased the shear strength by 33 and 40%, respectively, compared to that of solid beams with the same steel fiber volume fraction. For the beams without steel fibers having a/d of 0.6, creating an opening in the shear span decreased the shear strength by 50% compared to that of the solid beam. Creating web openings in deep beams having a/d of 0.6 and v_f of 0.5 and 1% decreased the shear strength by 51 and 40%, respectively, compared to that of solid beams with the same steel fiber volume fraction. Deep beams with web openings became stiffer with the increase in steel fiber volume fraction.

Sahoo et al. (2012) studied the behavior of steel fiber-reinforced concrete deep beams with a/h of 0.97 and large square openings located at

the bottom corner near the support having w_0/a and h_0/h of 0.34 and 0.32, respectively. Steel fibers were added at v_f of 1.5%. The reinforcing bars in two specimens were detailed as per a selected strut-and-tie (STM) model. In other specimens most of the reinforcing bars required by the STM were eliminated and replaced by steel fibers, in which steel bars were used only for longitudinal tensile reinforcement. The researchers concluded that steel fiber-reinforced concrete deep beams with v_f of 1.5% v_f reached a capacity higher than the design load and exhibited significant post-peak residual strength and a ductile mode of failure. The initial stiffness of steel fiber-reinforced specimens was nearly equal to that of the RC beams without steel fibers. The steel fiber-reinforced specimens showed a very gradual post-peak descending branch in the load-displacement response, indicating significant contribution of the steel fibers to the residual strength of the tested beams.

Zewair et al. (2021) studied the effect of three types of steel fibers on the shear behavior of RC deep beams with a/d of 1 and a circular opening placed in the middle of the shear span having w_0/a and h_0/h of 0.31. Three different types of steel fibers were considered in this study: straight, hooked and corrugated. Steel fibers were added at v_f of 1%. The improvements in the shear capacity with respect to that of a reference beam without steel fibers were 29, 20 and 21% due to the addition of 1% of straight, hooked and corrugated steel fibers, respectively. The beams with steel fibers were stiffer than a benchmark beam without steel fibers. The deflections at peak load of all the tested beams were almost equal to a value of 3 mm, except for the beam with corrugated steel fibers where it was 3.8 mm.

1.5.2.3 Shear Behavior of RC beams with Recycled Aggregates and Steel Fibers

To date, little effort has been devoted to investigating the shear behavior of RC beams containing RCAs and steel fibers, despite the

importance of the topic. To the best knowledge of the author, only one study by Chaboki et al. (2019) was available in the literature.

Chaboki et al. (2019) investigated the effect of the addition of steel fibers at v_f of 1 and 2% to improve the shear strength of slender beams with a/h of 2.5 made with 50 and 100% RCAs. The RCAs were obtained from buildings demolition waste. The total effective w/c of the concrete was kept constant at 0.41. In their study, the researchers tested a total of twenty-seven RC beams with different steel fiber content and RCA replacement percentages. In these beams, stirrups were used at spacing values of 10 and 20 cm or not used at all. Three beams were selected as control, without steel fibers and RCAs. The inclusion of steel fibers enhanced the shear behavior of RCA-based concrete beams. In the absence of stirrups, the addition of steel fibers resulted in a significant increase in the shear capacity. Nevertheless, the shear strength gain was less pronounced for beams with traditional transverse reinforcement.

1.5.3 Published Analytical Models
1.5.3.1 Solid Deep Beams

The nominal shear capacity of RC deep beams (V_n) can be expressed by Equation 1.1, where V_c is the concrete contribution to the shear resistance including the dowel action and effect of steel fibers, and V_w is the contribution of the internal web shear reinforcement to the shear capacity. The concrete contribution to the shear capacity, V_{cd}, including the influence of dowel action is affected by the mechanical properties of the concrete, fiber volume fraction (v_f), flexural steel reinforcement ratio (ρ), and the shear span-to-effective depth ratio (a/d). The contribution of the internal web shear reinforcement, V_w, is influenced by the type of steel, area of shear reinforcement bars, and number of shear reinforcing bars intersected by the critical shear crack.

$$V_n = V_{cd} + V_w \qquad\qquad 1.1$$

Narayanan & Darwish (1987) proposed Equation 1.2 for the average concrete shear stress at shear failure (i.e. ultimate shear stress), v_u, which is defined by V_{cd}/bd, where b is the beam width and d is the effective depth of the beam. The magnitude of e in Equation 1.2 depends on a/d; $e = 1$ when $a/d > 2.8$ and $e = 2.8(d/a)$ when $a/d \leq 2.8$ whereas d_f is a bond factor that accounts for the bond characteristics of steel fibers and equals 0.5 for round fibers, 0.75 for crimped fibers, and 1 for indented fibers. The parameter τ is the average fiber matrix interfacial bond stress, 4.15 MPa.

$$v_u = e \left[0.24 f_{sp} + 80\rho \left(\frac{d}{a} \right) \right] + 0.41\tau \left(\frac{l_f v_f d_f}{D_f} \right) \qquad\qquad 1.2$$

Ashour et al. (1992) proposed Equation 1.3 to predict the ultimate shear stress of RC beams with $a/d \geq 2.5$ and Equation 1.4 for beams with $a/d < 2.5$.

For $a/d \geq 2.5$:

$$v_u = \left[2.11 \sqrt[3]{f_c'} + 7 \left(\frac{l_f v_f d_f}{D_f} \right) \right] \left(\rho \frac{d}{a} \right)^{1/3} \qquad\qquad 1.3$$

For $a/d < 2.5$:

$$v_u = \left[2.11 \sqrt[3]{f_c'} + 7 \left(\frac{l_f v_f d_f}{D_f} \right) \right] \left(\rho \frac{d}{a} \right)^{1/3} \left[2.5 \left(\frac{a}{d} \right) \right] + 0.41\tau \left(\frac{l_f v_f d_f}{D_f} \right) \left[2.5 - \left(\frac{a}{d} \right) \right] \quad 1.4$$

Kwak et al. (2002) proposed Equation 1.5 as a modified version of that developed earlier by Narayanan & Darwish (1987) to predict the ultimate shear stress of RC beams. The factor k in Equation 1.5 depends on a/d; $k = 1$ for $a/d > 3.4$ and $k = 3.4(d/a)$ for $a/d \leq 3.4$.

$$v_u = 3.7k\left(f_{sp}\right)^{2/3}\left[\rho\left(\tfrac{d}{a}\right)\right]^{1/3} + 0.8\left[0.41\tau\left(\tfrac{l_f v_f d_f}{D_f}\right)\right] \qquad 1.5$$

The contribution of the internal web shear reinforcement to the shear capacity, V_w, can be expressed by Equation 1.6 proposed by Kong et al. (1977) and adopted by CIRIA guide (1984), where C_s is an empirical coefficient equal to 100 MPa for plain round bars and 225 MPa for deformed bars, h is the beam depth, and A_w is the area of an individual web steel bar, y is the depth of the intersection between the web steel bar and a potential critical shear crack measured from the compression face of the beam, and α is the angle of intersection between the web steel bar and the potential critical shear crack. The potential critical shear crack in solid RC deep beams is typically assumed to be developed in the direction of the natural load path that is the line connecting the inner points of the load and support plates.

$$V_w = C_s \sum \left[\tfrac{A_w y}{h}\right]\sin^2\alpha \qquad 1.6$$

1.5.3.2 Deep Beams with Openings

Structural idealization of reinforced concrete deep beams with openings is shown in Figure 1.2. The shear capacity of steel fiber-reinforced RC deep beams with openings, V_n, can be estimated using Equation 1.7. In this equation, V_c = concrete contribution to the shear capacity, and V_s = contribution of steel bars to the shear resistance, including web reinforcement and dowel action ($V_w + V_d$). The value of V_c is mainly influenced by the mechanical properties of concrete and a/d whereas that of V_s is affected by the properties and location of the steel reinforcing bars crossed by the critical shear crack.
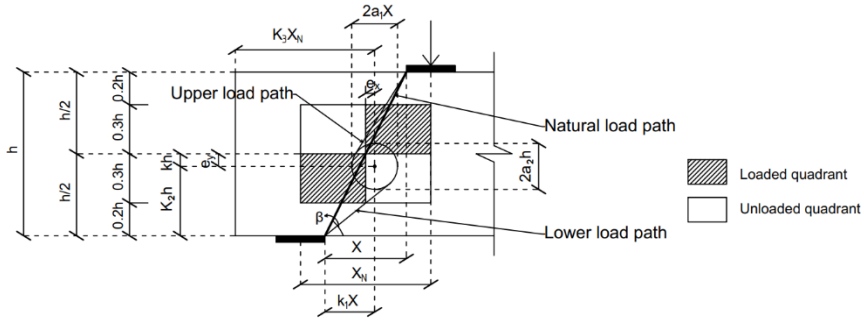
$$V_n = V_c + V_s \qquad 1.7$$

Figure 1.2: Structural idealization of deep beams with openings (Based on Kong & Sharp (1977), Shanmugam & Swaddiwudhipong (1988), and Ray & Reddy (1979))

According to Kong & Sharp (1977), the shear strength of a deep beam is significantly affected only when the opening interrupts the natural load path, which is considered in this study as the line joining edges of the load and support plates. In this model, the applied load is assumed to be transmitted to the support mainly by a lower path and partly by an upper path [Figure 1.2]. Based on this structural idealization, the researchers proposed Equation 1.8 to estimate the nominal shear capacity of RC deep beams with an opening that interrupts the natural load path. In this equation, K_1 and $K_2 =$ coefficients defining the position of opening, a_1 and $a_2 =$ coefficients defining the opening size, $X =$ clear shear span, $f_{sp} =$ cylinder-splitting tensile strength of concrete, $\lambda =$ empirical coefficient, equal to 1.5 for web bars and 1 for main bars, $A_b =$ area of an individual steel reinforcing bar, $y_1 =$ depth at which a typical bar intersects a potential critical diagonal crack (upper and lower load path in Figure 1.2), $\alpha_1 =$ angle of inclination between a typical bar and a potential diagonal crack depending on the failure mode (upper and lower load path in Figure 8), $C_1 = 1.4$ for normal weight concrete, $C_2 = 130$ N/mm^2 for plain round bars and 300 N/mm^2 for deformed bars, $h =$ total depth of the beam, and $b =$ width of the beam.

$$V_n = C_1 \left[1 - 0.35 \frac{(K_1+a_1)X}{(K_2-a_2)h}\right] f_{sp} b(K_2 - a_2)h +$$

$$\sum \lambda C_2 A_b \frac{y_1}{h} \sin^2 \alpha_1 \qquad\qquad 1.8$$

Shanmugam & Swaddiwudhipong (1988) proposed Equation 1.9 as a modified form of Kong and Sharp's (1977) semi-empirical formula for nominal shear strength prediction of steel fiber-reinforced concrete deep beams. Equations 1.10 - 1.12 were utilized to calculate the required components of Equation 1.9, where, $n = 1.1$, $f_1 =$ reduction factor to account for the size of openings, $f_2 =$ reduction factor to account for the degree of interruption of the opening, $k =$ the distance of the center of opening from the beam axis, $r =$ factor depending on the location of the center of opening which is equal to 1 in case the center of opening is located in the unloading quadrants and 2 in case the center of opening is located in the loaded quadrants. The remaining notations are defined in the previous paragraph similarly to the Kong & Sharp Equation 1.8.

$$V_n = C_1 f_1 f_2 \left[1 - 0.35 \frac{X}{h}\right] f_{sp}^n bh + \sum \lambda C_2 A_b \frac{y_1}{h} \sin^2 \alpha_1 \qquad\qquad 1.9$$

$$f_1 = (1 - a_1)\left(1 - \frac{a_2}{0.6}\right) \qquad\qquad 1.10$$

$$f_2 = \ \xi + 2(k_2)^r \sqrt{\frac{(k_1-k_2)^2}{[(a_1 X)^2+(a_2 h)^2]}} \leq 1 \qquad\qquad 1.11$$

$$\xi = 0.6 - 2k \geq 2 \qquad\qquad 1.12$$

Ray & Reddy (1979) proposed Equation 1.13 to predict the nominal shear strength of reinforced concrete deep beams with web openings. The researchers split V_s into two components, V_d to account for the dowel action and V_w to account for the web reinforcement (steel stirrups). In their study, the researchers postulated that the applied load may be assumed to be

transmitted to the supports through the natural load path connecting edges of the load and support plates even if the opening interferes with it. Equations 1.14 - 1.23 were utilized to calculate the required components of Equation 2.13. In these equations, $\psi_s = 0.65$, $\psi_w = 0.5$, A_s = area of tension steel, A_w = area of an individual web steel reinforcing bar, $f_y = 300$ MPa for deformed bars and 130 MPa for smooth bars, f'_c = cylinder compressive strength of the concrete, f_{sp} = cylinder-splitting tensile strength of concrete, b = beam width, h = beam depth, c is a parameter dependent on the concrete compressive strength and tensile splitting strength, λ_1, λ_2 and λ_3 are factors that account for the opening size and location, α = angle of inclination of web bar with horizontal, β = angle of inclination of the natural load path, X = clear shear span, X_N = nominal shear span, a_x = width of the opening, a_y = height of the opening, e_x and e_y = eccentricities of the opening, K_2 and K_3 = coefficients defining the opening location. m is the ratio of path length intercepted to total path length along the natural load path.

$$V_n = V_c + (V_d + V_w) \tag{1.13}$$

$$V_c = \frac{cbh(\lambda_1\lambda_2\lambda_3)}{\sin\beta\cos\beta(\tan\beta+\tan\varphi)} \tag{1.14}$$

$$V_d = (\psi_s A_s f_y)\left[\frac{\tan\beta\tan\varphi-1}{\tan\beta+\tan\varphi}\right] \tag{1.15}$$

$$V_w = \psi_w \sum A_w f_y \left[\frac{\sin\alpha\cot\beta+\cos\alpha}{(\tan\beta+\tan\varphi)/(\tan\beta\tan\varphi)} - \frac{\cos\alpha(1-\tan\alpha\tan\beta)}{\tan\beta+\tan\varphi}\right] \tag{1.16}$$

$$c = \sqrt{\frac{f'_c f_{sp}}{2}} \tag{1.17}$$

$$\tan\varphi = \frac{(f'_c-f_{sp})}{2\sqrt{f'_c f_{sp}}} \tag{1.18}$$

$$\lambda_1 = \begin{cases} 1 - \dfrac{K_3 X_n}{3K_2 h} & for \ K_3 X_N < K_2 h \\ \dfrac{2}{3} & for \ K_3 X_{nN} \geq K_2 h \end{cases} \qquad 1.19$$

$$\lambda_2 = 1 - m \qquad\qquad 1.20$$

$$\lambda_3 = \begin{cases} \left(0.85 + 0.3 \dfrac{e_x}{X_{net}}\right)\left(0.85 + 0.3 \dfrac{e_y}{Y_{net}}\right) \leq 1 & \textit{for center of opening in the unloaded quadrant} \\ \left(0.85 + 0.3 \dfrac{e_x}{X_{net}}\right)\left(0.85 - 0.3 \dfrac{e_y}{Y_{net}}\right) \leq 1 & \textit{for center of opening in the loaded quadrant} \end{cases}$$

$$1.21$$

$$X_{net} = X_n - a_x \qquad\qquad 1.22$$

$$Y_{net} = 0.6h - a_y \qquad\qquad 1.23$$

1.6 Research Significance

Utilizing recycled materials reduces the demand for natural resources and promotes environmental sustainability in the construction industry. However, the widespread use of RCAs in the construction industry is hindered by the lack of knowledge and contradicting information published in the literature on the structural behavior of RCA-based concrete members. The inclusion of steel fibers in RCA-based concrete structures would improve the structural performance, which would advocate for a wider acceptance of RCA for structural use, thus, supporting the concept of circular economy and sustainability. To date, no information is available in the literature on the shear behavior of steel fiber-reinforced RCA-based concrete deep beams (i.e. beams with $a/h \leq 2$). The shear response of RC deep beams made with 100% RCAs having steel fibers and web openings has received little attention. This research aims to fill this gap through a material characterization, numerical simulation, and laboratory testing of full-scale RC deep beams. New characterization test data were produced. New tensile softening laws necessary for numerical simulation of large-scale concrete elements were

developed. Numerical simulation models for large-scale deep beams made with RCAs and steel fibers were generated. A comparative analysis between numerical and experimental results was conducted to verify the accuracy and validity of the deep beam simulation models. The widespread use of RCA-based concrete in structural application would lead to more sustainable buildings and promote the concept of circular economy.

Chapter 2

Chapter 2: General Discussion

2.1 Research Design

The methodology adopted in the current study to achieve the research objectives is summarized in Figure 2.1. The main aim of this research is to examine the shear behavior of deep beams with and without web openings made with RCAs and steel fibers through finite element (FE) analysis and experimental validation. Characterization tests were conducted to determine key material properties and develop tensile softening laws to be used as input data in the analysis. The numerical deep models were made with a 100% RCAs to get the advantage of full replacement of NAs with RCAs to promote sustainability. Steel fiber were added to the RCA-based deep beams at v_f of 1, 2, and 3%. Predictions of the numerical deep beam models were validated through a comparative analysis with results obtained from laboratory tests. A numerical parametric study was conducted to investigate the effect of varying a/h, v_f, and presence of a web opening on the shear response. Details of the research design and methodology are presented in this section.
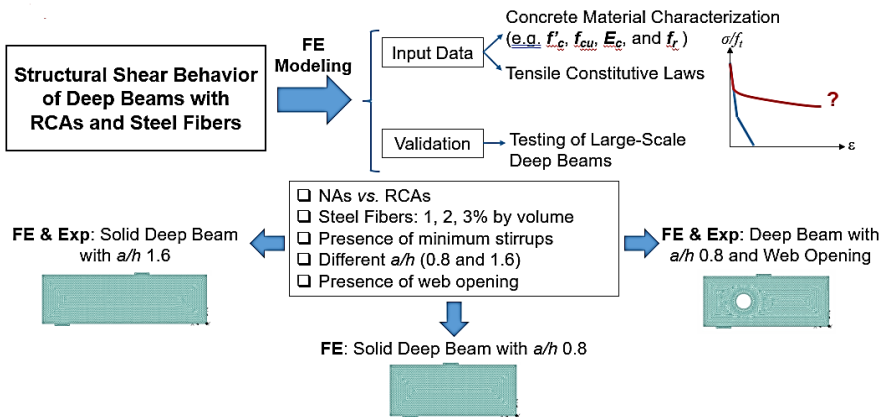

Figure 2.1: Overview on the Research Design

2.1.1 Material Characterization

A total of thirteen mixes were designed and prepared. The variables considered in the material characterization phase included: RCA replacement percentage (30, 70, and 100%) and v_f(1, 2, and 3%). An RCA replacement of less than 30% would not have a significant impact on sustainability. A 100% RCA replacement would maximize the contribution to sustainability but might require high amount of fibers for performance improvement. The 70% RCA replacement percentage is considered a medium level of replacement that would have a balance between sustainability and fiber content. A steel fiber volume fraction less than 1% would not have a significant impact on improving the performance of concrete made with RCAs. A steel fiber volume fraction higher than 3% would significantly reduce the concrete workability, result in agglomeration of steel fibers, and hence, may not be considered as a practical solution. The material characterization results were compared to a benchmark concrete mixture made with NAs without steel fibers. It should be noted that examination of the chemical composition of the steel fibers, homogeneity of steel fiber distribution within the concrete mixture, bridging effect of steel fibers, and intensity of concrete porosity is out of the scope of this research work.

2.1.1.1 Materials

The binder used in the concrete mixtures was the ASTM Type I ordinary Portland cement (OPC). Locally-abundant desert dune sand was employed as a sustainable fine aggregate in all mixes. The gradation curves of cement and dune sand are shown in Figure 2.2. The coarse aggregates included NAs and RCAs. The NAs were crushed dolomitic limestone with a nominal maximum particle size (NMS) of 19 mm obtained from the Emirate of Ras Al Khaimah, United Arab Emirates (UAE). The RCAs were collected from a local concrete recycling plant, located in the Emirate of Abu Dhabi,

with an NMS of 25 mm. The concrete recycling plant crushes old concrete structures with an unknown compressive strength. It is worth noting that the plant did not perform any chemical treatment to the obtained RCAs. The particle size distribution of different mixes/blends of NAs and RCAs used in this study are shown in Figure 2.3. All grading curves were within the upper and lower limit bounds specified by ASTM C33 (2016). Table 2.1 summarizes the physical properties of fine and coarse aggregates. Compared to NAs, RCAs had lower bulk density, higher water absorption, higher LA abrasion mass loss, lower specific gravity, and higher fineness modulus. Properties of RCAs were within the acceptable limits except for the water absorption, which was higher (ASTM C88, 2013; ACI Committee E-701, 2016; Hossain et al., 2007; ASTM C131, 2014).
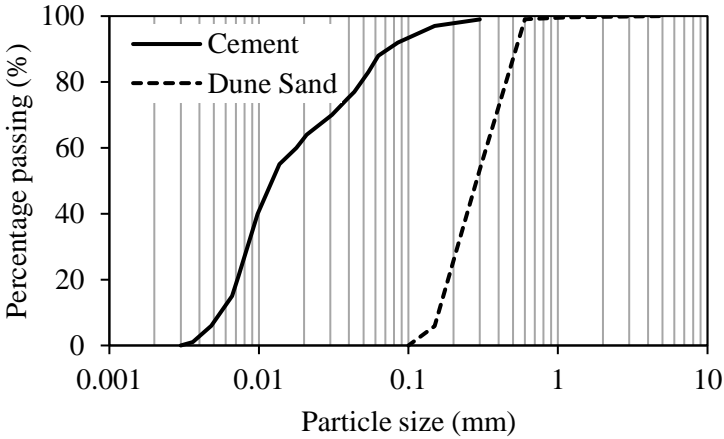

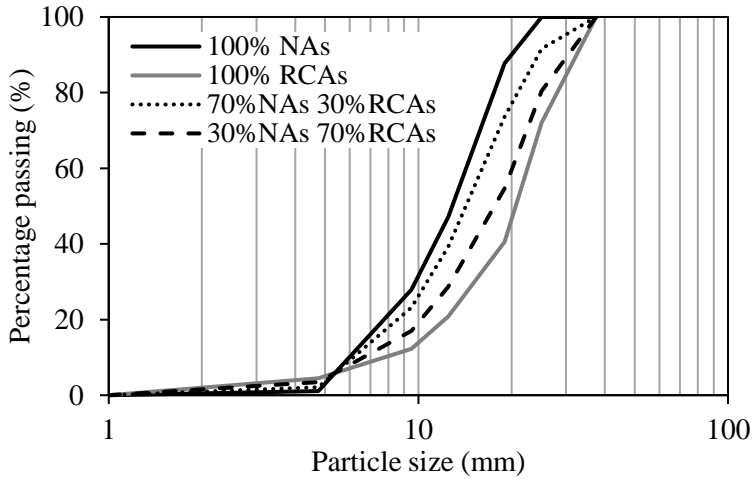Figure 2.2: Particle size distribution of cement and dune sand

Figure 2.3: Particle size distribution of different mixes of NAs and RCAs

Table 2.1: Physical properties of fine and coarse aggregates

Property	Unit	Standard Test	NAs	RCAs	Dune Sand
Dry-rodded density	kg/m^3	ASTM C29	1635	1563	1663
Absorption	%	ASTM C127	0.62	6.63	-
Los Angeles abrasion	%	ASTM C131	16.0	32.6	-
Surface area	cm^2/g	ASTM C136	2.49	2.50	116.8
Soundness (MgSO$_4$)	%	ASTM C88	1.20	2.78	-
Specific gravity	-	ASTM C127	2.82	2.63	2.77
Fineness modulus	-	ASTM C136	6.82	7.44	1.45

Dramix® 3D 65/35BG double hooked-end steel fibers, supplied by Bekaert, Dubai, UAE, were used in the current study. Double hooked-end steel fibers were selected due to their ability to provide better bond with concrete than straight steel fibers (Cunha, 2010). They are low carbon-cold drawn round steel fibers with a tensile strength of 1345 N/mm^2, Young's modulus of 210 GPa, mean diameter (D_f) of 0.55 mm, mean length (l_f) of 35 mm, and an aspect ratio (l_f/D_f) of 65 (Dramix, 2012). Dramix® conforms to ASTM A820 (2011), EN 14889-1 (2006), and ISO 13270 Class A (2013). Figure 2.4 shows a photograph of the steel fibers used in the present study. It

should be noted that the manufacturer does not recommend a maximum dosage of steel fibers in concrete mixtures. Generally, the maximum dosage of steel fibers depends on the concrete composition, placing method, and type of application. In the present study, trial mixes were carried out prior to casting of the beams to ensure adequate workability of the concrete and a homogeneous distribution of the steel fibers within the concrete mixture. Segregation, bleeding, and agglomeration of steel fibers were not observed in any of the mixtures. Similarly, preliminary trial mixes and tests should be done in practical setting to evaluate fresh and hardened properties of designed steel fiber-reinforced concrete mixtures with different dosages of steel fibers before adopting a particular mix design in construction projects.

Figure 2.4: Steel fibers used in this research

2.1.1.2 Mixture Proportioning

The proportions of all concrete mixtures employed in the current research are given in Table 2.2. The concrete mix design method of ACI 211.1 (2009) was first employed to develop a control NA-based concrete mixture with a design cylinder compressive strength (f'_c) of 30 MPa. The cement, dune sand, and water contents were kept constant in all mixtures at 470, 570, and 230 kg, respectively. Due to the slight variation in the specific

gravity of the RCAs compared to that of the NAs, in addition to the inclusion of steel fibers in some mixes, the corresponding volumes of the mixes containing RCAs/steel fibers slightly changed. This difference in volume was trivial and negligible, as shown in the last column of Table 2.2. Mixes were labeled as RX-SFY, where 'X' denoted the percentage of RCAs, relative to total amount of coarse aggregate, and 'Y' represented the steel fiber volume fraction (v_f). For instance, the control mix without RCAs and steel fibers is designated by R0-SF0. The RCA replacement percentage (RCA, %) was taken as 0%, 30%, 70%, 100%, while steel fiber volume fraction percentage (v_f, %) was altered between 0, 1, 2 and 3%.

Table 2.2: Mix proportions of different concrete mixes

| Mix Designation | Mass (kg) | | | | | | | Volume (m³) |
	Cement	RCA	NA	Dune Sand	Water	Steel Fibers	Total	
R0-SF0	470	0	1130	570	230	0	2400	1.00
R30-SF0	470	339	791	570	230	0	2400	1.01
R70-SF0	470	791	339	570	230	0	2400	1.02
R100-SF0	470	1130	0	570	230	0	2400	1.03
R30-SF1	470	339	791	570	230	78	2478	1.02
R70-SF1	470	791	339	570	230	78	2478	1.03
R100-SF1	470	1130	0	570	230	78	2478	1.04
R30SF2	470	339	791	570	230	156	2556	1.03
R70SF2	470	791	339	570	230	156	2556	1.04
R100SF2	470	1130	0	570	230	156	2556	1.05
R30-SF3	470	339	791	570	230	234	2634	1.04
R70-SF3	470	791	339	570	230	234	2634	1.05
R100-SF3	470	1130	0	570	230	234	2634	1.06

2.1.2 Details of Deep Beams

2.1.2.1 Test Matrix

The experimental program of the deep beam specimens testing is summarized in Table 2.3. Fourteen RC deep beam specimens were tested

under four-point loading. The large-scale deep beam specimens were divided into two groups S and N. Group S included seven solid RC deep beam specimens having *a/h* of 1.6. The beams in this group are designated using the notation SRX-SFY. The group N included seven RC deep beam specimens with *a/h* of 0.8 and web openings in their shear spans. The beams in this group are designated using the notation NRX-SFY. In the deep beam specimen notations, 'SRX' stands for solid deep beams with 'X' RCA replacement percentage, 'NRX' stands for deep beams with openings and with 'X' RCA replacement percentage and 'Y' is the steel fiber volume fraction (v_f). The notation SRX-SFY-S and NRX-SFY-S designate beams with internal shear reinforcement. In each group, two beams were made of NAs without steel fibers. One of them included minimum conventional steel stirrups while the other one was kept with neither steel stirrups nor steel fibers. The remaining five beams in each group were made of 100% RCAs. Out of these five beams, one beam had neither steel stirrups nor steel fibers, one beam had minimum conventional steel stirrups, and three beams contained steel fibers at v_f of 1, 2, and 3%.

Table 2.3: Test matrix of the deep beam specimens

Group	Specimen Designation	*a/h*	RCA (%)	v_f (%)	Presence of Traditional Shear Reinforcement	Presence of Openings
S	SR0-SF0	1.6	-	-	-	-
	SR0-SF0-S	1.6	-	-	√	-
	SR100-SF0	1.6	100	-	-	-
	SR100-SF0-S	1.6	100	-	√	-
	SR100-SF1	1.6	100	1	-	-
	SR100-SF2	1.6	100	2	-	-
	SR100-SF3	1.6	100	3	-	-
N	NR0-SF0	0.8	-	-	-	√
	NR0-SF0-S	0.8	-	-	√	√
	NR100-SF0	0.8	100	-	-	√
	NR100-SF0-S	0.8	100	-	√	√
	NR100-SF1	0.8	100	1	-	√
	NR100-SF2	0.8	100	2	-	√
	NR100-SF3	0.8	100	3	-	√

2.1.2.2 Test Specimens

Figure 2.5(a) and Figure 2.5(b) show the concrete dimensions and details of reinforcement of deep beam specimens in group S, with and without traditional shear reinforcement, respectively. Figure 2.6(a) and Figure 2.6(b) show the concrete dimensions and details of reinforcement of deep beam specimens in group N, with and without traditional shear reinforcement, respectively. In the deep beam specimens of group N, two circular openings, one in each shear span, were placed symmetrically about the midpoint of the beam to fully interrupt the natural load path as shown in Figure 2.6. The center of each opening was located at the mid-height of the beam (250 mm below the top surface) and at the middle of the shear span (200 mm away from the center of the support). This was done to induce an extreme discontinuity in the shear span. The openings had a diameter of 150 mm which corresponded to an opening height-to-depth ratio (h_0/h) of 0.3. All deep beam specimens in groups S and N had a width of 150 mm and a depth of 500 mm. The beams in group S had a length of 3300 mm and an effective span of 2900 mm. A distance of 200 mm from each side of the beam was left free to provide a sufficient development length for the longitudinal steel reinforcement. The *a/h* was 1.6, resulting in a shear span of 800 mm and a constant moment region of 1300 mm. The beams in group N had a length of 2500 mm and an effective span of 2100 mm. Accordingly, the value of *a/h* was 0.8, resulting in a shear span of 400 mm and a constant moment region of 1300 mm.

The beams were reinforced with four No. 25 (25 mm in diameter) longitudinal steel reinforcing bars at the tension side and two No. 25 (25 mm in diameter) at the compression side. Based on testing of three replicate steel samples, the average measured yield strength of the No. 25 was 539 MPa, whereas the ultimate tensile strength was 649 MPa. The elastic modulus of

the reinforcing steel bars was 200 GPa. The concrete cover to the center of the steel reinforcement was 50 mm, rendering an effective depth (d) of 450 mm. This arrangement of steel reinforcement was decided to ensure that a shear mode of failure would dominate. The traditional shear reinforcement, when employed, was detailed in accordance with the minimum shear reinforcement provisions of ACI 318-14 (2014) for deep beams, resulting in two curtains of No.5 (5 mm in diameter) plain steel bars spaced at 80 mm in both vertical and horizontal directions. Based on testing of three replicate steel samples, the average measured yield strength of the No. 5 was 505 MPa, whereas the ultimate tensile strength was 543 MPa. Steel plates (150 mm x 150 mm x 20 mm) were placed at the load and support points.
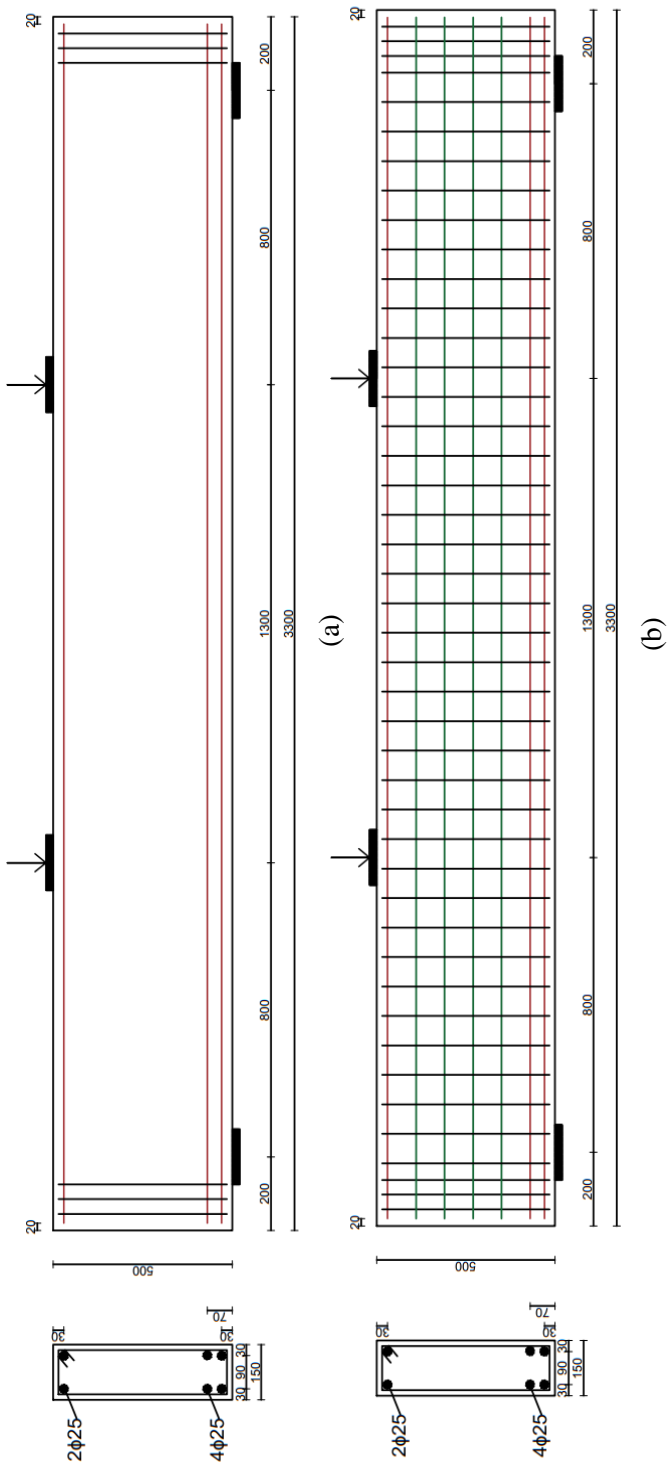
Figure 2.5: Details of deep beam specimens of group S (dimensions are in mm): (a) A beam without traditional shear reinforcement; (b) A beam with traditional shear reinforcement
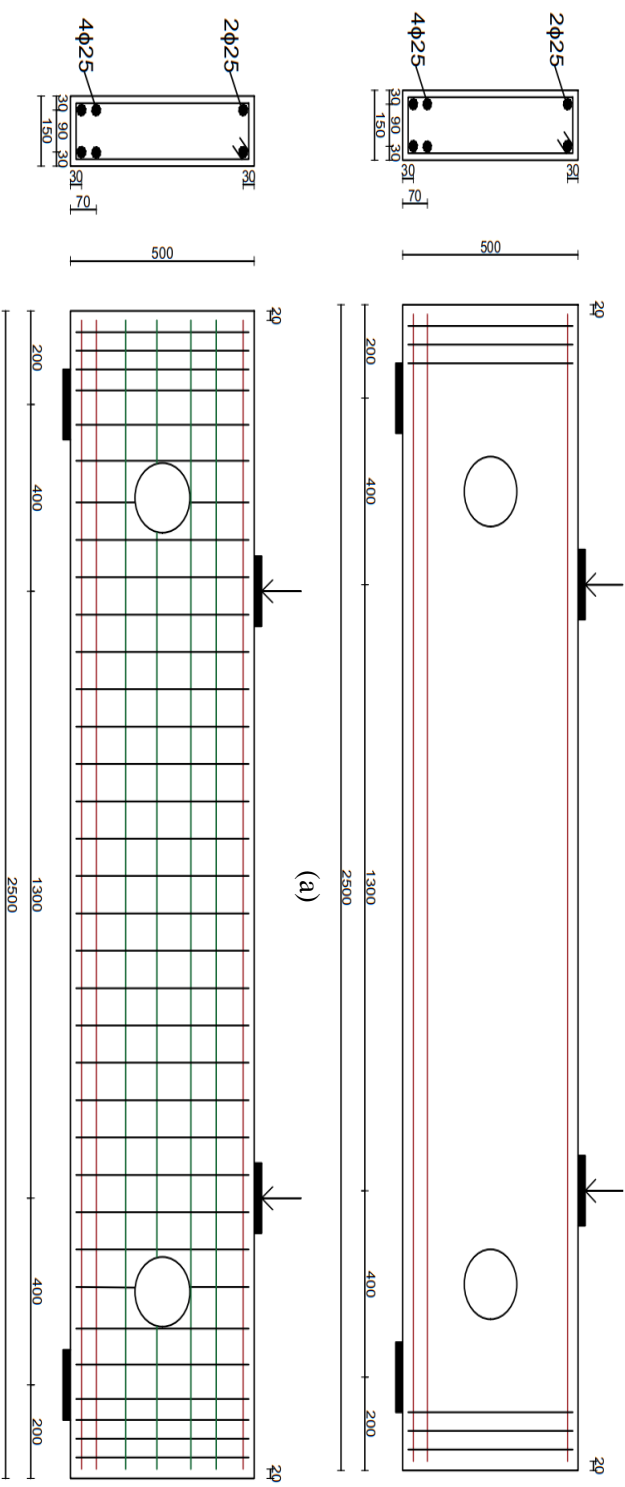
Figure 26: Details of deep beam specimens of group N (dimensions are in mm): (a) A beam without traditional shear reinforcement; (b) A beam with traditional shear reinforcement

2.1.3 Numerical Simulation

Fourteen three-dimensional (3D) FE models were developed to simulate the shear behavior of the tested large-scale RC deep beams using the FE software ATENA 3D (ATENA). The models employed realistic tensile and compressive constitutive laws that account for the nonlinear behavior of the concrete material. A quarter FE model was built for each beam to take advantage of the planes of symmetry and reduce the overall computational time. Monitoring points were added to the FE models to obtain values of the applied load, midspan deflection, and steel strains. Figure 2.9 (b) and Figure 2.10 (b) illustrate the locations of the monitoring points of a typical FE model for deep beams with stirrups from groups S and N, respectively.

2.1.3.1 Material Constitutive Laws

Although ATENA 3D software has built-in constitutive laws for conventional concrete, such laws are not available for concrete made with RCAs and steel fibers. These constitutive laws are developed by the users based on material characterization test data. The *CC3DnonLinCementitious2User* concrete material model was adopted in this investigation to simulate the concrete material by employing realistic tensile and compressive constitutive laws that account for the nonlinear behavior of material (ATENA). This concrete material model provides the users an option to edit and modify key values of the concrete material constitutive law such as the tensile softening behavior that describes the post-peak tensile strength of concrete which is crucial in the case of steel fiber-reinforced concrete. In case the input parameters are not known, the software automatically generates the parameters using default formulas based on the CEB FIP Model Code 90 (1993). In such case, the concrete cube compressive strength is the only parameter needed to be specified and the remaining parameters are generated by the software using built-in equations function of the concrete cube

compressive strength. The adopted concrete model combines constitutive models for tensile (fracturing) and compressive (plastic) behavior. The model employs Rankine failure criterion and exponential softening. The fracture model is based on the classical orthotropic smeared crack formulation and crack band model. The default crack model used in this concrete model is the fixed crack model. The hardening/softening plasticity model is based on Menétrey-Willam failure surface (ATENA). In this study, the input material parameters were based on results of concrete characterization tests. The basic input material parameters needed were the f_{cu}, f'_c, E_c, and f_t taken as $0.6f_r$ (Nilson et al., 2009).

A linear relationship characterizes the compressive stress-strain relation of the concrete material in the elastic phase with a slope equal to E_c. The pre-peak compressive stress-strain relationship is multilinear with the first change in slope starting at a corresponding stress of $0.25f'_c$. A second change in slope occurs at a corresponding stress of $0.8f'_c$. The plastic concrete strain at compressive strength (ε_{cp}) is generated by the software based on the cube concrete strength. The post-peak compressive stress-strain law is linearly descending and ends at the plastic concrete strain at zero stress (ε_d) generated by the software based on the given cube compressive strength. For steel-fiber reinforced concrete, the software manual recommends adopting a value of $\kappa\varepsilon_d$ for the concrete plastic strain at zero stress, where κ is a magnification factor equal to 100 (ATENA). It should be noted that adopting a magnification factor of 50 rather than 100 had no effect on numerical results, whereas deactivating the magnification factor reduced the shear capacity by less than 4%. Figure 2.7(a) shows the compressive hardening-softening law of the concrete. The tensile stress-strain response of concrete is characterized by an ascending branch followed by a multilinear softening response. The ascending branch of the stress-strain response of the concrete

in tension is characterized by a linear relationship in the pre-peak stage with a slope equal to E_c followed by a multilinear softening response. Figure 2.7(b) shows the tensile softening law of the concrete. As shown in Figure 2.7(b), plain concrete is characterized by a very negligible bilinear tensile post-peak response. The post-peak response of plain concrete is linearly descending to a stress value of $0.25f_t$ and then it continues to further decrease at a smaller slope (flatter slope) until it reaches the maximum plastic fracture strain (ε_{cfmax}) corresponding to a zero-stress value. After the stress value of $0.25f_t$, there is an option to account for tension stiffening effect for heavily reinforced concrete in ATENA software by keeping a constant stress value of $0.25f_t$ (Corresponding to a value of $C_{ts} = 0.25$ in the default concrete model). However, steel fiber-reinforced concrete is characterized by a significant post-peak residual tensile stress-strain response. The post-peak response of steel fiber-reinforced concrete is linearly descending to a stress value of $C_{sf}f_t$, where C_{sf} is a coefficient determined from inverse analysis, and then the response continues to decrease (linearly or multilinearly) until it reaches a maximum plastic fracture strain of ε_{cfmax} determined from inverse analysis.
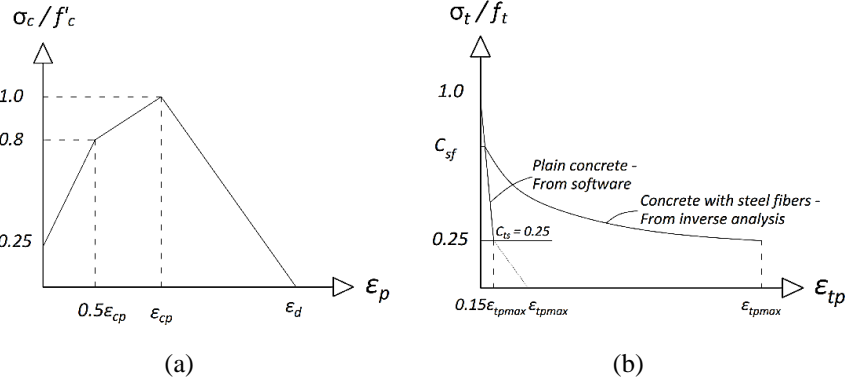

Figure 2.7: User concrete material model: (a) compressive hardening-softening behavior; (b) tensile softening behavior.

The concrete material model considers a reduction in compressive and shear strengths due to cracks. The default functions of the reduction factors are generated by the software. However, for concrete mixtures with steel fibers the compressive strength reduction function was deactivated by adjusting the function to a constant value of 1 as recommended by the software manual (ATENA). Steel Stress-Strain Response - The reinforcing steel bars were modeled using a bilinear stress-strain relationship with a post-yield strain hardening. The stress increases with strain linearly at a slope equal to the Young's modulus of steel (E_s) until yielding. The post-yield modulus (E_{sp}) was assumed as 1% of E_s (pre-yield modulus). The steel plates at the support and loading points were modeled using a linear-elastic behavior.

2.1.3.2 Element Types

The concrete beam and steel plates were modeled as solid 3D macro-elements. Openings were then generated in the desired beam models. The steel reinforcements were modeled as one-dimensional discrete elements with 2 nodes embedded in the concrete macro-element as shown in Figure 2.8 (a). A perfect bond was assumed between concrete and steel bars. ATENA software recommends having a minimum of 4–6 elements in the shortest dimension of the member to warrant solution convergence while minimizing the computational time (ATENA). The smallest possible mesh size of 15 mm was used in the analysis based on a conducted mesh sensitivity analysis (Kachouh et al., 2020). In ATENA software, only prismatic macro-elements can be meshed using brick elements. Any irregularities, such as circular openings can prevent the execution of brick meshes. In that case, tetrahedron mesh or mixed mesh could be considered (ATENA). In this research, 3D solid tetrahedral elements with 4 nodes were used to model all the deep beams as shown in Figure 2.8 (b). Figure 2.9 (a) and Figure 2.10 (a)

show the beam geometry and mesh configuration of a typical FE model of a deep beam of Group S and N, respectively. Figure 2.9 (b) and Figure 2.10 (b) show the Reinforcement details of a typical FE model of a deep beam of Group S and N, respectively.
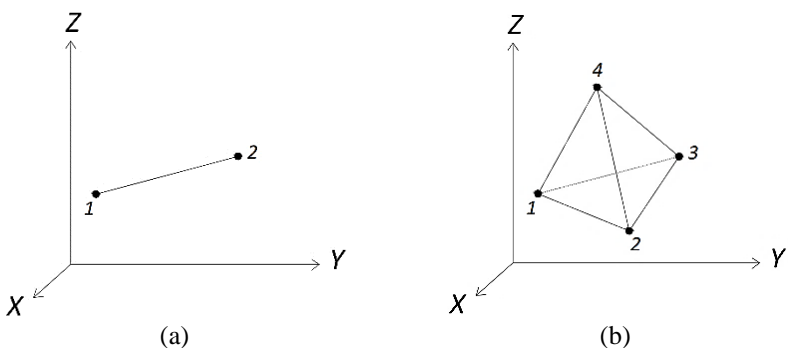

Figure 2.8: Element types: (a) Steel reinforcements, (b) Concrete beams

2.1.3.3 Boundary Conditions and Loading

The top and bottom steel plates were connected to the beam through fixed contacts. A restriction of vertical and transverse displacements was applied on the supporting plates by means of a line support placed at the middle of the bottom surface of the plate. A displacement-controlled applied load was induced at the middle of the top steel plate at a rate of 0.1 mm per step. In the analysis, the standard Newton-Raphson iterative solution method implemented in ATENA was adopted. The iteration had to satisfy a tolerance limit of convergence criteria. The default convergence tolerance criteria used in ATENA was 1%. The surfaces of the planes of symmetry were restrained from movement in a direction perpendicular to the other symmetrical part of the beam through surface supports. Figure 2.9 (a) and Figure 2.10 (a) show the boundary conditions a typical FE model of a deep beam of Group S and N, respectively.
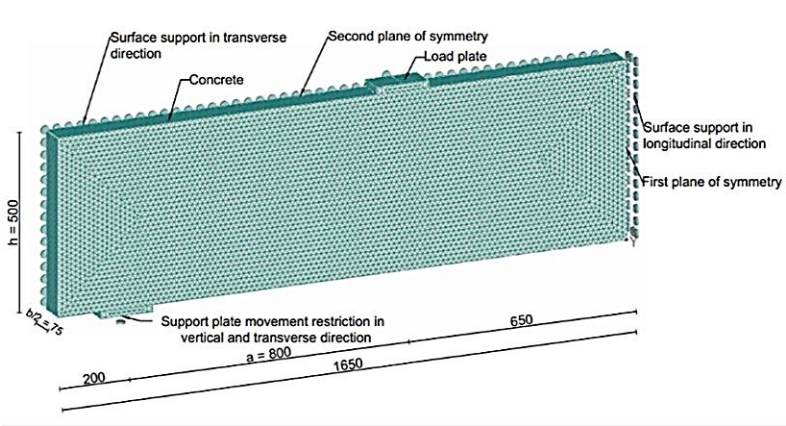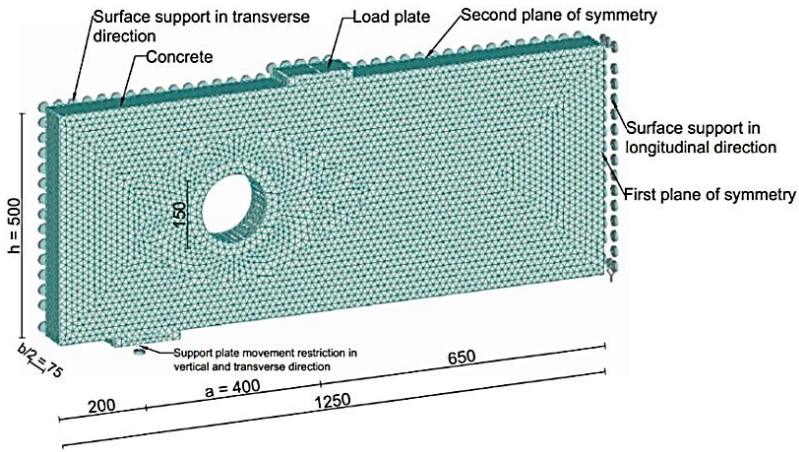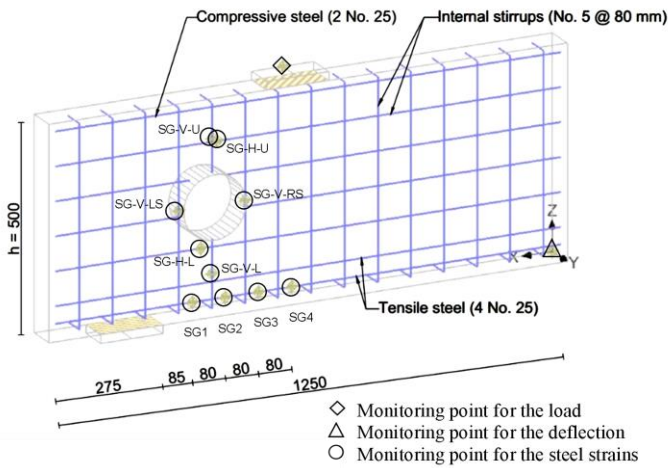
(a)
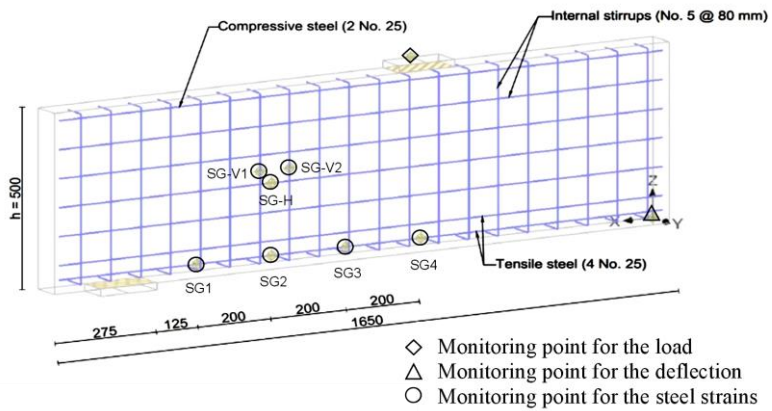
(b)

Figure 2.9: A typical deep beam model of group S (dimensions are in mm):
(a) Beam geometry configuration and boundary conditions; (b)
Reinforcement details and monitoring points

(a)

(b)

Figure 2.10: A typical deep beam model of group N (dimensions are in mm): (a) Beam geometry configuration and boundary conditions; (b) Reinforcement details and monitoring points

2.2 Data Collection

2.2.1 Sample Preparation

Mixing, casting, placing, consolidation, and curing was performed in accordance with the guidelines of ASTM C192 (2015). Concrete mixture constituents were mixed in a laboratory mechanical mixer. The steel fibers

were placed in warm water for few minutes until they become separated. The quantity of water needed in the mix design was based on using the aggregates in a saturated surface dry (SSD) condition. To account for the water absorption capacity of the NAs and RCAs, the dry aggregates were first placed into the mixer. The amount of water needed for the aggregates to reach the SSD condition was then added and mixed with the coarse aggregates for 3 minutes. The steel fibers, if existed, were then mixed with the coarse aggregates to ensure a uniform dispersion of fibers. The cement and dune sand were then added at a later stage and mixed for another 2 min. Finally, the amount of free water, per the mix design, was gradually added and mixed with other components for an additional 2 min. This mixing procedure ensured a homogenous and uniform mixture. Fresh concrete samples were cast in two layers and compact-formed using a vibrating table for up to 10 seconds to ensure proper consolidation, as per ASTM C192 (2015). Specimens were then covered with plastic sheets, demolded after 24 hours, and cured in a water tank at $23 \pm 2°C$ until time of testing. Three replicate specimens were prepared for each material characterization test.

2.2.2 Testing Procedure
2.2.2.1 Material Characterization Tests

Material characterization tests were carried out on more than 300 specimens including: 100 mm cubes, 100 x 200 mm cylinders (diameter and height), 100 mm x 100 mm x 500 mm (width x height x length) prisms, 150 x 300 mm cylinders (diameter and height), 150 x 150 mm cylinders (diameter and height) and 100 x 50 mm discs (diameter and thickness). Table 2.4 summarizes the experimental tests conducted for material characterization along with the corresponding standards.

Table 2.4: Material characterization tests

	Property	Standard Test	Specimen Size (mm)
Fresh Properties	Fresh concrete density	ASTM C138 (2017)	Fresh concrete
	Slump	ASTM C143 (2015)	Fresh concrete
	Compacting factor	BS EN 12350-4 (2009)	Fresh concrete
	Vebe consistency	ASTM C1170 (2008)	Fresh concrete
Mechanical Properties	Hardened concrete density	ASTM C642 (2013)	Cylinder: 100 x 200
	Cubical compressive strength	BS 12390-3 (2009)	Cube:100
	Cylindrical compressive strength	ASTM C39 (2015)	Cylinder: 100 x 200 and 150 x 300
	Modulus of elasticity	ASTM C469 (2014)	Cylinder: 100 x 200
	Splitting tensile strength	ASTM C496 (2017)	Cylinder: 150 x 300
	Uniaxial tensile strength	RILEM TC 162-TDF (2001)	Notched cylinder: 150 x 150
	Four-point bending test	ASTM C1609 (2012)	Prism: 100 x 100 x 500
	Three-point bending test	RILEM TC 162-TDF (2002)	Notched prism: 100 x 100 x 500
Durability Properties	Water Absorption	ASTM C642 (2013)	Disc: 100 x 50
	Capillary Sorptivity	ASTM C1585 (2013)	Disc: 100 x 50
	Ultrasonic pulse velocity	ASTM C597 (2016)	Cube:100
	Abrasion resistance	ASTM C1747 (2013)	Disc: 100 x 50
	Bulk resistivity	ASTM C1760 (2012)	Cylinder: 150 x 300

Fresh concrete properties included slump, compacting factor, vebe consistency, and fresh concrete density. Figure 2.11 shows a schematic representation of the four-point bending test used to determine the modulus of rupture and to examine the post-cracking behavior. Figure 2.12 shows a schematic representation of the three-point bending test conducted on notched prism used to examine the effect of different parameters on the fracture energy. The notched three-point-bending test conducted in this study was suggested by RILEM (2002) and it has been adopted by the fib Model Code (2010) with referral to European Standard (2005). Figure 2.13 shows the test setup of the direct uniaxial tension test used to examine the post-cracking uniaxial tensile strength. Figure 2.14 shows the test setup for the splitting tensile strength test used to determine the indirect splitting tensile strength. Durability properties included water absorption calculated using Equation 2.1, capillary sorptivity calculated using Equation 2.2 to determine the rate of water absorption up to a maximum of 6 hours, ultrasonic pulse velocity, abrasion resistance, and bulk resistivity calculated using Equation 2.3 for plain concrete mixtures without steel fibers only because the presence of steel fibers or other embedded electrically conductive materials may yield unrepresentative bulk resistivity results.

$$\text{Water absorption (\%)} = \frac{\text{SSD mass (g)-Oven-dry mass (g)}}{\text{Oven-dry mass (g)}} \times 100\% \qquad 2.1$$

$$\text{Absorption, } I \text{ (mm)} = \frac{\text{Change in mass at time t (g)}}{\text{Exposed area (mm}^2\text{) x Density of water (g/mm}^3\text{)}} \qquad 2.2$$

$$\text{Bulk Resistivity (k}\Omega.\text{cm)} = \frac{\text{Applied voltage (V) x (Avg. sample diameter (mm))}^2}{1273.2 \text{ x Current at 1 minute (mA) x Avg. sample length (mm)}}$$

$$2.3$$
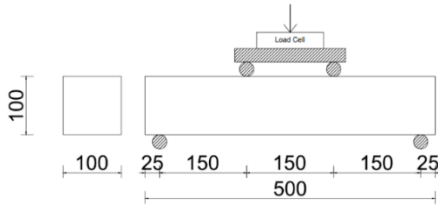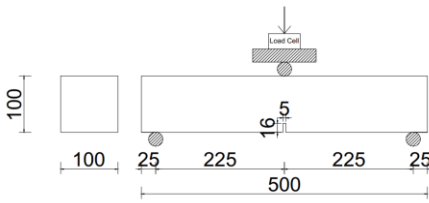
Figure 2.11: Four-point bending test: (a) Schematic representation (dimensions are in mm); (b) Test Picture
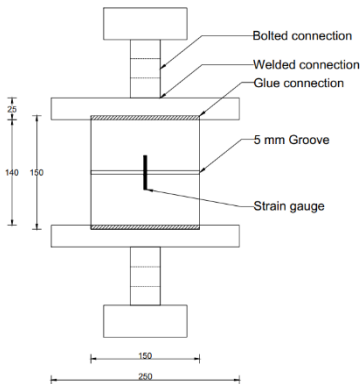

Figure 2.12: Three-point bending test: (a) Schematic representation (dimensions are in mm); (b) Test Picture

Figure 2.13: Uniaxial tensile test: (a) Schematic representation of the experimental test setup (dimensions are in mm); (b) Test in progress
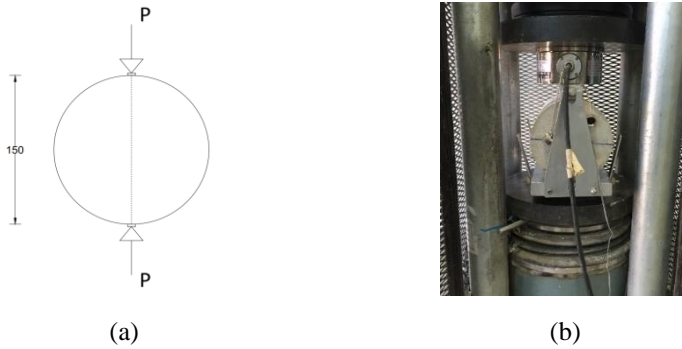
Figure 2.14: Splitting tensile test: (a) Schematic representation of the experimental test setup (dimension is in mm); (b) Test in progress

2.2.3 Tension Function of Concrete with Steel Fibers

The post-cracking residual tensile strength identified as the post-peak stress-strain (σ-ε) relationship in tension is essential for modelling steel fiber-reinforced concrete members in any finite element software. Flexural tests on prisms following the ASTM C1609 (2012) standards along with an inverse FE analysis were employed to develop tensile softening constitutive laws for concrete made with RCAs and steel fibers. Furthermore, uniaxial tension tests were performed following the RILEM TC 162-TDF (2001) recommendations.

2.2.3.1 Inverse Analysis

The post-peak behavior of steel fiber-reinforced recycled aggregate concrete mixes was identified by conducting inverse analysis of the load-deflection curves obtained from the flexural tests on prisms using finite element software ATENA. The inverse analysis technique started by developing FE models for the tested prisms and setting up specific tensile parameters in a user-defined tensile softening law of the concrete. The value of the uniaxial tensile strength, f_t was kept constant at $0.6f_r$, where f_r is the average flexural strength of concrete (Nilson et al., 2009). The other input parameters of the post-cracking tension function were modified, and several

iterations were considered until the difference between the numerical and experimental load-displacement curves of the prisms became negligible.

Figure 2.15(a), Figure 2.15(b), and Figure 2.15(c) illustrate the experimental and predicted load-deflection curves with the corresponding tension function of concrete prisms made with R100-SF1, R100-SF2, and R100-SF3 concrete mixtures, respectively. These figures show that the flexural load capacity and toughness increased with an increase in the steel fiber volume fraction. The tension function of the concrete with steel fibers is approximated with a bilinear law. When the concrete reaches its tensile strength, f_t, the tensile stress drops to a value of approximately $0.6f_t$, then decreases linearly with an increase in the tensile strain. The tension function of the concrete with v_f of 2 and 3% exhibited a slightly reduced rate of degradation in the tensile stress after cracking relative to that of the concrete with v_f of 1%. The agreement between the predicted and experimental load-deflection responses of the prisms verified the validity of the tension function developed from the inverse analysis. Figure 2.16 shows the tensile softening constitutive law of the user concrete material model used in the FE numerical modeling.
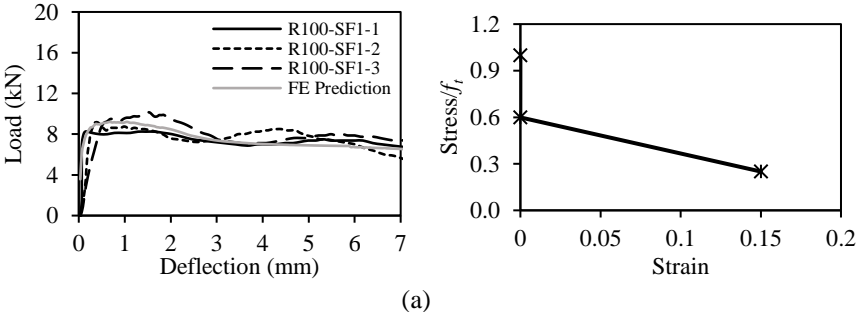

(a)

Figure 2.15: Experimental and predicted load-deflection curves with the corresponding tension function: (a) R100-SF1; (b) R100-SF2; (c) R100-SF3
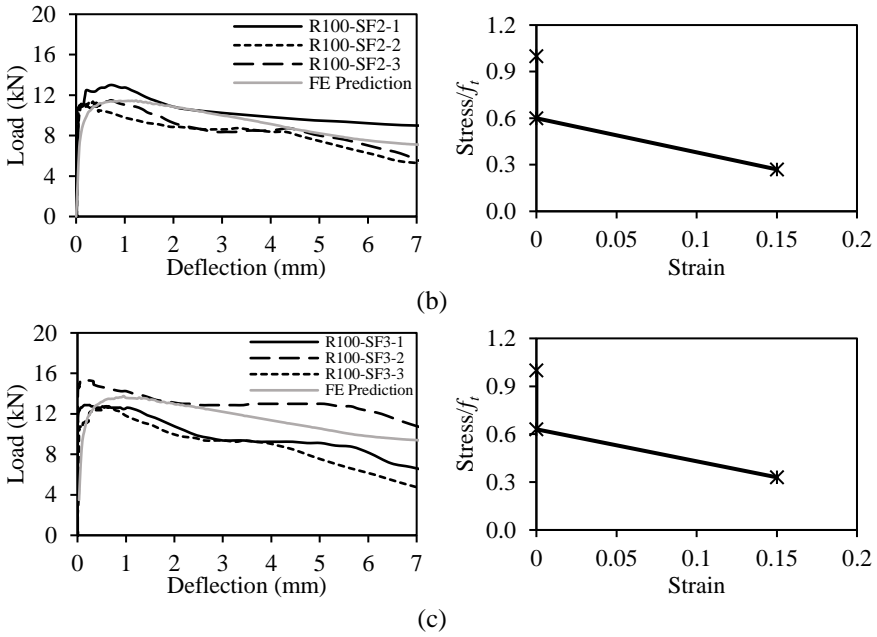
(b)

(c)

Figure 2.15: Experimental and predicted load-deflection curves with the corresponding tension function: (a) R100-SF1; (b) R100-SF2; (c) R100-SF3 (continued)
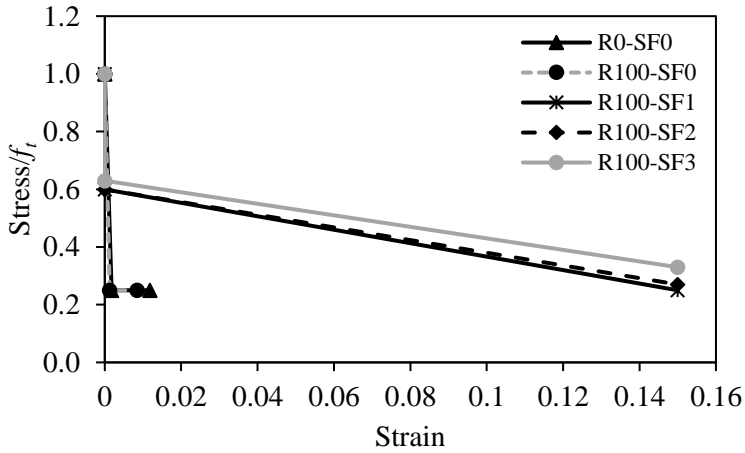

Figure 2.16: Tensile softening laws of concrete adopted in the numerical modeling

2.2.4 Deep Beam Tests

2.2.4.1 Specimens Preparation

The deep beam specimens were cast in a horizontal position to facilitate the casting process. The reinforcement steel cages were placed inside plywood molds prior to casting. It should be noted that in practical application the beams are cast vertically which might cause difference in concrete homogeneity between the bottom and top parts of the beam. The mixing procedure described earlier in section 2.2.1 was adopted. The concrete mixture was placed compacted by a vibrator, and then leveled. The concrete surface was smoothened using a finishing trowel. Segregation, bleeding, and agglomeration of steel fibers were not observed during casting. The deep beam specimens were cured using wetted burlaps for seven consecutive days, then air-cured for a minimum of 28 days. Figure 2.17 shows photographs of steel fiber-reinforced concrete mixtures during placement and while using a finishing trowel to smoothen the surface. Figure 2.18 shows a photograph of a concrete beam after being trowel-finished. The slump of fresh concrete was tested directly after the mixing process. Additional concrete cubes, cylinders and prisms were sampled for the concrete material characterization, compacted on a vibration table, demolded after 24 hours, and then placed in a water tank for moist curing until the time of testing after 28 days. Three replicate specimens were prepared for each test. The openings in the deep beam specimens of Group N were made after concrete casting through coring. It should be noted that laboratory testing of large-scale RC structural elements, such as the deep beams of the current study, are costly, time-consuming, and labor intensive. As such, only one specimen was tested for each parameter. Nevertheless, the numerical investigation included in the current study is meant to offset this limitation.

<center>(a)   (b)</center>

Figure 2.17: Casting of steel fiber-reinforced concrete beams: (a) Placement of concrete; (b) Surface Smoothening using a finishing trowel
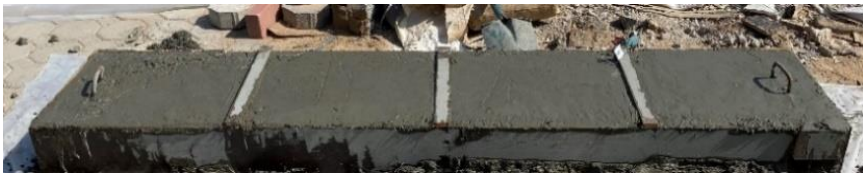

<center>Figure 2.18: A trowel-finished concrete beam</center>

2.2.4.2 Test Setup and Instrumentation

Two actuators, 1300 mm apart, were used to apply the load to the top surface of the beams. The applied loads of the actuators were recorded by two load cells. Initially, the tests were conducted under a load-controlled rate of 0.5 kN/sec. At approximately 80% of the expected shear capacity, the loading scheme was switched to a displacement control at a rate of 0.6 mm/min for safety consideration. Three linear variable differential transducers (LVDTs) were placed below the beam, one at midspan and one at each support, to measure the net midspan deflection. The net midspan deflection was calculated as the difference between the measured deflection at the midspan

and the average of the deflection at the supports. For beams in group S, four strain gauges (SGs), 5 mm long each, were bonded to the bottom layer of the longitudinal steel reinforcing bars within the shear span at a spacing of 200 mm to measure the tensile steel strain. Three SGs, 5 mm long each, were installed on one horizontal and two vertical stirrups located at the center of each shear span with shear reinforcement. Figure 2.19 shows the test setup of a solid deep beam. Figure 2.20 shows the test setup of a deep beam with web openings. Figure 2.21(a) shows the location of the SGs attached to steel reinforcing bars and stirrups. For beams in group N having web openings, the strains in the tension steel within the shear span were measured using four strain gauges (SGs), each having a length of 5 mm. These SGs were bonded to the bottom longitudinal steel reinforcement at a spacing of 80 mm within the shear span. In each shear span of the beams with steel stirrups, a 5-mm SG was installed on the vertical stirrup next to the opening. The locations of the SGs bonded to the tension steel and stirrups are illustrated in Figure 2.22(a). The SGs attached to the tensile steel bars within the shear span were used to examine the steel strain profile and verify the arch action effect/mode of failure. The SGs of the shear reinforcement were used to check stirrup's yielding and examine the effect of test parameters on the rate of increase of the stirrup strain. Five SGs, 60 mm long each, were bonded to the concrete surface of beams in group S to measure the concrete strains. The concrete SGs were placed longitudinally at the midspan and under the loading points and diagonally at the middle of each shear span. Figure 2.21(b) shows the location of the concrete SGs attached to the concrete surface for beams in group S. Concrete SGs were also attached to the concrete surface of the beams with stirrups but not shown in Figure 2.21(a) for clarity. The SGs attached to the concrete surface were used to check level of strain in the concrete and better understand the effect of test parameters on the behavior of the tested beams. For beams in group N, the longitudinal concrete strains were

measured using three SGs of 60 mm length bonded to the concrete surface longitudinally at the midspan and under the load plates. Four SGs of 60 mm length were also bonded to the concrete surface in the diagonal direction in the upper and lower chords of each shear span to measure the concrete strain in the diagonal direction in each chord. The locations of the concrete SGs used in all deep beams with openings are shown in Figure 2.22(b). The load cells, LVDTs, and SGs were connected to a data acquisition system. Before conducting the tests, the front surfaces of the beams were painted white to facilitate tracing of cracks. Cracks developed during testing were marked, and the corresponding load values were recorded.
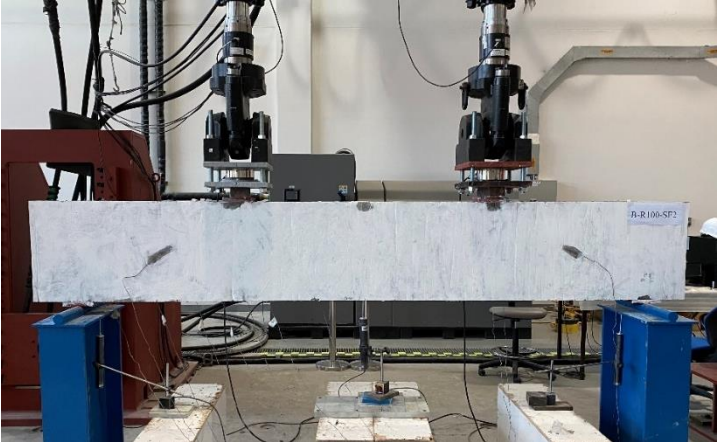

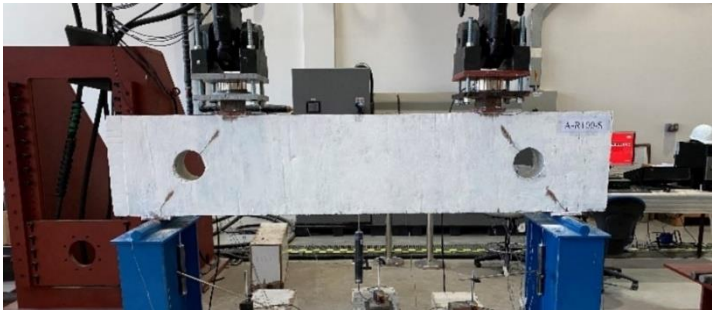
Figure 2.19: Test setup of solid deep beam

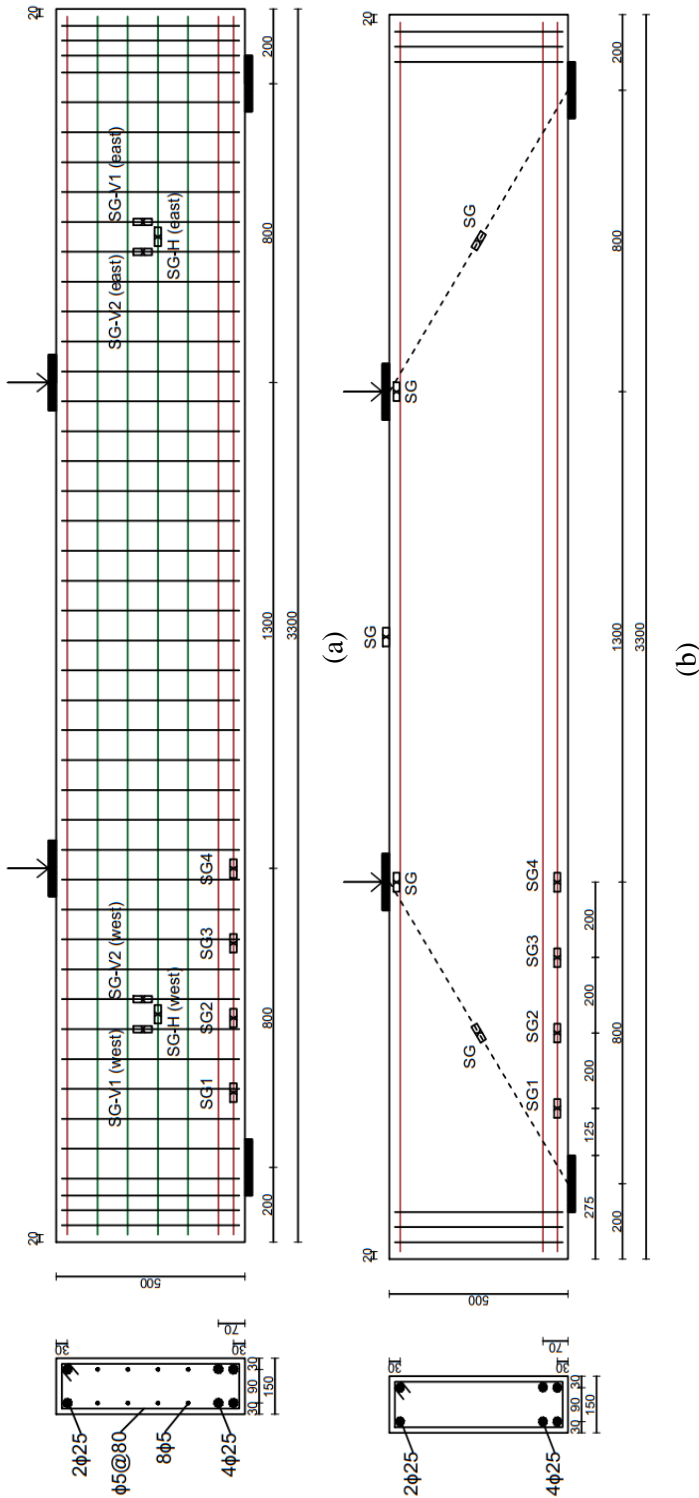Figure 2.20: Test setup of deep beam with openings

Figure 2.21: Details of deep beam specimens (dimensions are in mm): (a) A beam with traditional shear reinforcement; (b) A beam without traditional shear reinforcement
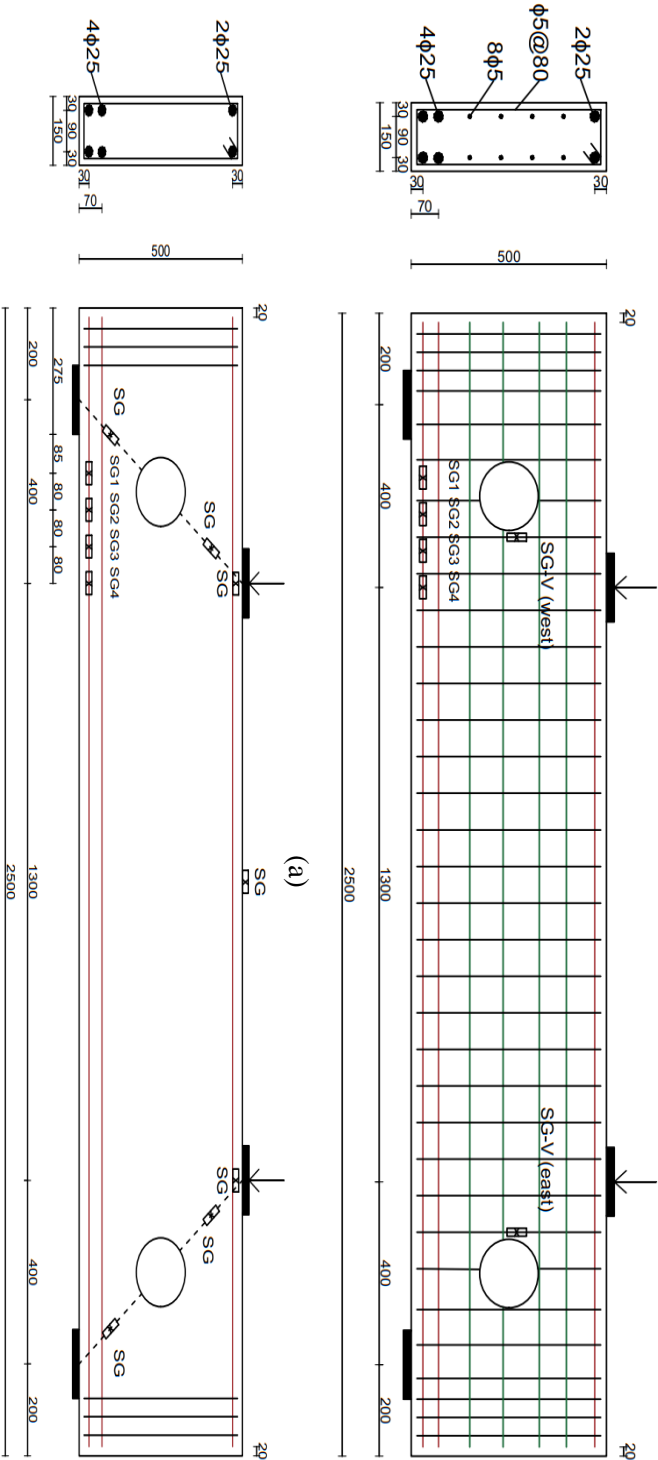
Figure 2.22: Details of deep beam specimens (dimensions are in mm): (a) A beam with conventional steel stirrups; (b) a beam without conventional steel stirrups

2.3 Results

This section presents and discusses the main findings obtained in the four main phases of this research: material characterization, large-scale deep beam testing, analytical predictions, and numerical simulations.

2.3.1 Characterization of Concrete made with RCAs and Steel Fibers

2.3.1.1 Fresh Properties

The fresh properties of concrete are evaluated in this section based on the fresh density, slump, vebe consistency and compacting factor.

Fresh Density - The fresh density of the thirteen concrete mixes prepared for material characterization are presented in Table 2.5. The values ranged from 2357 to 2815 kg/m^3. The density decreased as the RCA replacement percentage increased. Approximately 12% reduction in fresh concrete density was observed by increasing the RCA replacement percentage from 0% to 100%. The lower dry-rodded density of the RCAs, displayed in Table 2.1, contributed to the reported reduction in the fresh density. The existing mortar attached to RCAs could also create a rough, porous surface texture that possibly increased the air content. Concrete mixtures with steel fibers exhibited higher fresh density values relative to those of their plain counterparts. The fresh density of the mixtures with RCAs and steel fibers was insignificantly different than that of the control mixture made with NAs. The yield was calculated as shown in Table 2.5. It should be noted that the variation in the yield values between different concrete mixes could be attributed to a variation between the properties obtained from testing of samples of different constituents and the actual properties of the batched materials.

Slump – The slump of the thirteen concrete mixes is presented in Table 2.5. The slump of the control mix with NAs was 150 mm. The concrete mixtures with RCAs exhibited lower slump in the range of 95 – 135 mm. Such reduction in slump is owed to the rough surface texture and irregular geometric shape of RCAs (Manzi et al., 2013; Wagih et al., 2013). The addition of steel fibers further reduced the slump. The slump decreased with an increase in the steel fiber volume fraction. The mixtures with $v_f = 3\%$ exhibited negligeable slump. It should be noted that, trial mixes were carried out prior to concrete casting to ensure adequate workability of the concrete and a homogeneous distribution of the steel fibers within the concrete mixture. Segregation, bleeding, and agglomeration of steel fibers were not observed in any of the mixtures. However, in practical applications superplasticizers should be used to improve the workability of concrete mixes made with RCAs and steel fibers.

Table 2.5: Fresh density and slump of concrete mixes

Mix Designation	ρ_f (kg/m^3)	Yield[*]	Slump (mm)
R0-SF0	2677	0.90	150
R30-SF0	2655	0.90	135
R70-SF0	2430	0.99	117
R100-SF0	2357	1.01	95
R30-SF1	2680	0.92	120
R70-SF1	2595	0.95	100
R100-SF1	2500	0.99	86
R30-SF2	2750	0.93	30
R70-SF2	2658	0.96	25
R100-SF2	2600	0.98	20
R30-SF3	2815	0.94	0
R70-SF3	2710	0.97	0
R100-SF3	2640	1.00	0

[*] The Yield is the ratio of batched quantities to fresh densities.

Table 2.6 presents the results of the fresh properties of mixes used to cast the large-scale RC deep beams. It is evident that the addition of steel fibers decreased the slump, increased the vebe time, and decreased the compacting factor. The addition of high steel fiber v_f of 3%, significantly reduced the workability of the concrete. The slump of mix R100-SF3 was only 11% of that of its counterpart mix R100-SF0 without steel fibers. The vebe time of mix R100-SF3 was 10 times that of R100-SF0. The reduced slump and increased vebe time of the concrete mixtures with steel fibers indicate stiffer mixes with low workability. It should be noted that the slump values of these mixes are different than those of the mixes of the first phase (Table 2.5), possibly due to a change in the weathering condition at the time of casting or the time between placing and testing.

Table 2.6: Fresh concrete properties of the mixes used to cast the large-scale deep beams

Mix Designation	Slump (mm)	Vebe Time (sec)	Compacting Factor
R0-SF0	228	0.83	0.98
R100-SF0	183	1.26	0.97
R100-SF1	85	2.39	0.94
R100-SF2	60	5.38	0.90
R100-SF3	20	12.16	0.77

2.3.1.2 Mechanical Properties

The mechanical properties of concrete are evaluated in this section based on the hardened density, compressive strength, modulus of elasticity, splitting tensile strength, uniaxial tensile strength and modulus of rupture (i.e. flexural strength).
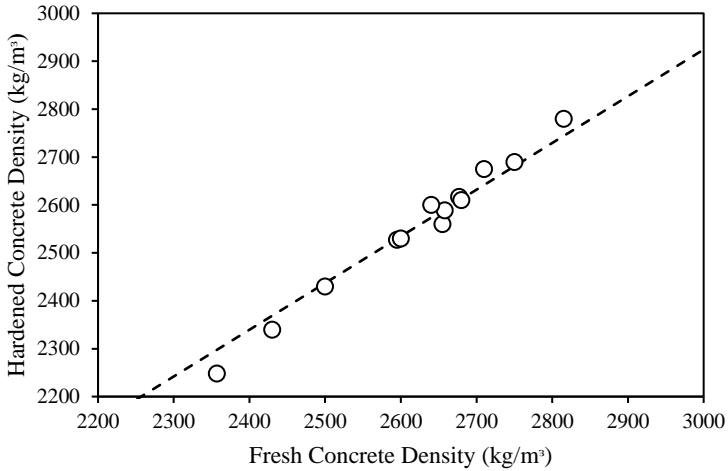
Figure 2.23: Relationship between fresh and hardened concrete density

Hardened Density - Figure 2.23 shows a strong correlation (correlation coefficient, $R^2 = 0.97$) between fresh (ρ_f) and hardened (ρ_h) concrete densities. The best fit relationship between the two densities indicates that: $\rho_h = 0.97\rho_f$

Compressive Strength - Table 2.7 presents the compressive strength of concrete mixes at the ages of 3, 7 and 28 days. Although the initial 3-day strength of the mixes with RCAs were lower than that of the NA-based control mix, their strength gain over time was generally higher. It seems that the reduced RCAs quality and the weak bond between the old and new mortar is mainly responsible for the low early strength. With time, the hydration reaction progressed, providing a better bond and rendering this weakness less prominent. The inclusion of steel fibers with $v_f \geq 2\%$ resulted in a higher early-age (3-day) compressive strength but reduced the strength gain with time, to some extent, compared to that of the mixes with $v_f < 2\%$. It is also worth noting that the strength gains exhibited by the RCA-based mixes with $v_f = 3\%$ were insignificantly different from those exhibited by the NA-based control mix. It is worth noting that the normal experimental scatter as per the

ASTM C39 (2015) standard is assessed based on a coefficient of variation of 3.2%. In this research, the coefficient of variation of the compressive strength of concrete cylinders ranged between 1% and 7%. The coefficient of variation of the compressive strength of concrete cubes ranged between 1% and 5%.

The development of the cylinder compressive strength of concrete mixes is illustrated in Figure 2.24. The development of the cylinder compressive strength followed a bilinear relationship, typically known as a common feature for conventional concrete. The high rate of increase in the compressive strength occurred within the first 3 days due to the higher rate of hydration. Results of Figure 2.24 show that the concrete compressive strength at different ages was majorly affected by the RCA content. As expected, the control mixture R0-SF0 achieved the highest strength at the age of 3, 7 and 28 days. Although the control mix was designed to achieve a 28-day design cylinder compressive strength of 30 MPa, as per the procedure of ACI 211.1 (2009), the measured cylinder compressive strength was 21% higher at 36.4 MPa. The substitution of 30% of NAs with RCAs without steel fibers reduced the compressive strength by 15%. However, the compressive strength of R30-SF0 was still above the design strength mark of 30 MPa. The substitution of 70% and 100% of NAs with RCAs without steel fibers reduced the compressive strength by 29% and 32%, respectively. The compressive strengths of the mixes with 70% and 100% RCAs were below the design strength. This can be attributed to the inferior properties of RCAs compared to those of the NAs.

Table 2.7: Compressive strength of concrete cylinders and cubes

Mix Designation	Compressive Strength (MPa)					
	$f_{c,3D}$	$f_{c,7D}$	f'_c	f_{cu}	$f_{c,3D}/f'_c$	$f_{c,7D}/f'_c$
R0SF0	23.5 (2.0)	28.4 (0.5)	36.4 (1.4)	42.6 (1.7)	0.65	0.78
R30SF0	17.8 (1.3)	22.1 (2.3)	30.8 (0.3)	33.8 (1.8)	0.58	0.72
R70SF0	13.9 (0.6)	17.1 (0.2)	25.8 (1.5)	27.0 (0.3)	0.54	0.66
R100SF0	13.7 (2.0)	17.2 (0.3)	24.7 (0.5)	26.0 (1.2)	0.55	0.70
R30SF1	15.9 (0.8)	21.7 (0.6)	32.0 (1.4)	35.0 (0.4)	0.50	0.68
R70SF1	13.0 (0.7)	17.3 (0.5)	28.5 (1.6)	30.6 (0.9)	0.46	0.61
R100SF1	12.6 (0.5)	16.8 (1.2)	26.1 (0.6)	28.1 (0.4)	0.48	0.64
R30SF2	20.6 (2.3)	24.2 (1.5)	33.1 (0.6)	36.4 (1.1)	0.62	0.73
R70SF2	17.2 (1.0)	19.5 (1.5)	29.3 (0.8)	31.8 (1.1)	0.59	0.67
R100SF2	16.5 (1.4)	18.4 (1.7)	26.9 (1.9)	28.4 (1.3)	0.61	0.68
R30SF3	22.9 (1.1)	27.5 (0.9)	34.3 (0.2)	38.8 (1.6)	0.67	0.80
R70SF3	20.2 (2.1)	22.9 (2.2)	30.6 (2.1)	33.4 (1.5)	0.66	0.75
R100SF3	19.4 (2.2)	22.6 (1.5)	28.0 (0.9)	29.6 (0.9)	0.69	0.81

$f_{c,3D}$ = Concrete compressive strength at the age of 3 days.
$f_{c,7D}$ = Concrete compressive strength at the age of 7 days.
*Values between parentheses represent the standard deviation.

For mixes with 30% RCAs, the addition of steel fibers at v_f of 1, 2, and 3% improved f'_c by 4, 7, and 11%, respectively, compared to their plain counterparts. For mixes with 70% RCAs, the addition of steel fibers at v_f of 1, 2, and 3% improved f'_c by 10, 14, and 19%, respectively, compared to their plain counterparts. For mixes with 100% RCAs, the addition of steel fibers at v_f of 1, 2, and 3% improved f'_c by 6, 10, and 13%, respectively, compared to their plain counterparts. It is worth noting that the effect of steel fibers on f'_c was more pronounced at RCAs replacement of 70%. In addition, the impact of steel fibers on f'_c reduced at RCA replacement of 100%, probably because the concrete was too weak to show an effect for steel fibers. It should be noted that, the addition of steel fibers in volume fractions of 1, 2, and 3% to 30% RCA concrete mixtures resulted in compressive strengths in the range of 32-34 MPa, thus exceeding the 30-MPa design cylinder strength. The compressive strength was still however lower than that of R0-SF0 made with NAs. The compressive strengths of the concrete mixes with 70% RCA replacement and v_f of 1,2 and 3% were 78, 80, and 84% of that of R0-SF0 and 95, 98, and 100% of the 30 MPa design cylinder compressive strength, respectively. Upon complete replacement of NAs by RCAs, concrete mixes with v_f of 1, 2, and 3% had compressive strengths values of 87, 90, and 93% of the 30-MPa design cylinder compressive strength, respectively. The addition of steel fibers provided a denser concrete, and hence, slightly improved the compressive strength of the mixes with RCAs

Table 2.7 also presents the ratio of f'_c/f_{cu}. The NA-based control specimen R0-SF0 had a ratio of 0.85. An increase in RCA replacement percentages in plain concrete led to an increase in f'_c/f_{cu}. This indicated that the difference between the cube and cylinder compressive strengths decreased when more RCAs was used in the concrete mix. It seems that the slenderness effect of cubes under compression is not as apparent when NAs

is replaced by RCAs. Values of f'_c/f_{cu} for the mixtures with steel fibers were insignificantly different from that of their plain counterparts made with RCAs. Figure 2.25 (a) and Figure 2.25 (b) show the typical shear mode of failure under compression for a concrete cylinder without and with steel fibers, respectively. Figure 2.26 (a) and Figure 2.26 (b) show the typical failure mode of tested cubes without and with steel fibers, respectively. The cracks generated at failure were approximately parallel to the direction of applied load.
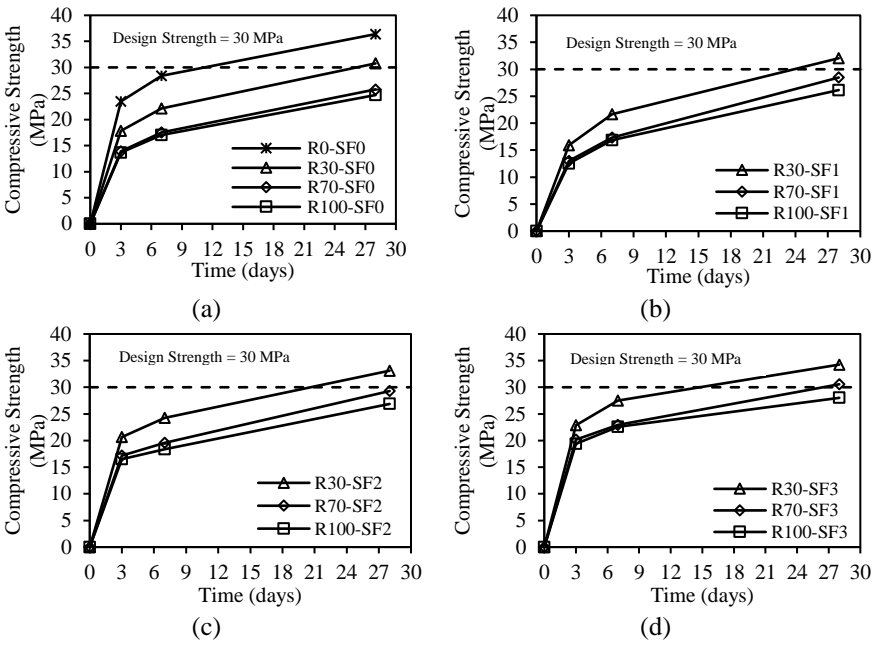

Figure 2.24: Development of compressive strength of concrete mixes with steel volume fractions: (a) 0%; (b) 1%; (c) 2%; (d) 3%

<center>(a)</center>

<center>(b)</center>

Figure 2.25: Failure modes of concrete cylinders under compressive tests: (a) R100-SF0, (b) R100-SF1

<center>(a)</center>

<center>(b)</center>

Figure 2.26: Failure modes of concrete cubes under compressive tests: (a) R0-SF0, (b) R100-SF3

Modulus of Elasticity - Figure 2.27 shows the results of the modulus of elasticity of concrete mixes with different RCAs and steel fiber contents. A reduction in the E_c value with an increase in the percentage of RCA replacement. For plain concrete mixes, 30, 70, and 100% RCA replacements resulted in respective decreases in E_c of 19, 42, and 46% compared to that of the NA-based control mix, R0-SF0. This is consistent with other findings reported in previous investigations (Xiao et al., 2005; Xie et al., 2015). This reduction in E_c may be due to the presence of cement mortar attached to RCAs, creating a more porous and less dense concrete structure. The addition of steel fibers at v_f of 1, 2 and 3% led to average increases of 8, 11 and 17%

in E_c, respectively, compared to those of plain RCA-based concrete counterparts. Steel fibers may have delayed initiation of microcracks, controlled/restricted growth cracks after initiation, hence, slightly reduced deformation at the same stress. Yet, it should be noted that the increase in the modulus of elasticity of the steel fiber concrete mixes having a 100% RCA replacement percentage was insignificant. Apparently, the effect of RCA replacement on E_c was more prominent than that of steel fiber addition.
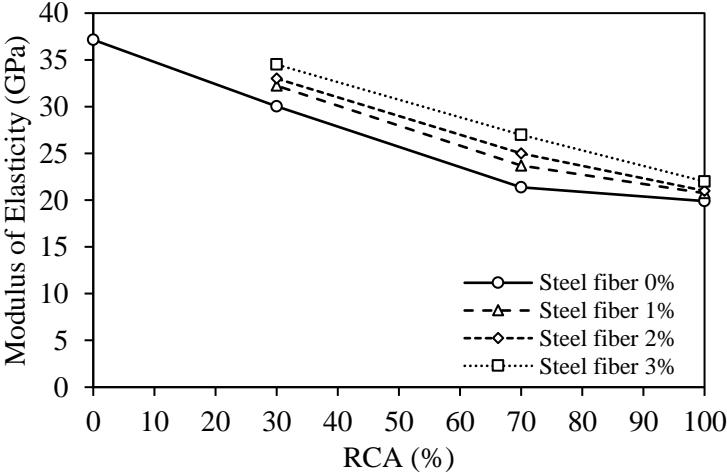

Figure 2.27: Modulus of elasticity of concrete mixes with different RCAs and steel fiber contents

Modulus of elasticity results of the mixtures examined in the current study were modeled based on regression analysis. Two models were proposed, as presented in Equation 2.4 and Equation 2.5, to predict the values of E_c (in GPa) with reasonable accuracy ($R^2 = 0.96$). Equation 2.4 relates E_c to f'_c (in MPa) as a linear function with a y-intercept, similar to that proposed by ACI 363. In comparison, Equation 2.5 provides similar prediction accuracy but as a power function. Equations 2.4 and 2.5 are applicable in the range of f'_c of the mixtures examined in the current study.

$$E_c = 18.1\sqrt{f_c'} - 71.7 \qquad\qquad 24 \leq f_c' \leq 37\ MPa \qquad\qquad\qquad 2.4$$

$$E_c = 0.055 f_c'^{1.82} \qquad\qquad 24 \leq f_c' \leq 37\ MPa \qquad\qquad\qquad 2.5$$

The obtained relationships in Equation 2.4 and Equation 2.5 are compared to those developed by ACI Committee 363 (1997), ACI Committee 318 (2014), Dilli et al. (2015), Ahmed & Shah (1985), CEB-FIP (1990) and Mendis (2003). Figure 2.28 presents the predicted versus experimental modulus of elasticity. The equations introduced in this work gave a reasonable accuracy with values converging around the 45°-line. The model suggested by Dilli et al. (2015) significantly underestimated the modulus, while those proposed by Shah and Ahmed (1985) and Mendis (2003) tended to overestimate it. Furthermore, the equation given by the ACI Committee 363 (1997) slightly overestimated the modulus for values lower than 22 GPa and accurately predicted the modulus for values between 22 and 30 GPa, after which it underestimated the experimentally obtained modulus of elasticity. Similarly, the model proposed by CEB-FIP (1990) overestimated the modulus for experimental values lower than 30 GPa and tended to underestimate modulus of elasticity values higher than 30 MPa. Clearly, the presence of steel fibers and RCAs rendered codified and other equations reported in the literature of typical concrete mixes unsuitable.
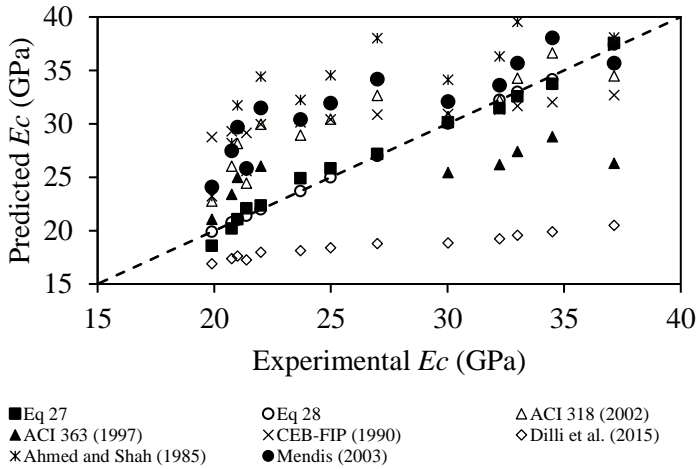
Figure 2.28: Correlation between modulus of elasticity and 28-day cylinder compressive strength

Splitting Tensile Strength - The splitting tensile strength, f_{sp}, of the concrete mixes are summarized in Table 2.8. It is worth noting that the normal experimental scatter as per the ASTM C496 (2017) standard is assessed based on a coefficient of variation of 5%. In this research, the coefficient of variation of the splitting tensile test results ranged between 2% and 20%. The inclusion of 30% RCAs did not reduce the splitting strength of the concrete. A 10% reduction was recorded at 70% RCA replacement percentage. Complete replacement of NAs by RCAs decreased the splitting tensile strength by 21%. The addition of steel fibers remarkably increased the splitting tensile strength to a level even higher than that of the control mix R0-SF0. The addition of steel fibers at v_f of 1, 2 and 3% to the mix made with 100% RCA resulted in 58, 72 and 85% increases in the splitting tensile strength, respectively, compared to that of the plain mix R100-SF0. The splitting tensile strength of all mixes with steel fibers exceeded that of the control mix made with NAs. The steel fibers bridging effect provided concrete with better resistance to tensile crack initiation and propagation.

Figure 2.29 (a) and Figure 2.29 (b) show the typical mode of failure under splitting tensile tests of concrete cylinders without and with steel fibers, respectively. As shown in the figure, the cylinder without steel fibers split at the onset of failure, whereas that with steel fibers remained intact.

| (a) | (b) |

Figure 2.29: Failure modes of concrete cylinders under splitting tensile tests: (a) R0-SF0, (b) R100-SF1

Uniaxial Tensile Strength - The direct uniaxial tensile strength, f_t, of the concrete mixes are summarized in Table 2.8. The replacement of NAs by 30, 70 and 100% RCAs resulted in a decrease in the tensile strength by 14, 23, and 18%, respectively. The addition of steel fibers did not always increase the uniaxial tensile strength of the RCA-based specimens. At RCA replacement percentage of 30%, the addition of 2% of steel fiber volume fraction resulted in an increase in the uniaxial tensile strength from 1.49 MPa to 1.89 MPa compared to its counterpart with v_f of 1%. For mixes made with 70% and 100% RCAs, the increase in steel fiber volume fraction from 1% to 2% did not result in additional increase in the uniaxial tensile strength. The addition of a higher steel fiber v_f of 3% did not result in a further increase in the uniaxial tensile strength. In fact, some of the results of the mixes made with v_f of 3% were even lower than those made with lower steel fiber volume fraction. This behavior might be attributed to the fact that the uniaxial tensile strength under this test configuration was very sensitive to the original concrete tensile strength. It seems that due to the test configuration the tensile

strength was reached at the onset of crack initiation and steel fibers contributed mainly to the post-cracking behavior rather than improving. This behavior verifies the statement of the RILEM (2002) standard that the direct uniaxial tensile test is not intended for determination of the tensile strength, but the tensile post-peak behavior. The post-peak tensile strength was improved with the addition of steel fibers as shown in Figure 2.31(b), (c), and (d). Similar findings were reported by Shi et al. (2020). Figure 2.30 (a) and Figure 2.30 (b) show the typical mode of failure under direct uniaxial tensile tests of a concrete cylinder without and with steel fibers, respectively. The failure occurred at the notch pre-cut along the perimeter of the cylinder at the mid-height. The plain cylinder failed suddenly at the onset of crack initiation, whereas that with steel fibers exhibited a significant deformation after crack initiation until complete failure took place.

Table 2.8: Splitting and uniaxial tensile strength test results

Mix Designation	f_{sp} (MPa)	f_t (MPa)
R0-SF0	2.31 (0.2)	1.62 (0.1)
R30-SF0	2.30 (0.1)	1.40 (0.1)
R70-SF0	2.10 (0.2)	1.24 (0.1)
R100-SF0	1.82 (0.2)	1.33 (0.1)
R30-SF1	3.29 (0.2)	1.49 (0.4)
R70-SF1	3.03 (0.4)	1.38 (0.1)
R100-SF1	2.87 (0.2)	1.54 (0.1)
R30-SF2	4.01 (0.5)	1.89 (0.2)
R70-SF2	3.69 (0.5)	1.35 (0.2)
R100-SF2	3.13 (0.4)	1.53 (0.1)
R30-SF3	4.61 (0.1)	1.49 (0.1)
R70-SF3	4.21 (0.1)	1.34 (0.1)
R100-SF3	3.37 (0.7)	1.24 (0.2)

*Values between parentheses represent the standard deviation.

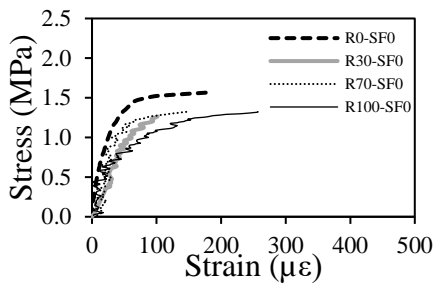(a)   (b)
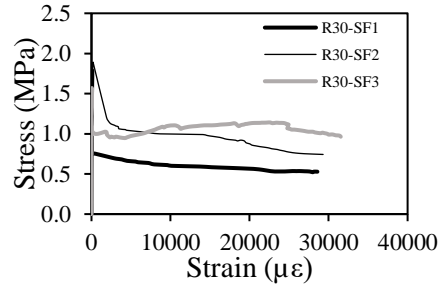
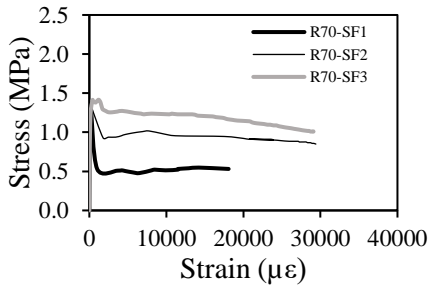Figure 2.30: Failure modes of concrete cylinders under direct uniaxial tensile tests: (a) R0-SF0, (b) R100-SF3

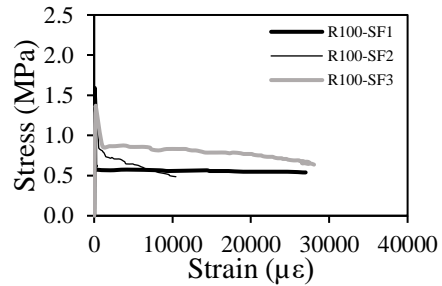(a)   (b)

(c)   (d)

Figure 2.31: Tensile strength test results: (a) Plain concrete mixes; (b) RCA 30%; (c) RCA 70%; (d) RCA 100%

Four-point Bending Test Results - Figure 2.32 illustrates the load-deflection curves of the concrete prisms tested under four-point bending. A typical representative curve is presented for each mix. The behavior of the plain concrete specimens was nearly linear elastic up to peak load, followed by a sudden drop without post-peak phase. The slope of the load-deflection

curve of the plain specimens decreased with increasing the RCA replacement percentage, possibly because of the reduced modulus of elasticity of the plain concrete mixes made with RCAs.
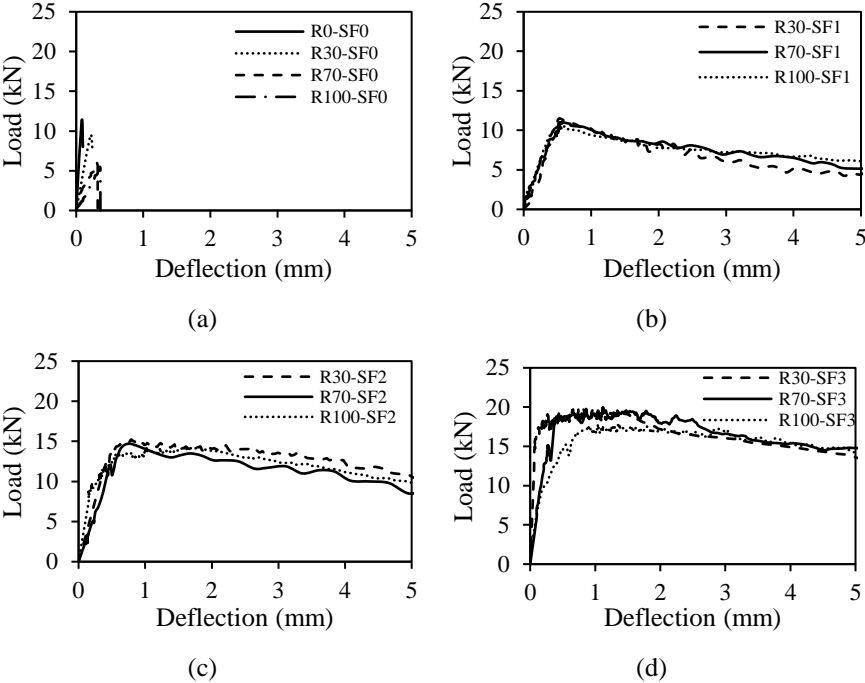

Figure 2.32: Load-deflection curves of RCA mixes with v_f of steel fibers: (a) 0%; (b) 1%; (c) 2%; (d) 3%

Increasing the RCA replacement percentage insignificantly influenced the slope of the linear ascending branch at v_f of 1% but slightly decreased the slope at v_f of 3%. Plain concrete mixes fractured abruptly after the peak-load was reached and had no post-peak response. In contrast, steel fiber-reinforced concrete mixes were characterized by a long post-peak tail, reflecting the residual flexural strength of the specimens. The post-peak profile for steel fiber-reinforced concrete mixes was found to be similar. In fact, the rate at which the residual strength was provided was analogous regardless of RCA replacement percentage. Nevertheless, the value of the

residual strength was dependent on that of the peak strength. Figure 2.33 (a) and Figure 2.33 (b) show photos of typical specimens without and with steel fibers after testing, respectively. For plain concrete prisms, a single localized crack formed, then propagated rapidly in the vertical direction causing a sudden brittle mode of failure. In contrast, the prisms with steel fibers exhibited a vertical crack originated at the bottom face, and then propagated gradually to the upper face, with a decreased width. The prisms with steel fibers did not separate into two parts at failure.

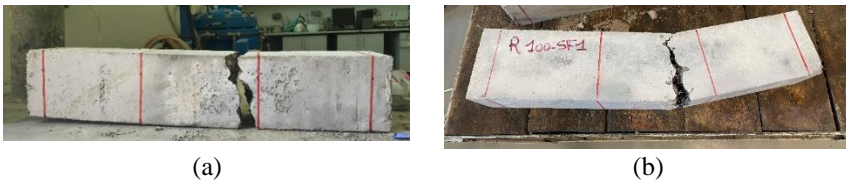(a)   (b)

Figure 2.33: Failure modes of concrete under four-point bending; (a) R0SF0, (b) R100SF1

Table 2.9 summarizes the four-point bending test results. Plain concrete mixes made with 30, 70, and 100% RCAs exhibited 16, 46, and 51% reductions in the modulus of rupture, f_r, respectively, compared to that of the control mix R0-SF0. This behavior can be attribute to the inferior properties of RCA, weak interface zone between the old mortar attached to RCA and the new mortar, and porous structure of RCA. Previous studies reported a similar reduction in flexural strength with an increase in RCA replacement percentage (Salem & Burdette, 1998; Topçu & Şengel, 2004). In contrast, the modulus of rupture of the steel fiber-reinforced concrete mixes, regardless of RCA replacement percentages, was almost equal or superior to that of NA-based mix. The value of f_{sp}/f_r of the control mix is 0.46. The values of f_{sp}/f_r of plain RCA-based mixes were in the range of 0.55 to 0.78 with an average of 0.69. The values of f_{sp}/f_r of RCA-based mixes with steel fiber at v_f of 1, 2, and 3% were on average 0.61, 0.54, and 0.47, respectively.

Table 2.9: Four-point bending test results

Mix Designation	f_r (MPa)	δ_p (mm)	f_{150}^{100} (MPa)	T_{150}^{100} (J)
R0-SF0	5.03 (0.4)	0.08	-	0.73
R30-SF0	4.21 (0.1)	0.21	-	0.98
R70-SF0	2.70 (0.1)	0.31	-	1.11
R100-SF0	2.47 (0.4)	0.35	-	1.39
R30-SF1	5.17 (0.6)	0.53	2.68	24.08
R70-SF1	4.95 (0.5)	0.54	3.22	24.65
R100-SF1	4.83 (0.2)	0.54	3.25	25.24
R30-SF2	6.86 (1.1)	0.78	5.23	39.68
R70-SF2	6.61 (1.2)	0.79	5.55	39.65
R100-SF2	6.40 (0.9)	1.23	6.10	39.59
R30-SF3	8.97 (0.1)	1.12	7.22	53.01
R70-SF3	8.82 (1.0)	1.16	7.47	53.57
R100-SF3	8.00 (1.1)	1.37	7.51	54.81

*Values between parentheses represent the standard deviation.

Analytical Model Correlating Compressive Strength to Modulus of Rupture - Several equations were developed using regression analysis to correlate the modulus of rupture of conventional plain concrete to its compressive strength (ACI 318-14, 2014; ACI 363, 1992; Perumal, 2015; Xu & Shi, 2009). However, models to predict the modulus of rupture of steel fiber-reinforced RCA concrete have not been previously proposed. A linear regression analysis was performed using Minitab software package to establish a statistical relationship to predict the modulus of rupture, f_r, from f'_c, v_f and RCA replacement percentage. The reliability of the proposed analytical model was assessed using the analysis of variance. While the two variables f'_c and v_f were found to be significant at the 95% confidence level having a P-value of 0, RCA variable was noted to be insignificant with a P-value of 0.138. Therefore, RCA, as a variable, was removed and a new regression analysis was performed with the two significant variables, f'_c and v_f. As a result, Equation 2.6 was developed. In this regression analysis, f'_c and v_f were found to be significant at the 95% confidence level having a P-value of 0. In addition, the contributions of v_f, f'_c and the error were 76.6, 21.5, and

1.9%, respectively. The linear correlation coefficient, R^2, was also found to be 0.98, indicating that the proposed equation provides an accurate estimation of the modulus of rupture obtained from the experiment. In comparison, previous codified and research equations generally underestimate the flexural strength of steel fiber-reinforced concrete made with RCA, as shown is Figure 2.34.

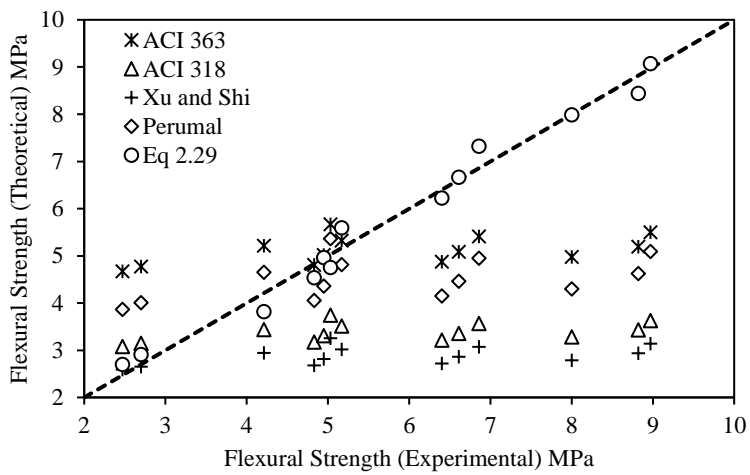$$f_r = 1.93\sqrt{f_c'} + 1.55v_f - 6.90 \qquad 24 \le f_c' \le 37 \; MPa \qquad 2.6$$

Figure 2.34: Predicted versus experimental values of flexural strength

Residual Flexural Strength - The flexural residual strengths, f_{150}^{100}, at a deflection of $L/150$, are presented in Table 2.9. It is worth noting that plain concrete mixes do not exhibit a post-peak behavior, and therefore, do not present any residual strength. The relationship between the residual flexural strength f_{150}^{100} and RCA replacement percentage at different values of v_f are shown in Figure 2.35. At a specific value of v_f, the RCA replacement percentage had little impact on the residual flexural strength. Conversely, the increase in steel fiber v_f resulted in a significant increase in f_{150}^{100}. An

interpretation of the results shows an average of 85 and 144% increases in residual flexural strength at v_f of 2 and 3%, respectively, compared to that of the mixes with v_f of 1%. Clearly, the influence of steel fiber incorporation is more dominant than that of the RCA replacement.
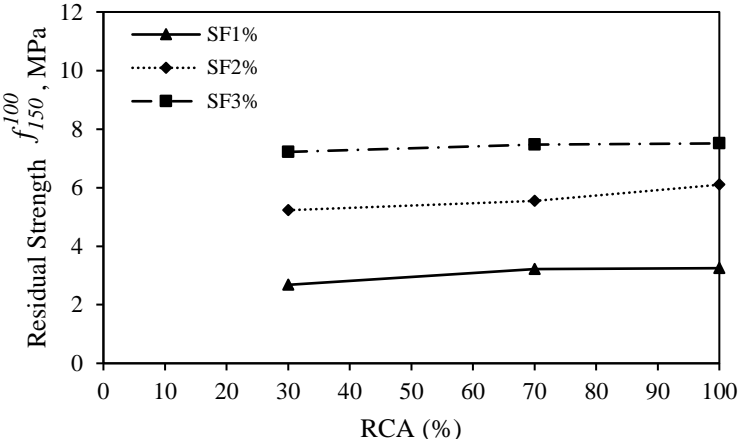

Figure 2.35: Effect of steel fibers and RCAs on the residual flexural strength of concrete

Flexural Toughness - The flexural toughness values of the plain concrete mixes ranged from 0.73 to 1.39 J. The steel fiber-reinforced RCA counterparts exhibited flexural toughness values of up to 54.81 J. Clearly, the addition of steel fibers significantly improved the flexural toughness.

The relationships between flexural toughness and RCA replacement percentage at different values of v_f are presented in Figure 2.36. An increase in RCA replacement percentage has insignificant effect on the flexural toughness. Yet, increasing the steel fiber volume fraction in the specimens with the same RCA content led to a higher flexural toughness. The flexural toughness of the mixtures with v_f of 2 and 3% was, on average, 61 and 118% higher than their counterpart mixes with v_f of 1%. It can be thus concluded

that higher energy absorption capacity, i.e. toughness, was obtained by increasing steel fiber content, owing to the steel fibers bridging capacity at crack surfaces and mechanical performance improvement of concrete.
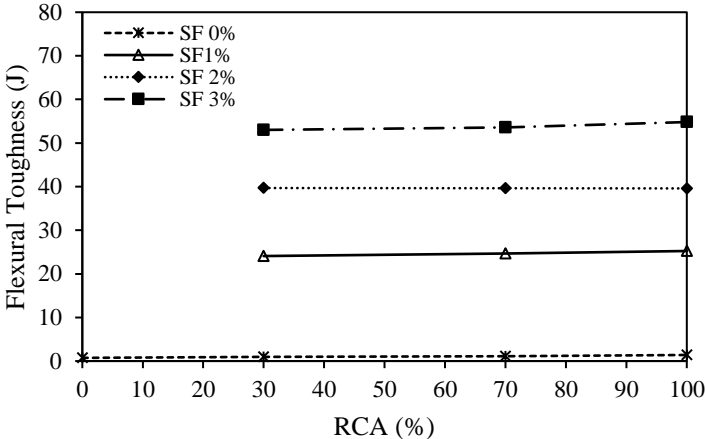

Figure 2.36: Effect of steel fibers and RCA replacement percentage on the flexural toughness

Three-Point Bending Test Results – Figure 2.37 shows the load-crack mouth opening displacement (CMOD) curves of the concrete prisms tested under three-point bending. A 60-mm-long strain gauge was bonded horizontally to the concrete surface at the notch location to calculate the crack mouth opening displacement (CMOD) from the measured strain. The control concrete mix, R0-SF0, exhibited a near-linear-elastic up to the peak load, followed by a sudden drop in resistance after the peak, as shown in Figure 2.37(a). In other plain concrete mixes, the increase in the RCA replacement percentage resulted in a decrease in the peak load and tended to increase the corresponding peak CMOD.

The load-CMOD curves of steel fiber-reinforced concrete mixes are divided into three parts. The first part is characterized by an elastic response

up to initiation of a crack at the tip of the notch and corresponds to the pre-cracked concrete specimen. For each steel fiber volume fraction, there was no notable change in the load-CMOD curves as the RCA replacement percentage increased. The second part of the curve represents propagation of the crack upward toward the compression face of the prism, which caused a deviation from linearity until the peak load was attained. The third part of the curve represents the post-peak phase, which is characterized by a gradual reduction of load with an increase in CMOD. From Figure 2.37(b-d), it is clear that the RCA replacement did not alter the load-CMOD curves of the mixes with steel fibers.
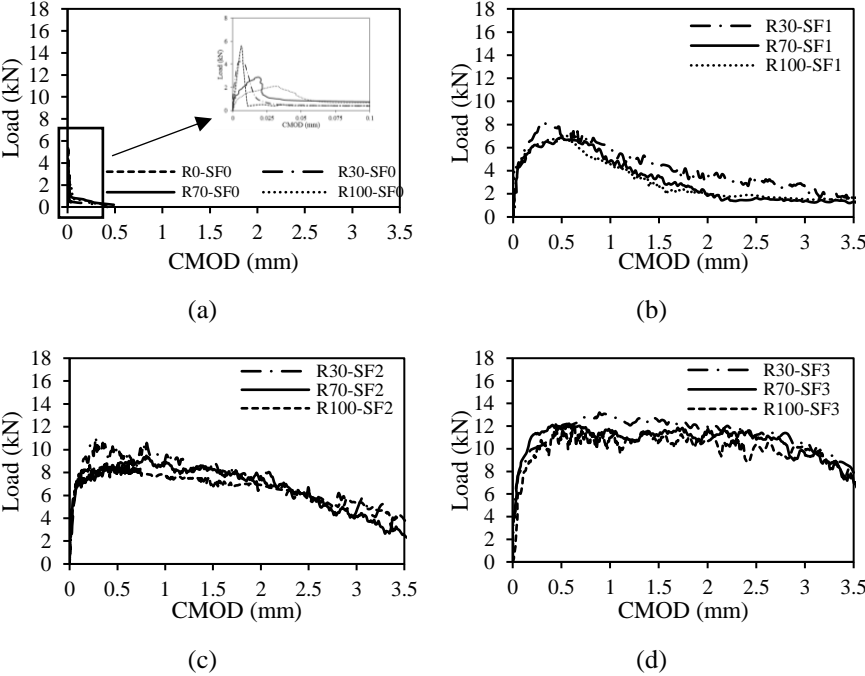

Figure 2.37: Load-CMOD curves of RCA mixes with steel fibers (SF): (a) SF 0%; (b) SF 1%; (c) SF 2%; (d) 3%

Increasing the steel fiber volume fraction in mixes with the same RCA replacement percentage resulted in an increase in load-carrying capacity

and CMOD at peak load. This behavior illustrates the dominant effect of steel fiber addition on load bearing capacity compared to that caused by the RCA replacement percentage. Figure 2.38 (a) and Figure 2.38 (b) show photos of typical specimens without and with steel fibers after testing, respectively. For plain concrete prisms, a single localized crack formed, then propagated rapidly in the vertical direction causing a sudden brittle mode of failure. In contrast, the prisms with steel fibers exhibited a vertical crack originated at the bottom face, and then propagated gradually to the upper face, with a decreased width. The prisms with steel fibers did not separate into two parts at failure.

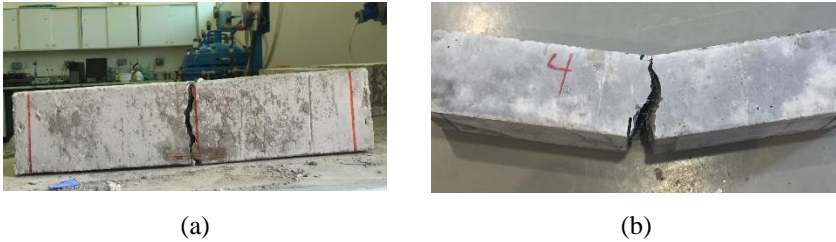(a)   (b)

Figure 2.38: Failure modes of concrete under three-point bending; (a) R0SF0, (b) R100SF1

Results of the limit of proportionality strength and the residual flexural strengths obtained from the three-point bending tests are reported in Table 2.10. Compared to the results of the control mix, R0-SF0, RCA replacement percentages of 30, 70, and 100% in plain concrete mixes resulted in reduced f_L by 22, 47, and 64%, respectively. Plain concrete mixes had no residual flexural strengths. On the other hand, as v_f increased, limit of proportionality and residual flexural strengths increased. It can also be noticed that the addition of steel fibers was generally more influential toward the residual strengths compared to the strength at the limit of proportionality. These results further verify the effectiveness of steel fibers to improve the flexural characteristics of concrete made with RCAs.

Table 2.10: The limit of proportionality strength and the residual flexural strengths.

Mix Designation	f_L (MPa)	$f_{R,1}$ (MPa)	$f_{R,2}$ (MPa)	$f_{R,3}$ (MPa)	$f_{R,4}$ (MPa)
R0-SF0	5.26 (0.4)	-	-	-	-
R30-SF0	4.11 (0.2)	-	-	-	-
R70-SF0	2.77 (0.4)	-	-	-	-
R100-SF0	1.91 (0.2)	-	-	-	-
R30-SF1	4.88 (0.5)	6.41	2.58	1.72	1.24
R70-SF1	4.59 (0.2)	6.41	3.25	1.63	1.43
R100-SF1	4.50 (0.3)	6.43	4.21	3.19	1.63
R30-SF2	5.64 (1.0)	8.13	6.51	5.93	3.36
R70-SF2	5.52 (0.8)	8.29	7.84	6.12	4.47
R100-SF2	5.26 (1.2)	9.18	8.61	6.41	4.64
R30-SF3	7.17 (0.9)	10.24	10.14	9.95	6.6
R70-SF3	6.79 (0.5)	11.19	10.81	10.33	6.98
R100-SF3	5.55 (0.7)	11.52	11.86	10.71	7.53

*Values between parentheses represent the standard deviation.

The load-CMOD, relationships are obtained. The load-CMOD curve is characterized by a number of reference points. The load at the limit of proportionality, F_L, is defined as the maximum load registered up to a CMOD of 0.05 mm. F_1, F_2, F_3 and F_4 are defined as the load values at CMOD of 0.5, 1.5, 2.5, and 3.5 mm, respectively (RILEM, 2002). The results of the tests are often expressed in terms of flexural tensile stress obtained by assuming a linear stress distribution over the mid-span cross section. As such, f_L is the flexural tensile strength derived from F_L, and $f_{R,1}$, $f_{R,2}$, $f_{R,3}$ and $f_{R,4}$ are the respective residual flexural tensile strengths derived from F_1, F_2, F_3 and F_4. The strength corresponding to the limit of proportionality, f_L, and the residual flexural strengths, $f_{R,i}$, are calculated using Equation 2.7 and Equation 2.8.

$$f_L = \frac{3F_L l}{2bh_{sp}^2}$$
<div style="text-align:right">2.7</div>

$$f_{Ri} = \frac{3F_{Ri} l}{2bh_{sp}^2}$$
<div style="text-align:right">2.8</div>

Where l is the prism span length (mm), b is the prism width (mm) and h_{sp} is the distance between the tip of the notch and the top of the specimen (mm).

To characterize the post-cracking behavior of steel fiber-reinforced concrete structures, RILEM TC 162-TDF (2002) recommends calculating the equivalent flexural strengths, f_{eq2} and f_{eq3} using Equation 2.9. These equivalent stresses are related to the material energy absorption capacity up to corresponding deflections of δ_2 and δ_3, where $\delta_2 = \delta_L + 0.65$ mm, $\delta_3 = \delta_L + 2.65$ mm, and δ_L = deflection at F_L. According to RILEM TC 162-TDF (2002), $f_{eq,2}$ and $f_{R,1}$ are used on the design at the serviceability limit state, while $f_{eq,3}$ and $f_{R,4}$ are used on the design at the ultimate limit state.

$$f_{eq,2} = \frac{3}{2} \frac{D^f_{BZ,2}}{0.5} \frac{l}{bh_{sp}^2} \; ; f_{eq,3} = \frac{3}{2} \frac{D^f_{BZ,3}}{2.5} \frac{l}{bh_{sp}^2} \qquad\qquad 2.9$$

Where l is the prism span length (mm), b is the prism width (mm), h_{sp} is the distance between the tip of the notch and the top of the specimen (mm), and $D^f_{BZ,2}$ and $D^f_{BZ,3}$ are portions of the area under the F-δ curve that are attributed to the effect of steel fibers, as explained hereafter.

The energy absorption capacity $D_{BZ,2}$ and $D_{BZ,3}$ are expressed as the area under the load-deflection curve up to deflection δ_2 and δ_3, respectively. They consist of two parts: one part representing the plain concrete expressed as D^b_{BZ} and another signifying the influence of steel fibers expressed as $D^f_{BZ,2}$ and $D^f_{BZ,3}$. As shown in Figure 2.39, the line dividing the pre- and post-cracking zones in the F-δ curve connects the point on the curve corresponding to F_L with another on the abscissa $\delta_L + 0.3$ mm.

The fracture energy, G_F, represents the energy consumed in crack propagation. It is computed by estimating the area under the F–δ curve of the

specimen up to a deflection of 3 mm, as per RILEM TC 50-FMC and Barros & Sena-Cruz (2001). Equation 2.10 is used in the calculation of G_F.

$$G_F = \frac{W_0 + mg\delta_0}{b(h\text{-}a_0)}$$ 2.10

Where W_0 represents the area under the F–δ curve, m is the mass of the specimen, g is the gravitational acceleration, δ_0 is the specified deflection of the specimen (3 mm), b is width of the specimen, h is the height of the specimen and a_0 is the notch height.
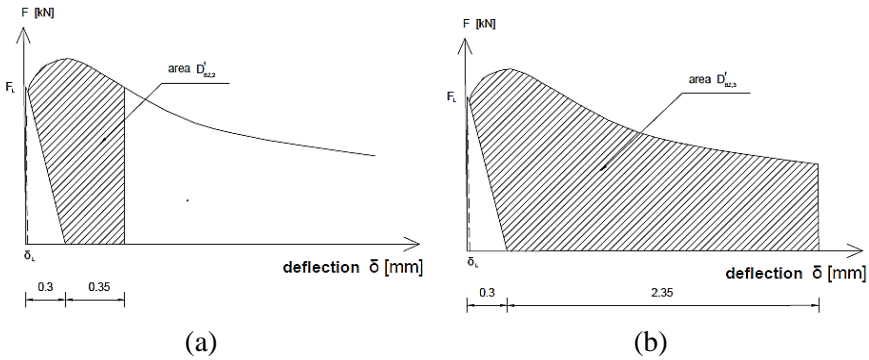

Figure 2.39: Evaluation of equivalent flexural tensile strength parameters: (a) $f_{eq,2}$; (b) $f_{eq,3}$

Results of the equivalent flexural tensile strengths and fracture energy of the specimens tested under three-point bending are summarized in Table 2.11. The plain concrete mixes had no post-peak residual strength. Therefore, their values of $D_{BZ,2}^f$, $D_{BZ,3}^f$, $f_{eq,2}$, and $f_{eq,3}$ were null. Increasing the RCA replacement percentage insignificantly reduced the equivalent flexural strengths. On the other hand, an increase in v_f led to an increase in the equivalent flexural strengths. Indeed, $f_{eq,2}$ and $f_{eq,3}$ of the specimens with steel fibers on average increased by 30 and 75%, with every 1% steel fiber volume fraction. Clearly, the addition of steel fibers had a more prominent effect on

$f_{eq,3}$ than $f_{eq,2}$ than that caused by the inclusion of RCAs. These findings are similar to those reported for the residual flexural strengths.

Table 2.11: Equivalent flexural strengths and energy absorption capacities from three-point bending tests

Mix Designation	$D^f_{BZ,2}$ (kN.mm)	$D^f_{BZ,3}$ (kN.mm)	$f_{eq,2}$ (MPa)	$f_{eq,3}$ (MPa)	W_0 (J)	G_F (N/m)
R0-SF0	-	-	-	-	0.12	60.12
R30-SF0	-	-	-	-	0.16	63.88
R70-SF0	-	-	-	-	0.20	64.79
R100-SF0	-	-	-	-	0.21	64.37
R30-SF1	4.08	11.52	7.81	4.41	13.01	1594.52
R70-SF1	3.42	8.45	6.54	3.23	9.75	1204.97
R100-SF1	3.54	8.61	6.77	3.29	9.76	1204.46
R30-SF2	5.30	19.52	10.14	7.47	21.83	2645.92
R70-SF2	4.64	18.25	8.88	6.98	20.16	2445.34
R100-SF2	4.90	17.92	9.38	6.86	20.11	2438.35
R30-SF3	6.59	29.98	12.61	11.47	33.80	4072.49
R70-SF3	6.37	28.18	12.19	10.78	31.82	3834.94
R100-SF3	5.59	26.40	10.70	10.10	29.76	3588.39

The fracture energy of the plain concrete mixes was insignificantly different. The inclusion of RCAs in plain concrete specimens reduced the peak load but increased the deflection (i.e. the reduction in the peak load was compensated by an increase in the deflection), hence, no change in G_F resulted from the use of RCAs in plain concrete specimens. The inclusion of RCAs affected G_F of the specimens with steel fibers. For concrete specimens with 1% steel fiber v_f, increasing the RCA replacement percentage from 30% to 70% resulted in a reduction in G_F by 24%. Further increase in RCA replacement percentage resulted in an insignificant additional reduction in G_F. For concrete specimens with 2% steel fiber v_f, increasing the RCA replacement percentage from 30% to 70% resulted in a reduction in G_F by 8%. Further increase in RCA replacement percentage resulted in an insignificant additional reduction in G_F. For concrete specimens with 3%

steel fiber v_f, increasing the RCA replacement percentage from 30% to 70% and 100% resulted in a reduction in G_F by 6% and 12%, respectively. The addition of steel fibers remarkably increased G_F. At 30% RCAs, the addition of steel fiber v_f of 1, 2, and 3% resulted in an increase in G_F by 25, 41, and 64 times that of their plain counterpart. At 70% RCAs, the addition of steel fiber v_f of 1, 2, and 3% resulted in an increase in G_F by 19, 38, and 59 times that of their plain counterpart. At 100% RCAs, the addition of steel fiber v_f of 1, 2, and 3% resulted in an increase in G_F by 19, 38, and 56 times that of their plain counterpart.

Three-Point vs Four-Point Bending Tests - In this work, three- and four-point bending tests were used for evaluating the flexural behavior and post-peak strength capacities of steel fiber-reinforced concrete made with RCAs. These tests are characterized by different load locations and specimen geometry. Consequently, the stress redistribution in the mid-span section varies as well. The results from these two tests were used to correlate the flexural behavior of un-notched prisms tested under four-point loading (ASTM C1609) to that of notched prisms tested under three-point loading (RILEM, 2002). The purpose is to provide prediction equations for three-point bending results from those of four-point bending.

Energy measurements from four- and three-point bending are characterized by the area under corresponding load-deflection curves. The flexural toughness, T_{150}^{100} (in J), and fracture energy, G_F (in N/m), calculated based on the ASTM C1609 and RILEM TC 162-TDF, are compared. Nevertheless, since the area under the F-δ curve in three-point bending is actually W_0 (in J), it is also compared to T_{150}^{100}. Figure 2.40(a) presents a linear relationship between W_0 and T_{150}^{100}. The high correlation coefficient ($R^2 =$ 0.97) indicates that it is possible to accurately predict the energy consumed in crack propagation and formation of new cracks in three-point bending (W_0)

from the energy absorption capacity of the four-point bending test specimen (T_{150}^{100}). Indeed, the developed equation (Equation 2.11) shows that the former is nearly half of the latter. Effectively, the un-notched specimen is more ductile than its notched counterpart. A similar relation is developed between G_F and T in the form of Equation 2.12 ($R^2 = 0.97$), as shown in Figure 2.40(b).

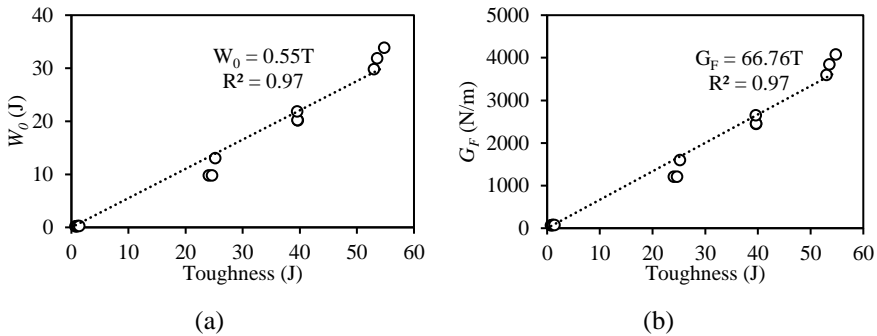$$W_0 = 0.55T_{150}^{100} \qquad\qquad\qquad 2.11$$

$$G_F = 66.76T_{150}^{100} \qquad\qquad\qquad 2.12$$

Figure 2.40: Flexural toughness versus (a) W_0 and (b) G_F

Another series of material characterization tests were conducted on concrete samples taken from the same concrete mixtures used to cast the large-scale deep beam specimens to measure key mechanical properties. Table 2.12 presents the results of the mechanical properties of mixes used to cast the large-scale deep beams. The average values along with the corresponding standard deviation of the 28-day concrete cylinder compressive strength, f'_c, cube compressive strength, f_{cu}, modulus of elasticity, E_c, splitting tensile strength, f_{sp}, and direct uniaxial tensile strength, f_t, are reported in Table 2.12. Figure 2.41 shows the stress-strain responses resulting from the direct uniaxial tensile test on concrete cylindrical specimens. Figure 2.42 illustrates idealized representation of the normalized uniaxial tensile stress-strain response of the steel fiber-reinforced concrete

mixes based on the average of the tested specimens for each mix. Figure 2.43 shows a comparison between the normalized post-peak tensile constitutive law resulting from the inverse analysis of the results of the flexural tests on prisms with the idealized tensile behavior resulting from the direct uniaxial tensile tests.

Table 2.12: Mechanical properties of concrete mixes used to cast the large-scale deep beams

Mixture Designation	f'_c (MPa)	f_{cu} (MPa)	f_{sp} (MPa)	f_t (MPa)	f_r (MPa)	E_c (GPa)
R0-SF0	36.4 ± 1.5	40.5 ± 1.8	3.1 ± 0.2	2.06 ± 0.3	3.41 ± 0.2	34.7 ± 1.8
R100-SF0	23.6 ± 0.4	24.7 ± 1.0	2.1 ± 0.2	1.52 ± 0.1	2.42 ± 0.5	19.8 ± 2.4
R100-SF1	25.8 ± 0.3	32.2 ± 0.6	3.1 ± 0.1	1.75 ± 0.4	4.12 ± 0.4	21.5 ± 2.9
R100-SF2	25.6 ± 1.4	30.0 ± 1.0	3.4 ± 0.2	1.81 ± 0.2	5.38 ± 0.4	20.7 ± 2.5
R100-SF3	25.0 ± 0.8	28.3 ± 0.7	4.1 ± 0.6	1.84 ± 0.1	6.14 ± 0.7	21.1 ± 1.6

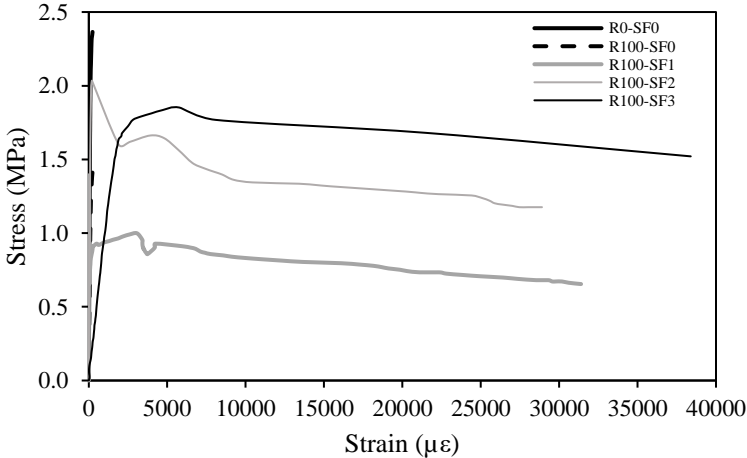*Values between parentheses represent the standard deviation.

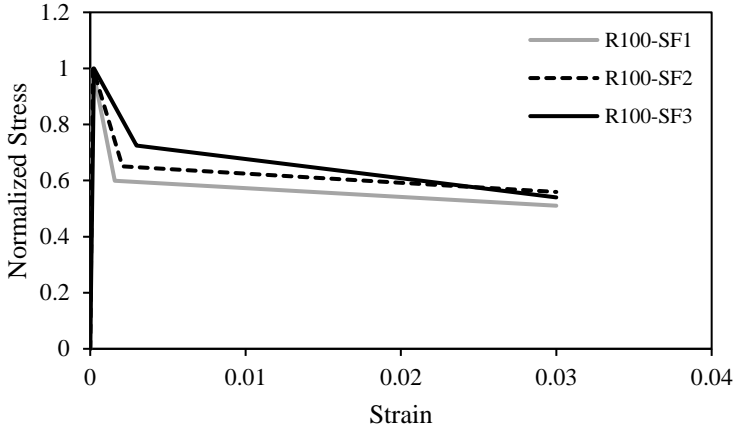Figure 2.41: Representative uniaxial tensile test stress-strain curves

Figure 2.42: Idealization of the normalized uniaxial tensile stress-strain response of mixes with steel fibers
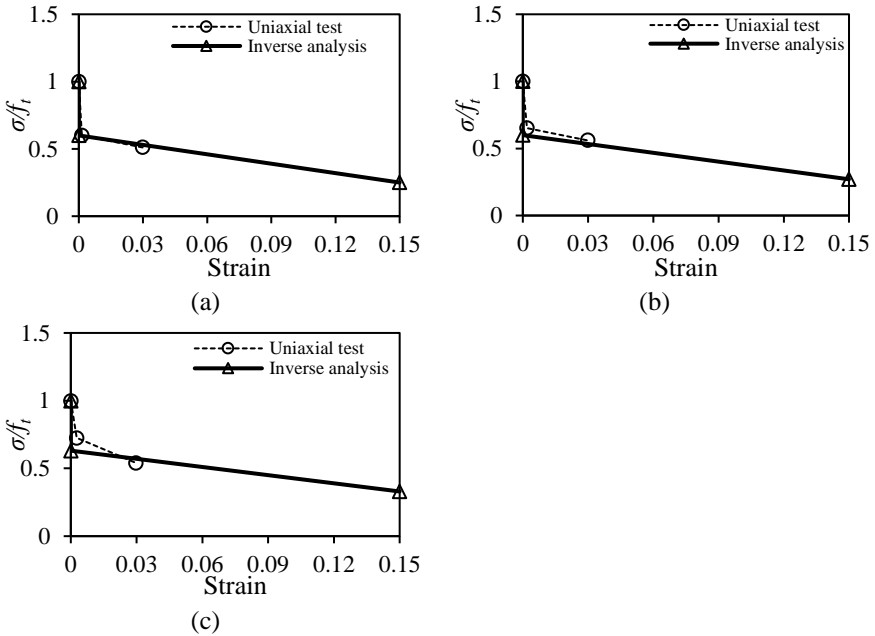

Figure 2.43: Comparison between the tension function obtained from the inverse analysis and that from the direct uniaxial tensile test: (a) R100-SF1; (b) R100-SF2; (c) R100-SF3

2.3.1.3 Durability Properties

Water Absorption and Sorptivity - Water absorption and sorptivity (rate of absorption) tests can be used as an indirect evaluation of the concrete porosity and probable future durability of concrete (Sanal, 2018). Results of water absorption and sorptivity tests are presented in Table 2.13. The NA-based control specimen (R0-SF0) exhibited the lowest water absorption and sorptivity of 5.72% and 0.023 mm/√s, respectively. The substitution of NAs by 30, 70, and 100% RCAs increased the water absorption by 37, 55, and 65%, and the sorptivity rate by 6, 19, and 27%, respectively. The increased water absorption of the mixes with RCAs can be ascribed to the porous structure of the mortar adhered to the RCAs, which may have provided extensive void sites, thus causing an increase in water absorption. The addition of steel fibers at v_f of 1, 2 and 3% reduced the water absorption by 6, 16 and 22%, respectively, relative to those of their counterparts' mixes made with RCAs without steel fibers. It seems that the inclusion of steel fibers in concrete mixtures densified the concrete matrix, and thus reduced the water absorption.

Table 2.13: Water absorption, initial rate of water absorption bulk resistivity and UPV results

Mix Designation	Water Absorption (%)	Initial Sorptivity (mm/√s)	Bulk Resistivity[1] (kΩ.cm)	UPV[2] (m/s)
R0-SF0	5.72	0.023	6.3 (moderate)	4831 (Excellent)
R30-SF0	7.83	0.030	4.4 (low)	3167 (Medium)
R70-SF0	8.90	0.037	4.0 (low)	2353 (Doubtful)
R100-SF0	9.41	0.040	3.8 (low)	2222 (Doubtful)
R30-SF1	7.30	0.029	-	3589 (Good)
R70-SF1	8.40	0.034	-	2898 (Doubtful)
R100-SF1	8.80	0.038	-	2703 (Doubtful)
R30-SF2	6.40	0.025	-	4000 (Good)
R70-SF2	7.30	0.029	-	3300 (Medium)
R100-SF2	8.30	0.033	-	2989 (Doubtful)
R30-SF3	5.98	0.022	-	4348 (Good)
R70-SF3	6.80	0.026	-	3800 (Good)
R100-SF3	7.70	0.030	-	3456 (Medium)

[1]Classification based on ACI-222R-01 (2008).
[2]Classification based on BS 1881: Part 203 standard.

The values of the rate of water absorption are plotted against the square root of the time in Figure 2.44. The slope of the sorptivity curve was higher for the first 30 minutes (42 $s^{0.5}$) than that over the remaining exposure time. This is mainly attributed to the respective filling of large and small pores at early and late stages. An increase in RCA replacement percentage in plain concrete mixes resulted in a higher water absorption and also yielded higher slopes [Figure 2.44(a)]. The slopes and total absorption decreased with an increase in the steel fiber volume fraction as shown in Figure 2.44(b-d). It is believed that steel fibers occupy the relatively larger void space in the concrete structure, hence, reducing the rate of water absorption. Nevertheless, the water absorption values of all mixes with steel fibers, except R30-SF3, were still higher than that of the control mix made with NAs. Only mix R30-SF3 had had water absorption and sorptivity values almost equal to those of R0-SF0.
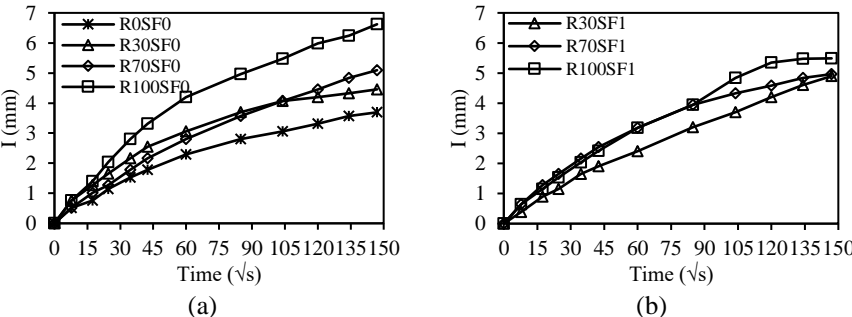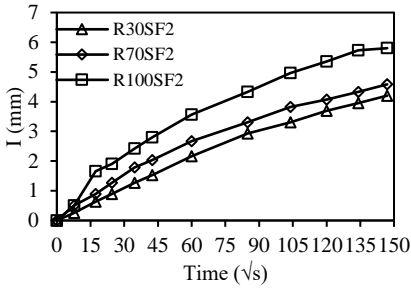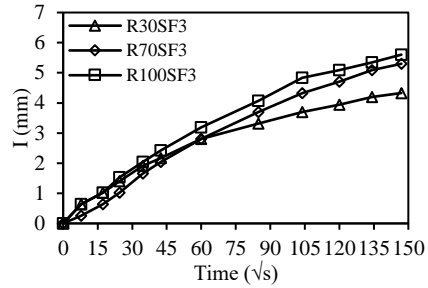

Figure 2.44: Capillary sorptivity of concrete mixes over time: (a) Plain mixes; (b) mixes with $v_f = 1\%$; (c) mixes with $v_f = 2\%$; (d) mixes with $v_f = 3\%$

Figure 2.44: Capillary sorptivity of concrete mixes over time: (a) Plain mixes; (b) mixes with $v_f = 1\%$; (c) mixes with $v_f = 2\%$; (d) mixes with $v_f = 3\%$ (continued)

Abrasion Resistance - Figure 2.45 shows the abrasion resistance of the concrete mixes. Plain concrete specimens with 30, 70, and 100% RCAs exhibited 2, 8, and 36% increases in the abrasion mass loss, respectively. This behavior is associated to the weaker abrasion resistance of the RCAs compared to the NAs, and the inferior hardened properties of the RCA-based concrete specimens compared to those of the NA-based control specimen. The addition of steel fibers considerably improved the abrasion resistance of the concrete specimens made with RCAs, as manifested by the significant reduction in their abrasion mass loss relative to those of their plain RCA-based counterparts. For concrete mixes with a 30% RCA replacement percentage, increasing the steel fiber volume fraction from 1 to 3% did not result in a further increase in the abrasion resistance. An average reduction of 47% in the abrasion mass loss was recorded for these specimens compared to that of the plain RCA-based counterparts, irrespective of steel fiber content. The addition of steel fibers at v_f of 1%, 2% and 3% to the mixes with 100% RCAs resulted in respective reductions of 27, 40 and 47% in the abrasion mass loss compared to that of their plain RCA-based counterparts. The improved abrasion resistance of the specimens with steel fibers can be attributed to the improved tensile properties of the corresponding concrete mixtures.
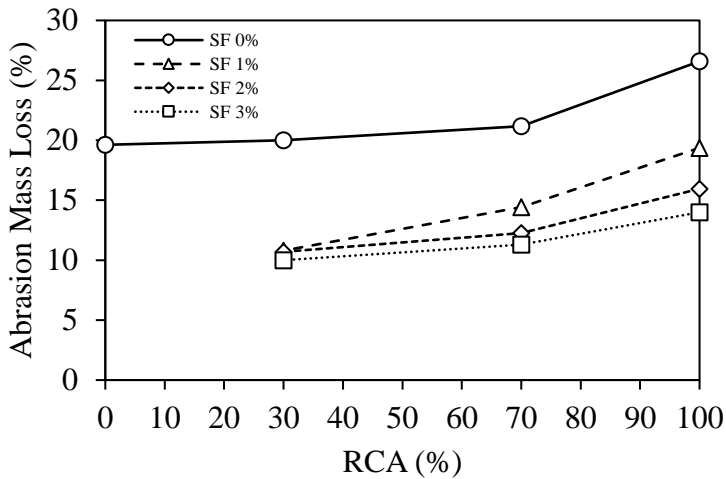
Figure 2.45: Effect of RCAs and steel fiber (SF) percentages on the abrasion resistance of concrete

Bulk Resistivity - Results of bulk resistivity tests are also given in Table 2.13. The steel fibers are electrically conductive materials, hence, bulk resistivity results of the specimens with steel fibers could be misleading. As such, only plain mixes with and without RCAs were considered in this experiment. The bulk resistivity values ranged between 3.8 and 6.3 kΩ.cm. The bulk resistivity value is an indication of corrosion protection. Based on ACI 222R-01 (2008), the resistivity value of the control mix R0-SF0 indicated a moderate corrosion protection. The replacement of NAs with RCAs reduced the resistivity value which changed the classification to low corrosion protection. The bulk resistivity of concrete was affected by the presence of RCAs. In fact, 30, 70, and 100% RCA replacement percentages led to 30, 36, and 40% reductions in the bulk resistivity, respectively, compared with that of the NA-based concrete specimen. This behavior can be attributed to the porous surface of the RCAs, in addition to the weak interface zone between the old and new cement paste, which may have resulted in a larger amount of pores in the RCA concrete mixes, thus causing

a higher water absorption. The mix with 30% RCAs exhibited a 30% reduction in the bulk resistivity. Higher RCA replacement percentages of 70% and 100% further reduced the bulk resistivity. The reduction in the bulk resistivity was almost proportional to the RCA replacement percentage.

Ultrasonic Pulse Velocity - The results of the UPV test conducted on concrete specimens at the age of 28 days are summarized in Table 2.13. Results ranged between 2222 and 4831 m/s with lowest and highest velocities recorded for the 100% RCA plain concrete and NA-based control mixes, respectively. For plain RCA-based concrete mixes, RCA replacements of 30, 70 and 100% resulted in 34, 51 and 54% respective reductions in the velocity relative to that of the NA-based control specimen. Such a reduction is a direct indication of the increased voids in specimens with RCAs. The addition of steel fiber v_f of 1, 2, and 3% to concrete mixtures made with 30% RCAs, resulted in an increase in UPV by 13%, 26% and 37%, respectively, compared to that of their plain counterpart. The addition of steel fiber v_f of 1, 2, and 3% to concrete mixtures made with 70% RCAs, resulted in an increase in UPV by 23%, 40% and 61%, respectively, compared to that of their plain counterpart. The addition of steel fiber v_f of 1, 2, and 3% to concrete mixtures made with 100% RCAs, resulted in an increase in UPV by 22%, 35% and 56%, respectively, compared to that of their plain counterpart. The BS 1881: Part 203 classified concrete specimens based on the UPV values. The control specimen R0-SF0 is classified as "excellent". The replacement of 30% of NAs with RCAs changed the classification to "medium". Higher RCA replacement percentages resulted in a "doubtful" classification. The addition of a minimum of 1% of steel fiber volume fraction improved the quality of the mixes with 30% of RCA replacement percentage, hence, these mixes were classified as "good". Mixes made with 70% of RCA replacement percentage needed a minimum of 2% of steel fiber volume fraction to achieve a "medium" classification. However, mixes made with 100% of RCA

replacement percentage needed a minimum of 3% of steel fiber volume fraction to achieve a "medium" classification. It should be noted that, despite being discrete, the presence of steel fibers may affect the results of the UPV test.
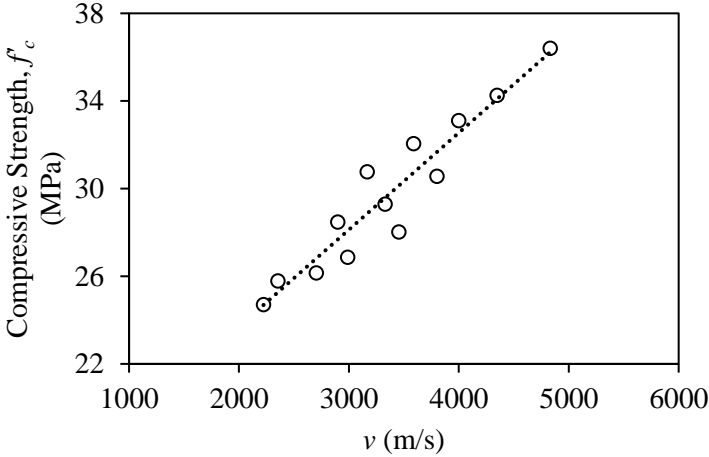

Figure 2.46: Relationship between UPV and f'_c

The UPV test results were correlated to the 28-day cylinder compressive strength, so that strength may be estimated through a non-destructive test method. As shown in Figure 2.46, a strong linear correlation exists between these two properties with a correlation coefficient, R^2, value as high as 0.91. Equation 2.13 presents the proposed linear regression equation to predict f'_c (MPa) using the velocity, v (m/s), values. It is clear that a denser concrete mix, characterized by a higher UPV value, leads to a higher compressive strength. Equation 2.13 is applicable in the range of f'_c of the mixtures examined in the current study.

$$f'_c = 0.0044v + 14.85 \qquad 24 \leq f'_c \leq 37\ MPa \qquad\qquad 2.13$$

2.3.2 Shear Behavior of Solid RC Deep Beams made with RCAs and Steel Fibers

The shear behavior of the tested solid deep beams is evaluated in this section. Results of the solid deep beam tests include the shear load-deflection response, shear cracking load, shear capacity, crack pattern, failure mode, and strain measurements.

2.3.2.1 Experimental Results

2.3.2.1.1 Shear Load-Deflection Response

The shear load-deflection responses of the tested solid beams are depicted in Figure 2.47. The shear load is the support reaction, and the reported deflection is located at the midspan. Specimens SR0-SF0 and SR100-SF0 without traditional shear reinforcement exhibited a load decay at the onset of shear cracking followed by a significant change in slope of the deflection response. Conversely, specimens SR0-SF0-S and SR100-SF0-S, with traditional shear reinforcement, exhibited a quasilinear response till the peak load. The RCA-based specimens SR100-SF0 and SR100-SF0-S exhibited a lower stiffness than those of their NA-based counterparts SR0-SF0 and SR0-SF0-S, respectively. The reduction in the beam stiffness was less pronounced in the presence of traditional shear reinforcement. The RCA-based specimens reached their shear capacity at midspan deflections higher than those of their NA-based counterparts. The increase in the deflection of RCA-based beams can be attributed to the lower Young's modulus of the RCA-based concrete mixtures and the porosity of RCA used (Kachouh et al., 2019; Kachouh et al., 2020).

The beams with steel fibers did not exhibit a load decay or a significant change in slope at the onset of shear cracking which improved the beams stiffness relative to that of SR100-SF0 made with RCAs without steel fibers. The midspan deflection values at shear cracking loads of the RCA-

based specimens with steel fibers were higher than those of the beams without fibers and further increased by increasing the fiber volume fraction.
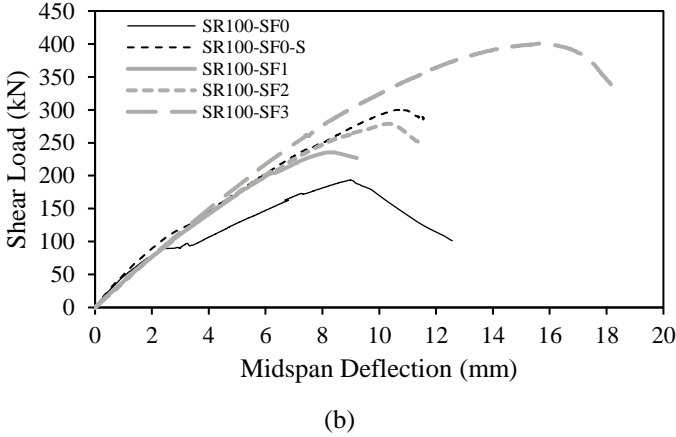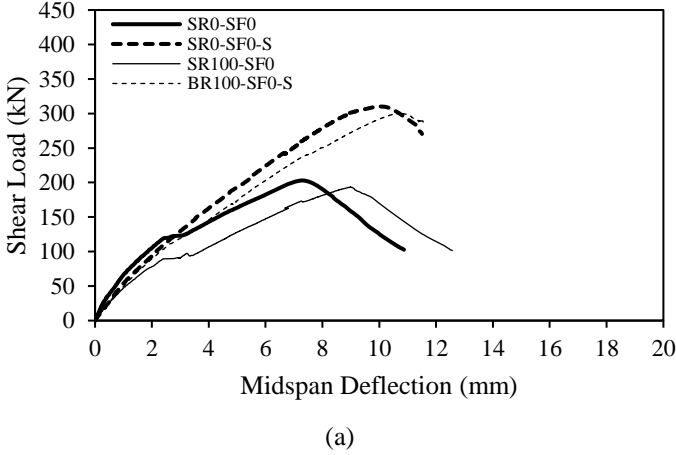

(a)

(b)

Figure 2.47: Shear load-deflection response: (a) Beams without steel fibers; (b) RCA-based beams with and without steel fibers

The shear cracking load, V_{cr}, and shear capacity, V_{max}, along with their corresponding deflections, Δ_{cr} and Δ_{max}, respectively, are reported in Table 2.14. The shear cracking load, V_{cr}, is defined as the load at which the first visible shear crack appears in the shear span. The shear cracking load and capacity of the RCA-based specimen SR100-SF0 were 25 and 5% lower

than those of SR0-SF0, respectively. The impact of using a 100% RCA rather than NAs was less significant in the presence of traditional shear reinforcement since only 12 and 2% reductions in the shear cracking load and capacity were recorded, respectively. The negligible shear strength reduction observed in the present study for the RCA-based beam with internal shear reinforcement is consistent with that reported in the literature for beams with internal steel stirrups having a/h of 2.5 (Chaboki et al., 2019). The reductions in the shear cracking load and capacity of the RCA-based specimens can be attributed to the inferior mechanical properties of the RCA-based mixture.

Table 2.14: Summary of test results

Specimen	Shear Cracking Stage		Ultimate Stage		Gain in Shear Capacity [*]
	V_{cr} (kN)	Δ_{cr} (mm)	V_{max} (kN)	Δ_{max} (mm)	
SR0-SF0	120	2.6	203	7.3	-
SR0-SF0-S	136	3.2	309	10.3	-
SR100-SF0	90	2.9	193	9.0	-
SR100-SF0-S	120	3.2	300	10.7	55%
SR100-SF1	160	4.6	235	8.3	22%
SR100-SF2	180	5.2	271	10.4	40%
SR100-SF3	250	7.1	401	15.8	108%

*With respect to the shear capacity of SR100-SF0

Table 2.14 also shows that the inclusion of steel fibers in the RCA-based beams resulted in a remarkable increase in their shear cracking load to a level even higher than that of the NA-based specimen SR0-SF0-S with traditional shear reinforcement. The shear capacity of the RCA-based beams with steel fibers was also improved. Specimens SR100-SF1, SR100-SF2, and SR100-SF3 exhibited shear capacity gains of 22, 40, and 107%, respectively, relative to that of SR100-SF0 without fibers. The increase in shear capacity can be attributed to the improved post-cracking resistance of the steel fiber-reinforced specimens and their ability to restrict crack propagation and growth. The shear capacities of SR100-SF1 and SR100-SF2 were approximately 80 and 90% of that of specimen SR100-SF0-S with traditional

shear reinforcement, respectively. Specimen SR100-SF3 with v_f of 3% exhibited a shear capacity even higher than those of SR0-SF0-S and BR100-SF0-S having traditional shear reinforcement.

2.3.2.1.2 Crack Pattern

Figure 2.48 shows the crack patterns observed at failure. All beams failed in shear as planned in the design to prevent a flexural mode of failure and allow the beam to develop its full shear capacity. All beams experienced an inclined shear crack at the mid-height of the shear span that propagated toward the load and support points. Additional cracks developed in the shear spans as the load progressed. Specimens SR0-SF0 and SR100-SF0 did not include traditional shear reinforcement nor steel fibers also exhibited splitting cracks in the shear span parallel to the longitudinal steel reinforcing bars. Specimen SR0-SF0 failed by crushing of concrete at the top part of the diagonal concrete strut in the west shear span. Specimen SR100-SF0 failed in a shear-compression mode of failure. The two specimens SR0-SF0-S and SR100-SF-S having traditional shear reinforcement without steel fibers exhibited a band of multiple cracks within the shear span, then eventually failed due to crushing of the concrete along the diagonal concrete strut. Specimen SR100-SF1 with v_f of 1% failed due to fracture of concrete across the major diagonal crack developed in the shear span accompanied by crushing of the top and bottom parts of the diagonal strut. Specimens SR100-SF2 and SR100-SF3 with v_f of 2 and 3%, respectively, failed due to crushing of the diagonal concrete strut in the shear span.
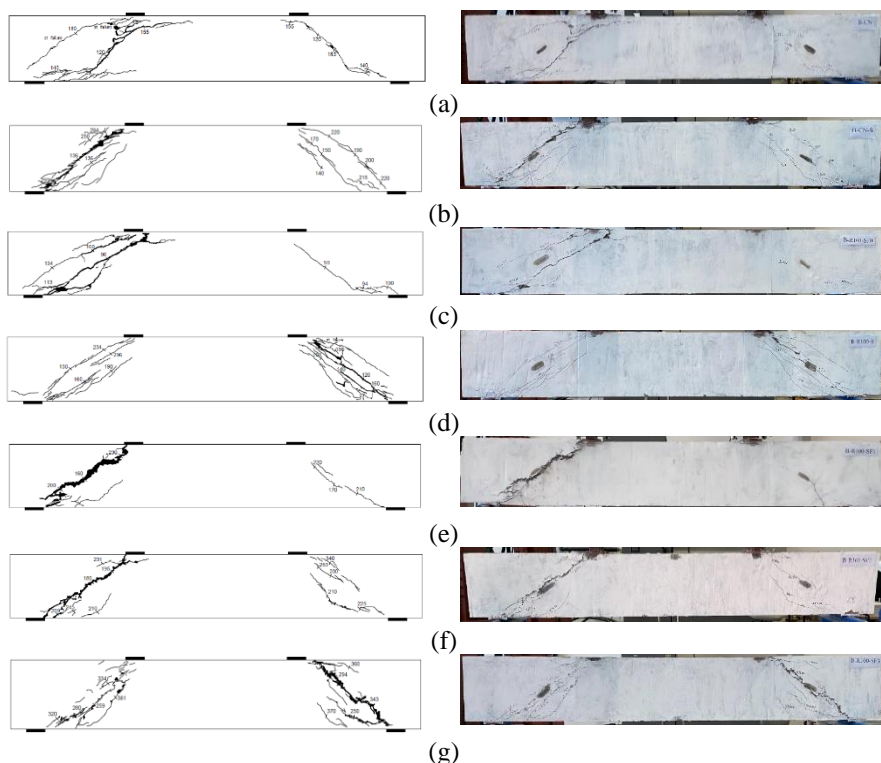
(a)

(b)

(c)

(d)

(e)

(f)

(g)

Figure 2.48: Crack pattern at failure: (a) SR0-SF0; (b) SR0-SF0-S; (c) SR100-SF0; (d) SR100-SF0-S; (e) SR100-SF1; (f) SR100-SF2; (g) SR100-SF3

2.3.2.1.3 Stirrup Strains

The relationships between the shear load and the maximum measured stirrup strains are illustrated in Figure 2.49. The stirrup strain profile can be divided into two or three phases depending on whether stirrups have yielded or not. The first phase represents the pre-cracking stage, while the second phase signifies the post-cracking stage, i.e., from shear crack initiation to stirrup yielding or beam failure. The third phase occurs only in the case of yielded stirrups, i.e., the post-yielding phase. The rate of increase of the stirrup strain of specimens SR0-SF0-S and SR100-SF0-S was insignificantly different. Only one vertical stirrup in specimen SR0-SF0-S exhibited a lower rate of stirrup strain than that experienced by other stirrups. The variation in

the rate of increase of stirrup strains may be ascribed to the location of SG with respect to the location of the shear cracks. Strain gauges that are intersected by major shear cracks are expected to exhibit higher strains than those away from the cracks. Strain measurements confirmed the yielding of shear reinforcement at different locations in specimens SR0-SF0-S and SR100-SF0-S prior to failure.
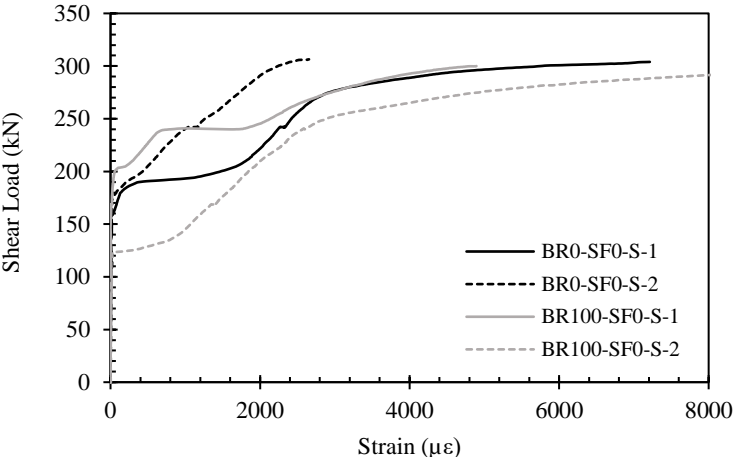

Figure 2.49: Shear load versus maximum stirrup strain relationships

2.3.2.1.4 Tensile Steel Strains

The tensile steel strain profiles of representative specimens at four different loading stages: 25, 50, 75, and 100% of the shear capacity, are shown in Figure 2.50, whereas the maximum measured tensile steel strains at the shear capacity are presented in Table 2.15. It is evident that the steel strains in all beams were less than the yield strain as planned in the design (ε_{yield} = 2695 με). The specimens exhibited almost a uniform steel strain profile within the shear span which confirmed the occurrence of the deep beam action.
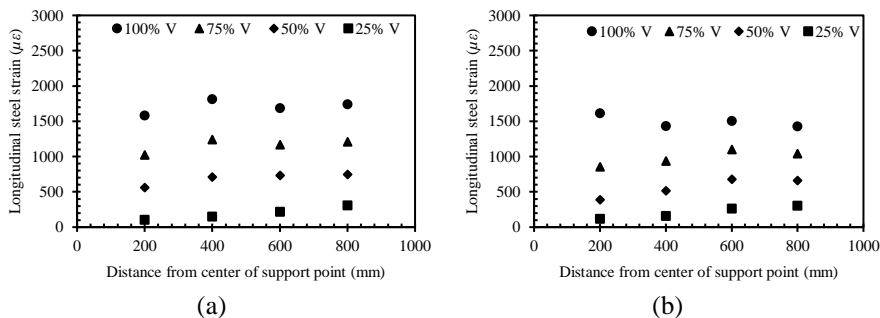
Figure 2.50: Steel strain profile: (a) SR0-SF0-S; (b) SR100-SF2

2.3.2.1.5 Concrete Strains

The maximum longitudinal and diagonal concrete strains measured at the shear capacity are reported in Table 2.15. It can be seen that the RCA-based control specimens SR100-SF0 and SR100-SF0-S exhibited higher maximum diagonal concrete strains compared to those of the NA-based control specimens SR0-SF0 and SR0-SF0-S, respectively, possibly because of the reduced Young's modulus of the RCA-based concrete. This behavior was less evident for the longitudinal concrete strains of the counterpart specimens. The maximum longitudinal concrete strains at the shear capacity of the specimens with traditional shear reinforcement were insignificantly different than those of their counterparts without shear reinforcement, except for the longitudinal concrete strain values of the counterpart specimens SR100-SF0 and SR100-SF0-S, which showed higher strains at the shear capacity in the presence of stirrups.

The RCA specimens with steel fibers exhibited higher maximum longitudinal concrete strains at the shear capacity than that of the control RCA-based specimen SR100-SF0. Their diagonal concrete strains at the shear capacity were higher than those of all other specimens. Specimen SR100-SF3 with v_f of 3% exhibited the highest longitudinal and diagonal concrete strain values at the shear capacity. The higher concrete strain values

exhibited by the steel fiber-reinforced RCA specimens can be ascribed to the confinement effect provided by the steel fibers and their ability to increase the strain capacity of the diagonal strut.

Table 2.15: Strain measurements at shear capacity

Specimen	Concrete Strain (με)		Max. longitudinal Steel Strain ε_s (με)	$\varepsilon_s/\varepsilon_y$
	Max. longitudinal strain	Max. diagonal strain		
SR0-SF0	2125	400	1100	0.41
SR0-SF0-S	1850	425	1812	0.67
SR100-SF0	1400	730	2427	0.90
SR100-SF0-S	2090	815	1991	0.74
SR100-SF1	1650	1150	1689	0.63
SR100-SF2	1670	1130	1613	0.60
SR100-SF3	3150	2280	2301	0.85

2.3.2.1.6 Analytical Prediction

The shear capacities predicted analytically based on published models are compared to those obtained from the tests in Table 2.16. The analytical approach of Narayanan & Darwish (1987) provided reasonable predictions for the shear capacity of the tested beams, except BR100-SF1 and BR100-SF2, where their shear capacities were overestimated by 17 and 26%, respectively. The analytical approach by Ashour et al. (1982) provided conservative predictions for the shear capacity of all of the tested beams, except BR100-SF2, where its shear capacity was overestimated by 14%. The deviation between predicted and experimental results was more significant for the beams without steel fibers. The model by Ashour et al. (1982) computes the contribution of the plain concrete to the shear resistance as function of the concrete compressive strength, f'_c, rather than the splitting tensile strength, f_{sp}. This fact may explain why the model by Ashour et al. (1982) tended to provide conservative predictions for the shear capacity. The model by Kwak et al. (2002) overestimated the shear capacity of the majority of the tested beams.

The difference between experimental results and those predicted by the models is considered within the typical margin of error considering the variability in shear test results. As such, it can be concluded that the three analytical models can provide reasonable predictions for the nominal shear capacity of the solid RC deep beams tested in the present study.

Table 2.16: Comparison between analytical and experimental results of the solid beams

Specimen	Experimental Results V_{max} (kN)	Analytical Results V_n (kN)			Ratio (V_n/V_{max})		
		Narayanan and Darwish	Ashour et al.	Kwak et al.	Narayanan and Darwish	Ashour et al.	Kwak et al.
SR0-SF0	203	218	169	258	1.07	0.83	1.27
SR0-SF0-S	309	305	256	345	0.99	0.83	1.12
SR100-SF0	193	192	146	200	0.99	0.76	1.04
SR100-SF0-S	300	280	233	286	0.93	0.78	0.95
SR100-SF1	235	275	230	287	1.17	0.98	1.22
SR100-SF2	271	341	310	332	1.26	1.14	1.23
SR100-SF3	401	416	389	398	1.04	0.97	0.99

2.3.2.2 Numerical Prediction and Model Verification of Solid Beams

2.3.2.2.1 Shear Load-Deflection Response

The shear load-deflection curves of the solid RC deep beam models are illustrated in Figure 2.51. The response of the deep beam models made with 100% RCAs without steel fibers was inferior to that of their counterparts made with NAs [Figure 2.51(a)]. The addition of steel fibers remarkably improved the shear capacity and stiffness of the RCA-based models [Figure 2.51(b)]. The stiffness of model SR100-SF2, with $v_f = 2$ %, coincided with that SR100-SF0-S having steel stirrups, while that of model SR100-SF3, with $v_f = 3$%, was superior to that of SR100-SF0-S. These findings are in agreement with those obtained from the experiments. The load-deflection responses predicted numerically are compared to those obtained experimentally in Figure 2.52. It is evident that the models predicted the response of the tested beams with good accuracy.
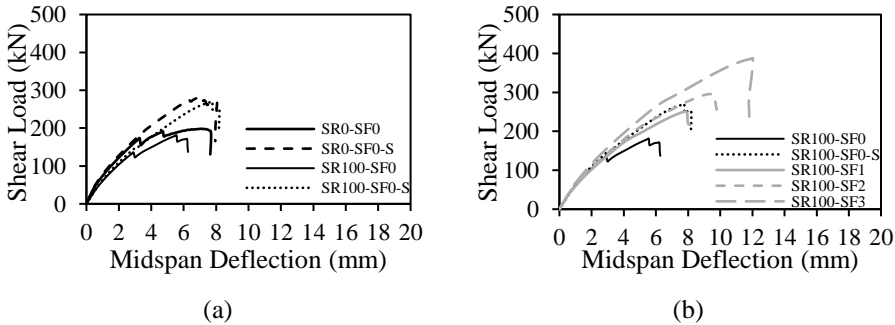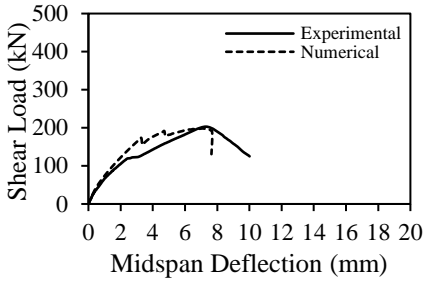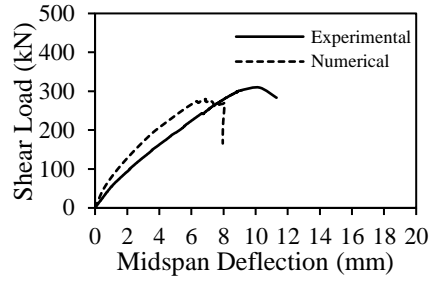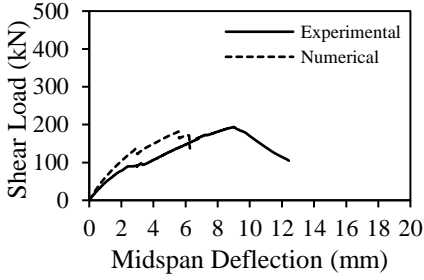

Figure 2.51: Numerical shear load-deflection response: (a) Beams without steel fibers; (b) RCA-based beams with and without steel fibers
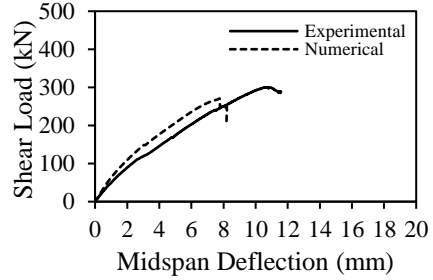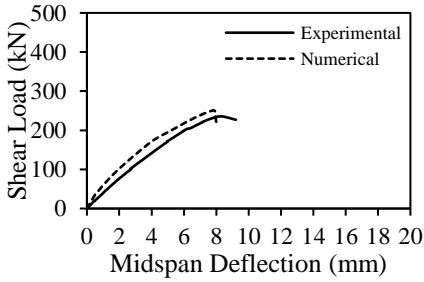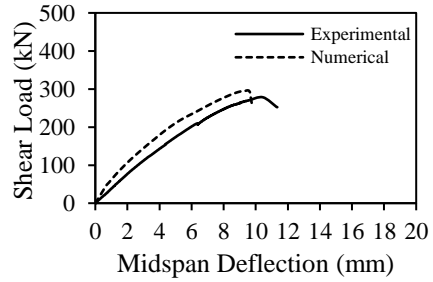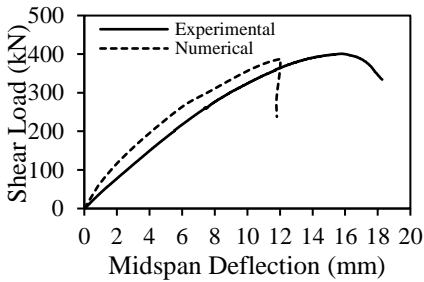
Figure 2.52: Numerical and experimental load-deflection responses: (a) SR0-SF0; (b) SR0-SF0-S; (c) SR100-SF0; (d) SR100-SF0-S; (e) SR100-SF1; (f) SR100-SF2; (g) SR100-SF3

Table 2.17: Comparison between numerical and experimental results

Model	Shear Capacity		Deflection Capacity		V_{FE}/V_{EXP}	Δ_{FE}/Δ_{EXP}
	V_{EXP} (kN)	V_{FE} (kN)	Δ_{EXP} (mm)	Δ_{FE} (mm)		
SR0-SF0	203	198	7.3	7.1	0.98	0.97
SR0-SF0-S	309	280	10.3	8.0	0.91	0.78
SR100-SF0	193	181	9.0	6.2	0.94	0.69
SR100-SF0-S	300	270	10.7	8.2	0.90	0.77
SR100-SF1	235	251	8.3	7.9	1.07	0.95
SR100-SF2	271	296	10.4	9.5	1.09	0.91
SR100-SF3	401	387	15.8	12.0	0.97	0.77
Average					0.98	0.83
Std Dev					0.07	0.10
COV (%)					7.03	11.95

The experimental and numerical shear capacities, V_{EXP} and V_{FE}, respectively, along with the deflections at failure, Δ_{EXP} and Δ_{FE}, are compared in Table 2.17. The difference between the numerical and experimental shear capacities was within 10% only. The ratio of V_{FE}/V_{EXP} was on average 0.98 with a corresponding standard deviation and coefficient of variation of 0.07 and 7%, respectively. The FE models insignificantly underestimated the beam deflection. The ratio of Δ_{FE}/Δ_{EXP} was on average 0.83 with a standard deviation of 0.10 and a coefficient of variation of 12%. Generally, the difference between numerical and experimental results could be due to a variation between actual properties of materials of the tested large-scale deep beams and those obtained from characterization test samples used as input data in the analysis. The difference between numerical and experimental results can be considered within the expected margin of error.

2.3.2.2.2 Crack Pattern

The crack patterns of the solid deep beams captured numerically are shown in Figure 2.53 (a). The minimum width of the displayed crack in FE models was set to be 0.1 mm. The deep beam models SR0-SF0 and SR100-SF0 exhibited initially an inclined shear crack in the shear span. At failure,

the models exhibited an additional shear crack in the shear span in addition to longitudinal splitting cracks parallel to the tension steel. The deep beam models with stirrups, SR0-SF0-S and SR100-SF0-S, showed a band of shear cracks in the shear span prior to failure. The steel fibers played a role similar to that of the steel stirrups and prevented the formation of longitudinal splitting cracks. The deep beam models with steel fibers failed in a diagonal compression model of failure.

The minimum principal concrete strain of the deep beam models prior to failure are shown in Figure 2.53 (b). The profile of the minimum principal concrete strain indicated the formation of a bottle-shaped strut in the shear span of the deep beam models with steel stirrups and a prismatic strut for the models with steel fibers. Photographs of the tested beams at failure are shown in Figure 2.53 (c). The crack patterns obtained from the tests, shown in Figure 2.53 (c), verified the formation of a band of shear cracks in the shear span of the deep beams with steel stirrups and concertation of inclined shear cracks along the natural load path of the beams with steel fibers. It should be noted that the deep beam models without steel fibers exhibited similar values of minimum principal concrete strain of approximately -0.006 to –0.008 prior to failure. The models with steel stirrups failed, however, at a higher shear capacity than that of their counterparts without stirrups, signifying the role of stirrups in reducing the rate of increase of the minimum principal concrete strain. The deep beam models with steel fibers exhibited minimum principal concrete strain values of approximately -0.006 to -0.01 at peak load but failed at a higher load relative to that of their counterparts without stirrups. The increased shear capacity of the steel-fiber reinforced models signified the effectiveness of the steel fibers in reducing the rate of in-crease of the minimum principal concrete strains.

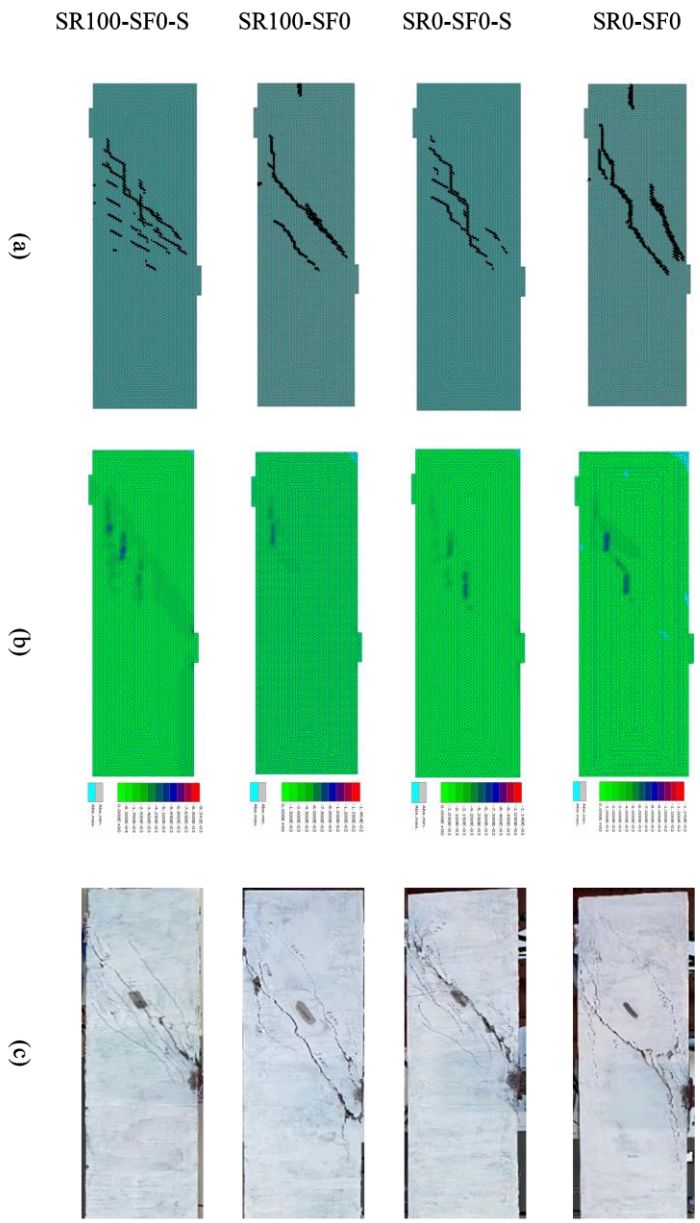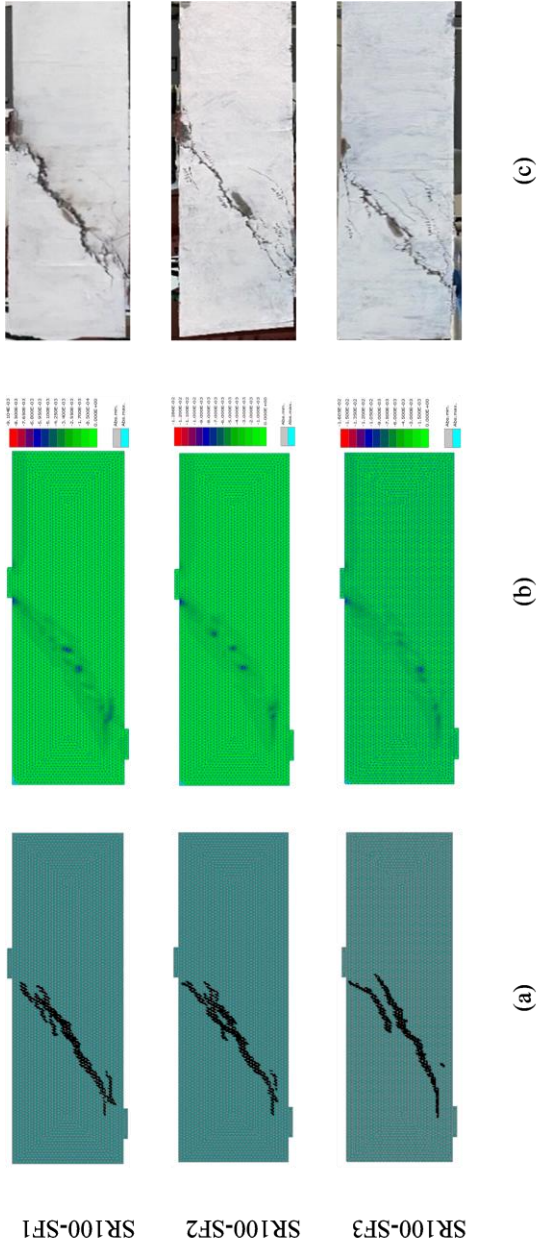SR100-SF0-S   SR100-SF0   SR0-SF0-S   SR0-SF0

(a)   (b)   (c)

Figure 2.53: Crack patterns and principal strains of group S: (a) Numerical crack patterns; (b) Minimum principal strains; (c) Experimental crack patterns

Figure 2.53: Crack patterns and principal strains of group S: (a) Numerical crack patterns;; (b) Minimum principal strains; (c) Experimental crack patterns (continued)

2.3.2.2.3 Stirrup Strains

The numerical stirrup strain responses of the model SR0-SF0-S are compared to those measured experimentally in the west and east shear spans in Figure 2.54 (a) and Figure 2.54 (b), respectively. Readings of SG-V2 were not captured experimentally in the east shear span due to malfunction of the SG. It should be noted that predicted strains of SG-V1 and SG-V2 were identical. Similarly, the rate of increase of the stirrup strain in the vertical stirrups recorded experimentally were insignificantly different, as shown in Figure 2.54 (a). Numerical data of the model SR0-SF0-S indicated failure of the beam without yielding of stirrups. This behavior was in alignment with the experimental data, expect in one location (SG-V1) in the west shear span. Numerical results indicated that no strains were recorded in the stirrups in the pre-cracking stage. Following shear cracking, the stirrup strains in-creased almost linearly until the model reached its shear capacity. This behavior was in agreement with the stirrup strains measured in the west and east shear spans as shown in Figure 2.54 (a) and Figure 2.54 (b).

The numerical stirrup strain responses of the model SR100-SF0-S are compared to those measured experimentally in the west and east shear spans in Figure 2.55 (a) and Figure 2.55 (b), respectively. The vertical stirrups in the model SR100-SF0-S made with RCAs exhibited higher strains than those exhibited by the horizontal stirrups, indicating more contribution to the shear resistance. Similarly, the vertical stirrup strains obtained from the tests tended to be higher than those of the horizontal stirrups in the west and east shear spans as shown in Figure 2.55 (a) and Figure 2.55 (b), respectively. The strain in the vertical stirrup of model SR100-SF0-S predicted numerically at peak load exceeded the yielding strain. Experimental results verified yielding of SG-V1 and SG-V2 in the west shear span (Figure 11a) and SG-V2 in the east shear span [Figure 2.55 (b)] prior to failure. The numerical results show that

the vertical stirrup strains of model SR100-SF0-S increased at a higher rate than that of SR0-SF0-S, indicating less contribution of RCAs to the shear resistance. This behavior was less evident in the experimental results that showed no significant difference in the rate of increase of the stirrup strains of the two tested beams, SR0-SF0-S and SR100-SF0-S.
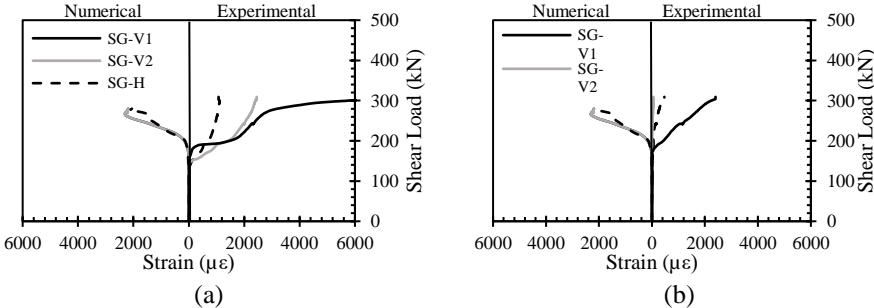

Figure 2.54: Numerical and experimental stirrup strain response of SR0-SF0-S: (a) West shear span; (b) East shear span
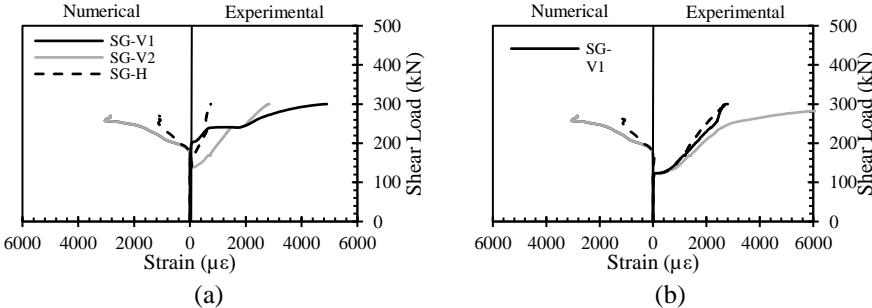

Figure 2.55: Numerical and experimental stirrup strain response of SR100-SF0-S: (a) West shear span; (b) East shear span

2.3.2.2.4 Tensile Steel Strains

The numerical and experimental tensile steel strain responses of the solid RC deep beam models are presented in Figure 2.56. The monitoring point of SG1 was located at a distance 125 mm away from the face of the support plate, whereas that of SG4 was under the load point. Other monitoring

points, SG2 and SG3, were located in between SG1 and SG4 at a spacing of 200 mm. The numerical and experimental steel strain responses showed a similar trend. The steel strain responses of the deep beam models SR0-SF0 and SR100-SF0 exhibited load decays due to development of shear cracks. No load decays occurred in the deep beam models with steel stirrups or steel fibers. The strains predicted numerically at SG1, which was close to the support, were lower than those recorded at other locations in all models. In agreement with the experimental results, the steel strains in other locations within the shear span were insignificantly different, verifying the arch action effect in all models. The tensile steel reinforcement did not reach the yielding strain in any of the models, which was verified experimentally.
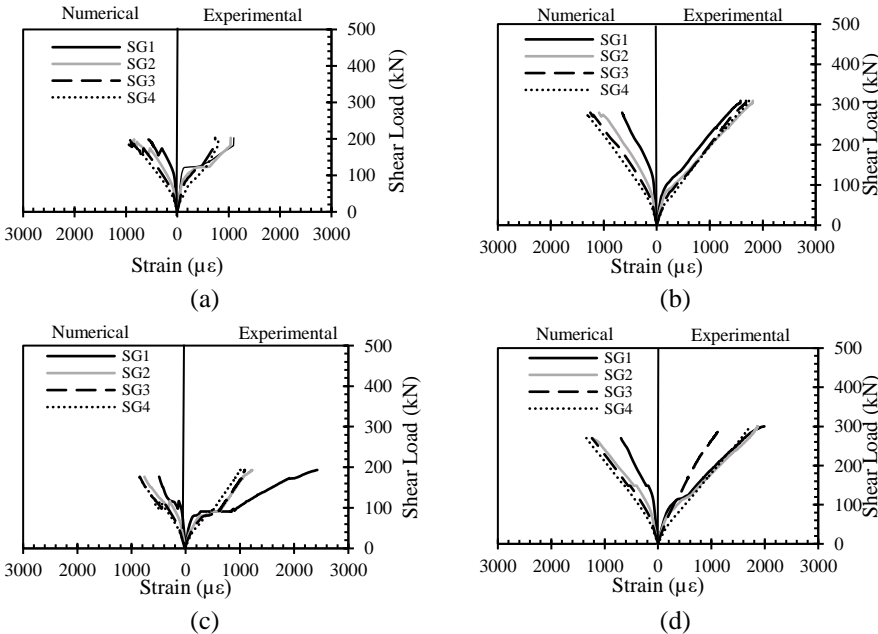

Figure 2.56: Numerical and experimental tensile steel strain responses: (a) SR0-SF0; (b) SR0-SF0-S; (c) SR100-SF0; (d) SR100-SF0-S; (e) SR100-SF1; (f) SR100-SF2; (g) SR100-SF3
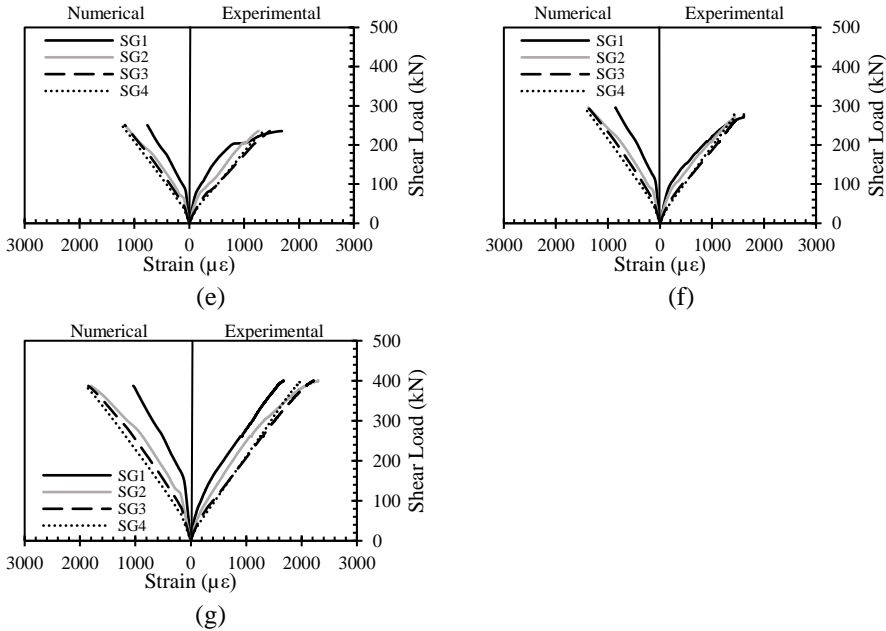
Figure 2.56: Numerical and experimental tensile steel strain responses: (a) SR0-SF0; (b) SR0-SF0-S; (c) SR100-SF0; (d) SR100-SF0-S; (e) SR100-SF1; (f) SR100-SF2; (g) SR100-SF3 (continued)

2.3.3 Shear Behavior of RC Deep Beams with Web Openings made with RCAs and Steel Fibers

2.3.3.1 Experimental Results

The shear performance of the RC deep beams with openings is evaluated and discussed in this section. The effect of test variables on the deflection response, cracking load, shear capacity, failure mode, and measured strains is elucidated.

2.3.3.1.1 Shear Load-Deflection Response

The shear load-deflection responses of the deep beams with openings are shown in Figure 2.57. The shear load is the support reaction, and the reported deflection is located at the midspan. It can be seen that up to a shear load of approximately 80 kN, the NA-based beams without conventional steel

stirrups, NR0-SF0 and NR100-SF0, had nearly an equal initial stiffness. As the load progressed, specimen NR100-SF0 started to exhibit a lower stiffness than that of NR0-SF0. Specimens NR0-SF0-S and NR100-SF0-S, with conventional steel stirrups, had an equal initial stiffness up to an approximate shear load of 40 kN, after which the RCA-based specimen NR100-SF0-S experienced a lower stiffness compared to that of its NA-based counterpart NR0-SF0-S. The conventional steel stirrups improved the stiffness of the beams. The improvement in beam stiffness resulting from the presence of conventional steel stirrups was less pronounced for the RCA-based specimen NR100-SF0-S rather than the NA-based specimen NR0-SF0-S. It seems that the severity of cracks in the RCA-based concrete specimen limited the effect of the conventional steel stirrups on the beam stiffness. The beams made with 100% RCAs without steel fibers experienced higher midspan deflections than those of their counterparts made with NAs. This behavior can be ascribed to the reduced Young's modulus of the concrete made with RCAs.

The addition of steel fibers clearly improved the stiffness and the overall performance of the beams made with 100% RCA. The beams with steel fibers did not experience a significant change in the slope of the deflection response at the time of cracking. Additionally, the stiffness of the beams having steel fibers were better than that of NR100-SF0-S having conventional steel stirrups. In fact, the stiffness of NR100-SF2 and AR100-SF3 almost coincided with that of NR0-SF0-S having NAs and conventional steel stirrups. The presence of steel fibers in the RCA concrete beams with web openings delayed initiation of shear cracks, limited their growth in the post-cracking phase, and hence, improved the beam stiffness. The improved stiffness of the RCA-based beams with fibers would result in less deflections under service load thus improving serviceability of structure.
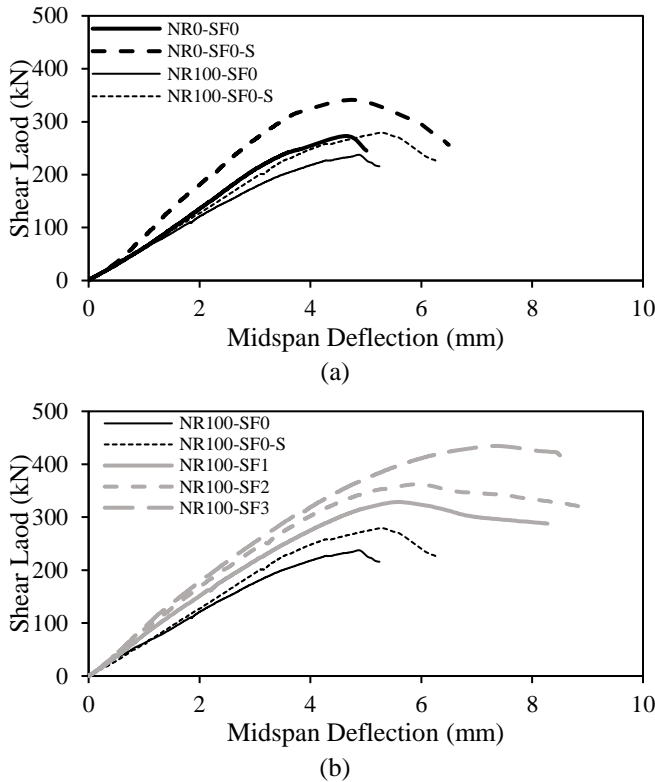
Figure 2.57: Shear load versus deflection relationship: (a) Beam specimens without steel fibers; (b) RCA beams with and without steel fibers

Table 2.18 summarizes the test results including the first visible shear cracking load, V_{cr}, shear capacity, V_{max}, and the corresponding deflections at first visible shear cracking load and at the shear capacity. The shear cracking load of specimens NR0-SF0-S and NR100-SF0-S with conventional steel stirrups were 30 and 15% higher than those of NR0-SF0 and NR100-SF0 without stirrups, respectively. Similarly, the inclusion of conventional steel stirrups increased the shear capacity of specimens NR0-SF0-S and NR100-SF0-S by 25 and 18%, respectively, compared with those of their respective counterparts NR0-SF0 and NR100-SF0. The inclusion of conventional steel stirrups in RC deep beam specimens with openings was less effective in delaying the appearance of shear cracks and improving the shear capacity

when 100% RCA was used. The failure mode of the tested beams was governed mainly by concrete properties. It seems that the inferior properties of the RCA-based concrete with web openings diminished the impact of the conventional steel stirrups on the shear cracking load and shear capacity. As shown in Table 2.18, the use of steel fibers increased in the shear cracking load of the RCA beams compared to that of their counterpart specimen NR100-SF0. Such an increase is owed to the improved tensile properties of the mixes with steel fibers. The shear cracking load of NR100-SF3 with $v_f =$ 3% was even higher than that of NR0-SF0-S made with NAs and conventional steel stirrups. The inclusion of steel fibers remarkably increased the shear capacity of the beams with openings made with 100% RCAs. Specimens NR100-SF1, NR100-SF2, and NR100-SF3 experienced shear strength gains of 39, 53, and 84%, respectively, compared to the strength of NR100-SF0. Specimen NR100-SF1 made with 1% of steel fibers experienced higher shear strength than that of NR100-SF0-S having conventional steel stirrups. Specimen NR100-SF2 with 2% steel fibers exhibited a shear capacity even higher than that of the NA-based specimen NR0-SF0-S having conventional steel stirrups. These results indicate that it is possible to use steel fibers in concrete deep beams with 100% RCAs and web openings in replacement of the minimum conventional steel stirrups required by ACI 318-14 (2014).

Table 2.18: Test results

Specimen	Shear Cracking Stage		Ultimate Stage		Gain in Shear Capacity [*]
	V_{cr} (kN)	Δ_{cr} (mm)	V_{max} (kN)	Δ_{max} (mm)	
NR0-SF0	100	1.5	273	4.7	-
NR0-SF0-S	130	1.4	341	4.8	25[*]
NR100-SF0	87	1.5	237	4.9	-
NR100-SF0-S	100	1.6	279	5.3	18[**]
NR100-SF1	100	1.3	329	5.6	39[**]
NR100-SF2	120	1.4	362	6.0	53[**]
NR100-SF3	140	1.5	435	7.4	84[**]

[*]Relative to the shear capacity of NR0-SF0.
[**]Relative to the shear capacity of NR100-SF0.

2.3.3.1.2 Crack Pattern

Figures 2.58 shows the crack patterns observed in the tested deep beam specimens with openings at failure. All specimens failed in shear as planned in the design to prevent a flexural mode of failure and allow the beam to develop its full shear capacity. Specimens NR0-SF0 and NR100-SF0 exhibited two independent diagonal splitting cracks formed in the upper and lower chords of the west shear span causing a frame-type mode of failure.

Specimen NR0-SF0-S and NR100-SF0-S having conventional steel stirrups, and those with steel fibers, NR100-SF1, NR100-SF2, and NR100-SF3, failed by crushing of the struts developed in upper and lower chords. It should be noted that the severity of cracks was less pronounced in specimen NR100-SF3. This behavior was mainly due to the inclusion of a higher steel fiber volume fraction of 3%. Reducing the severity of cracks results in better serviceability performance.
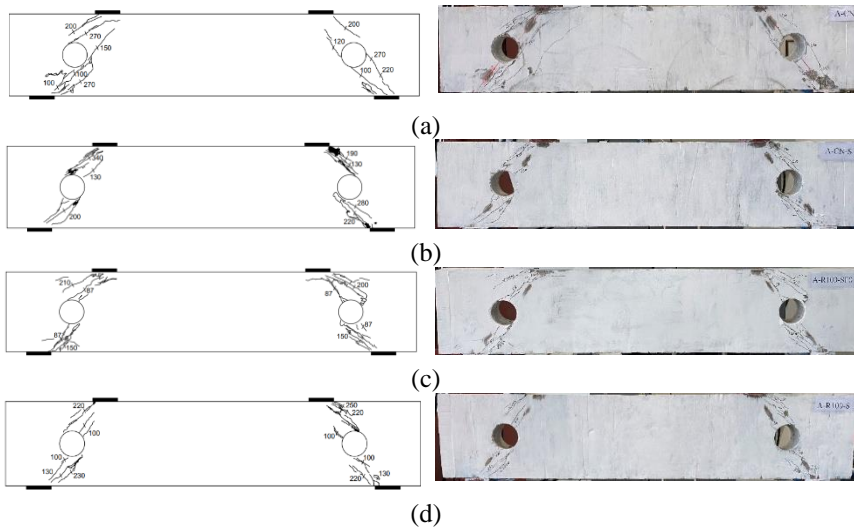

Figure 2.58: Crack pattern at failure: (a) NR0-SF0; (b) NR0-SF0-S; (c) NR100-SF0; (d) NR100-SF0-S; (e) NR100-SF1; (f) NR100-SF2; (g) NR100-SF3
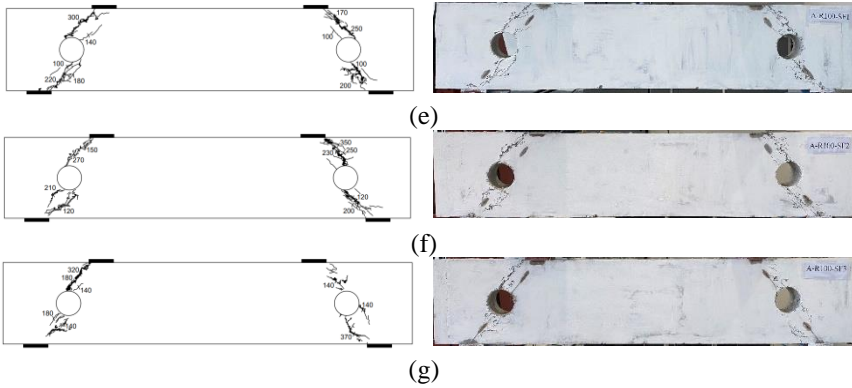
(e)

(f)

(g)

Figure 2.58: Crack pattern at failure: (a) NR0-SF0; (b) NR0-SF0-S; (c)
NR100-SF0; (d) NR100-SF0-S; (e) NR100-SF1; (f) NR100-SF2; (g)
NR100-SF3 (continued)

2.3.3.1.3 Stirrup Strains

Figure 2.59 shows the shear load-stirrup strain relationship. All the
measured strain in the vertical stirrups were below yielding. Initially, the steel
stirrups showed no or minimal strains. Following cracking, the stirrup strain
increased in a linear fashion until failure. The stirrup strain increased at a
higher rate in beam NR100-SF0-S with 100% RCAs compared to that of
NR0-SF0-S with NAs. The higher rate of increase of stirrup strain in the case
on RCA-based beam signifies a reduced contribution of the recycled
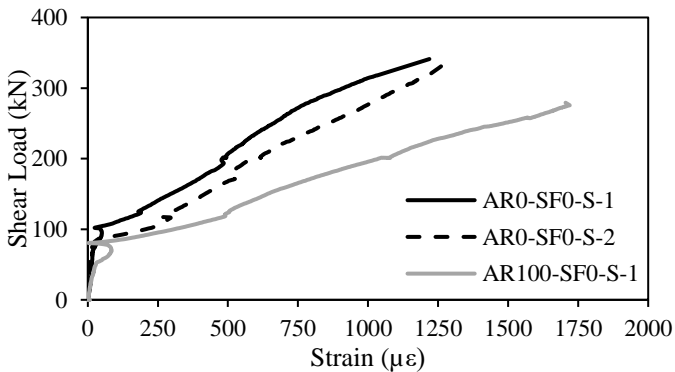aggregates concrete to the shear resistance.

Figure 2.59: Shear load versus maximum stirrup strain relationships

2.3.3.1.4 Tensile Steel Strains

Figure 2.60 presents results of strain measurements in the longitudinal steel reinforcing bars of representative specimens at four different loading stages.
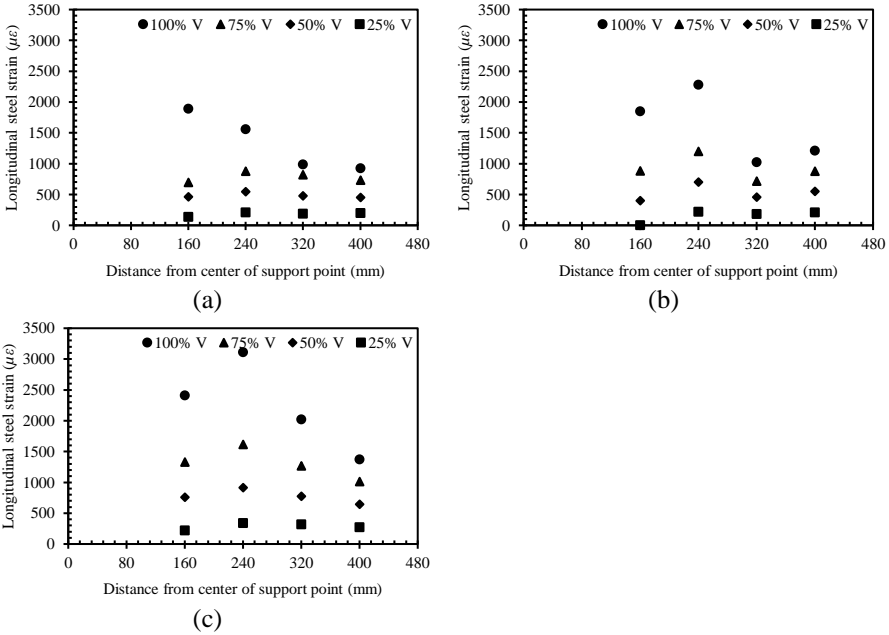

Figure 2.60: Steel strain profile: (a) NR100-SF0-S; (b) NR100-SF2; (c) NR100-SF3

Values of the maximum steel strains measured at peak load are given in Table 2.19. The tension steel did not reach the yield strain (εyield = 2695 $\mu\varepsilon$) except in one location in specimen NR100-SF3 at the distance of 240 mm away from the center of support. The strain in the tensile steel in other locations of specimen NR100-SF3 was below yielding. From Figure 2.58, it can be seen that the steel strains increased almost uniformly within the shear span up to 75% of the shear capacity verifying the behavior of a deep beam action (strut and tie action). Due to the severity of cracks in the bottom chord below the openings at the distance of 160 mm and 240 mm at the onset of

failure, the strain in the steel at 100% of the shear capacity was higher at these locations relative to that measured at other locations away from the openings and the cracks.

2.3.3.1.5 Concrete Strains

The maximum compressive concrete strains in the longitudinal and diagonal directions measured at the peak load are given in Table 2.19. Excluding specimen NR0-SF0, it can be seen that for the specimens without steel fibers, the maximum diagonal concrete strains were higher than those measured in the longitudinal direction indicating higher concrete deformations in the diagonal direction, possibly due to the presence of the web opening and shear cracking. In contrast, specimens with RCAs, except NR100-SF2, exhibited lower diagonal compressive concrete strains than those measured in the longitudinal direction. It seems that the presence of steel fibers reduced the deformation in the diagonal direction relative to those of the longitudinal direction due to the reduced severity of shear cracking. The specimens with steel fibers tended to exhibit higher diagonal and longitudinal concrete strains than those of their counterparts without steel fibers. This behavior can be attributed to the increase in the load-carrying capacity of the beams with steel fibers, which accommodated for additional concrete strain prior to failure.

Table 2.19: Maximum strains measured at peak load

Specimen	Concrete Strain ($\mu\varepsilon$)		Max. longitudinal Steel Strain ε_s ($\mu\varepsilon$)	$\varepsilon_s/\varepsilon_y$
	Max. longitudinal strain	Max. diagonal strain		
NR0-SF0	1470	616	1859	0.69
NR0-SF0-S	1062	1552	1990	0.74
NR100-SF0	1126	1672	2182	0.81
NR100-SF0-S	1102	1584	1890	0.70
NR100-SF1	2532	1144	1758	0.65
NR100-SF2	2120	2513	2282	0.85
NR100-SF3	3211	1965	3109*	1.15

*In one point only within the shear span.

2.3.3.1.6 Analytical Prediction

Table 2.20 shows a comparison of the shear capacities predicted analytically based on published models with those obtained from the tests. All models overestimated the shear capacity of the beams without steel fibers. This behavior was more evident in the absence of conventional steel stirrups. The deviation from experimental results was in the range of 32 to 49% for the beams without conventional steel stirrups and 9 to 30% for the beams with internal steel stirrups. In contrast, the models tended to provide reasonable or conservative prediction for the shear capacity of the RC deep beams made with 100% RCAs and steel fibers. Predicted results of the beams with steel fibers based on the analytical approach of Kong & Sharp (1977) were within a 12% error band. The analytical model by Shanmugam & Swaddiwudhipong (1988) tended to overestimate the value of the shear capacity of the beams with steel fibers by up to 17%. Predictions of the model by Ray & Reddy (1979) for the beams with steel fibers were conservative with predicted-to-measured shear capacity (V_n/V_{max}) of 0.71 to 0.98.

Table 2.20: Comparison between analytical and experimental results of the beams with openings

Specimen	Experimental Results V_{max} (kN)	Analytical Results V_n (kN)			Ratio (V_n/V_{max})		
		Kong and Sharp	Shanmugam and Swaddiwudhipong	Ray and Reddy	Kong and Sharp	Shanmugam and Swaddiwudhipong	Ray and Reddy
NR0-SF0	273	360	386	383	1.32	1.42	1.40
NR0-SF0-S	341	371	397	390	1.09	1.16	1.14
NR100-SF0	237	338	353	326	1.43	1.49	1.38
NR100-SF0-S	279	349	364	333	1.25	1.30	1.19
NR100-SF1	329	360	386	321	1.09	1.17	0.98
NR100-SF2	362	367	396	317	1.01	1.10	0.87
NR100-SF3	435	382	420	307	0.88	0.97	0.71

*2.3.3.2 Numerical Prediction and Model Verification of Beams with Openings*

2.3.3.2.1 Shear Load-deflection Response

The predicted shear load-deflection curves of the deep beam models containing openings are illustrated in Figure 2.61. The use of RCAs rather than NAs reduced the stiffness and shear capacity of the models, as shown in Figure 2.61 (a). The addition of steel fibers improved the stiffness and remarkably increased the shear capacity of the deep beam models, as shown in Figure 61 (b). The beam models having steel fibers exhibited an improved stiffness even better than that of NR100-SF0-S with NAs and conventional steel stirrups. It is worth noting that when the steel fiber-reinforced concrete models reached approximately 90% of the shear capacity, they started to exhibit an increased midspan deflection without a significant increase in load until failure. This plastic response can be attributed to the tension stiffening effect caused by steel fibers, which improved the deformability of the models.

The shear load-deflection responses of the models without steel fibers predicted numerically are compared to those obtained experimentally in Figure 2.62. The predicted response of the deep beam models without steel fibers tended to be stiffer than that obtained from the experiment. This behavior may be attributed to the existence of microcracks in the tested beams prior to testing caused by shrinkage or occurred during handling. Such microcracks would reduce the actual stiffness of the tested beams. The numerical shear load-deflection responses of the models with steel fibers are compared to those obtained from the tests in Figure 2.62. The difference between the numerical and experimental stiffnesses of the deep beam models with steel fibers was less significant relative to that of the models without steel fibers.
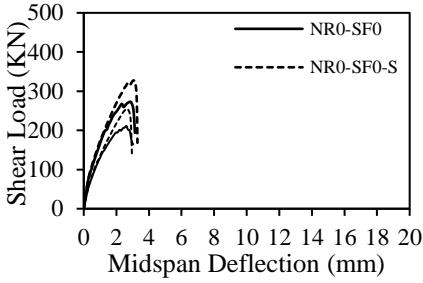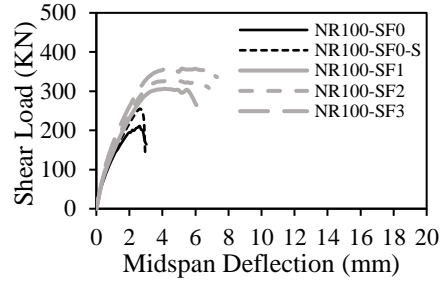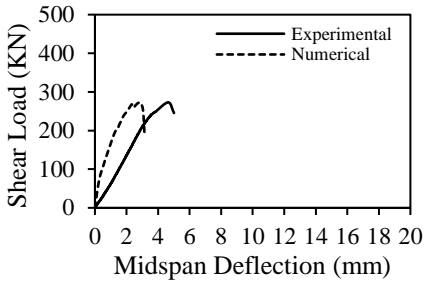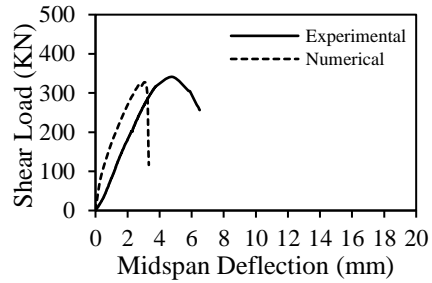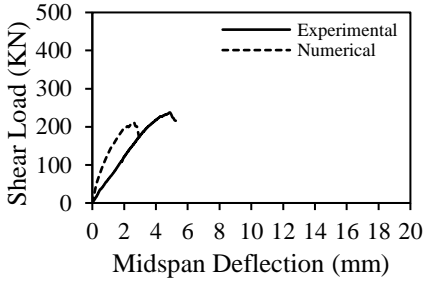
Figure 2.61: Numerical shear load-deflection response: (a) Beams without steel fibers; (b) RCA-based beams with and without steel fibers.

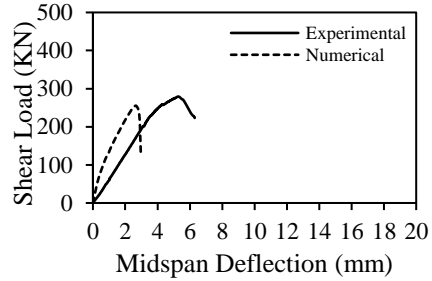Figure 2.62: Numerical and experimental load-deflection responses: (a) NR0-SF0; (b) NR0-SF0-S; (c) NR100-SF0; (d) NR100-SF0-S; (e) NR100-SF1; (f) NR100-SF2; (g) NR100-SF3
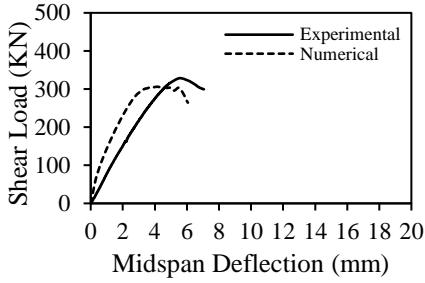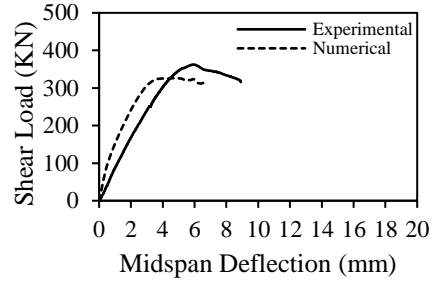
Figure 2.62: Numerical and experimental load-deflection responses: (a) NR0-SF0; (b) NR0-SF0-S; (c) NR100-SF0; (d) NR100-SF0-S; (e) NR100-SF1; (f) NR100-SF2; (g) NR100-SF3 (continued)
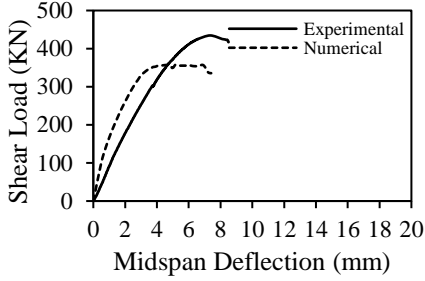
Table 2.21: Comparison between numerical and experimental results

Model	Shear Capacity		Deflection Capacity		V_{FE}/V_{EXP}	Δ_{FE}/Δ_{EXP}
	V_{EXP} (kN)	V_{FE} (kN)	Δ_{EXP} (mm)	Δ_{FE} (mm)		
NR0-SF0	273	273	4.7	2.9	1.00	0.62
NR0-SF0-S	341	327	4.8	3.0	0.96	0.63
NR100-SF0	237	211	4.9	2.6	0.89	0.53
NR100-SF0-S	279	255	5.3	2.7	0.91	0.51
NR100-SF1	329	306	5.6	5.4	0.93	0.96
NR100-SF2	362	326	6.0	5.9	0.90	0.98
NR100-SF3	435	358	7.4	6.0	0.82	0.81
Average					0.92	0.72
Std Dev					0.05	0.18
COV (%)					5.74	25.26

The experimental and numerical shear capacities, V_{EXP} and V_{FE}, respectively, along with the deflections at failure, Δ_{EXP} and Δ_{FE}, are compared in Table 2.21. The predicted shear capacities were within 11% error band,

except for one model NR100-SF3 with V_{FE}/V_{EXP} of 0.82. The ratio of V_{FE}/V_{EXP} was on average 0.92 with a corresponding standard deviation and coefficient of variation of 0.05 and 6%, respectively. The predicted deflections at failure for the models with steel fibers were generally in good agreement with those measured experimentally with Δ_{FE}/Δ_{EXP} in the range of 0.81 to 0.98. The models tended, however, to underestimate the deflection at failure of the beams without steel fibers. It is worth noting that the measured deflections at failure of the models without steel fibers were very small which made the ratio of Δ_{FE}/Δ_{EXP} very sensitive to any small difference (within 2 mm) between predicted and measured deflections. The ratio of Δ_{FE}/Δ_{EXP} of all models was on average 0.72 with a standard deviation of 0.18 and a coefficient of variation of 25%.

2.3.3.2.2 Crack Pattern

The crack patterns of the deep beam models with openings predicted numerically are shown in Figure 2.63 (a). The minimum width of the displayed crack in FE models was set to be 0.1 mm. All models initially exhibited a diagonal shear crack crossing the center of the opening. This crack did not propagate further as the load progressed. At higher loads, inclined shear cracks developed in the upper and lower chords in the direction of the corresponding load paths. The models without steel stirrups nor steel fibers failed due to the formation of independent diagonal splitting cracks in the direction of upper and lower load paths. The models with stirrups exhibited multiple parallel inclined cracks along in the direction of the upper and lower natural load paths prior to failure.

The minimum principal concrete strain of the deep beam models prior to failure are shown in Figure 2.63 (b). The profile of the minimum principal concrete strains of the models with steel stirrups or steel fibers verified the formation of diagonal struts in the direction of the upper and

lower load paths. The deep beam models without steel fibers exhibited an average minimum principal concrete strain value of approximately -0.008 at peak load. The models with steel stirrups failed, however, a higher shear capacity than that of their counterparts without stirrups, indicating a lower rate of increase of the minimum principal concrete strains relative to that of their counterparts without stirrups. The deep beam models with steel fibers at v_f of 1, 2, and 3% reached their shear capacity at minimum principal strain values of approximately -0.014, -0.018, and -0.020, respectively. The increased minimum principal strain capacities exhibited by the models with steel fibers enabled the models to sustain higher load and deflection capacities prior to failure than those of their counterparts without steel fibers. Figure 2.63 (c) shows photographs of the tested beams with openings at failure. The crack patterns obtained from the tests are in good agreement with those predicted numerically. Experimental results verified the frame-type mode of failure in the deep beams without shear reinforcement and the shear compression mode of failure along the upper and lower load paths in the deep beams with stirrups or steel fibers.
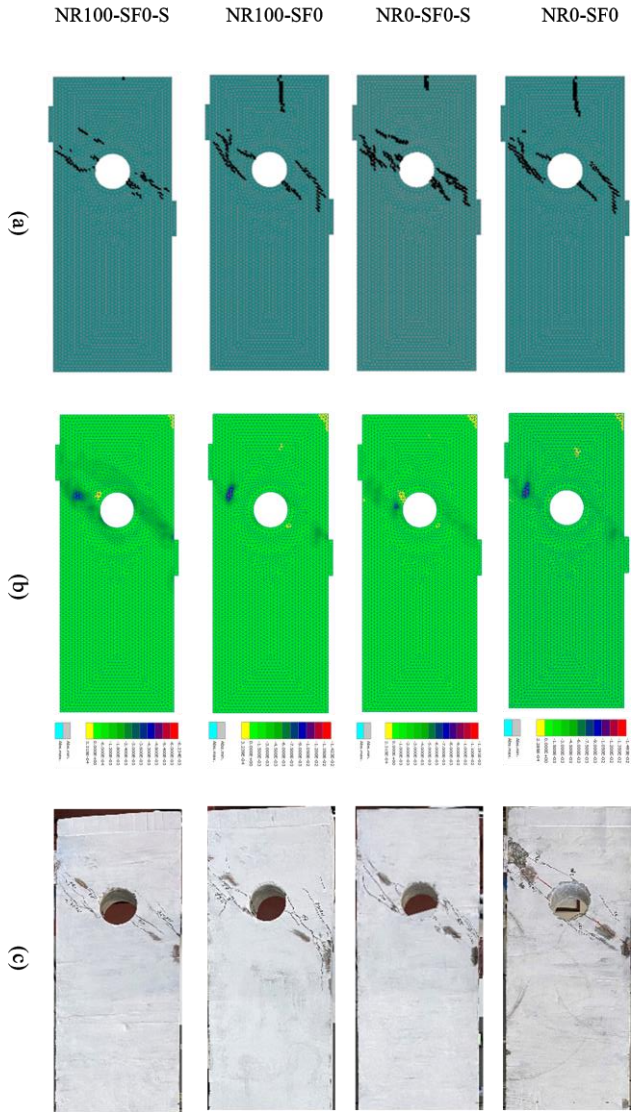
Figure 2.63: Crack patterns and principal strains; (a) Numerical crack patterns, (b) minimum principal strains, (c) Experimental crack patterns
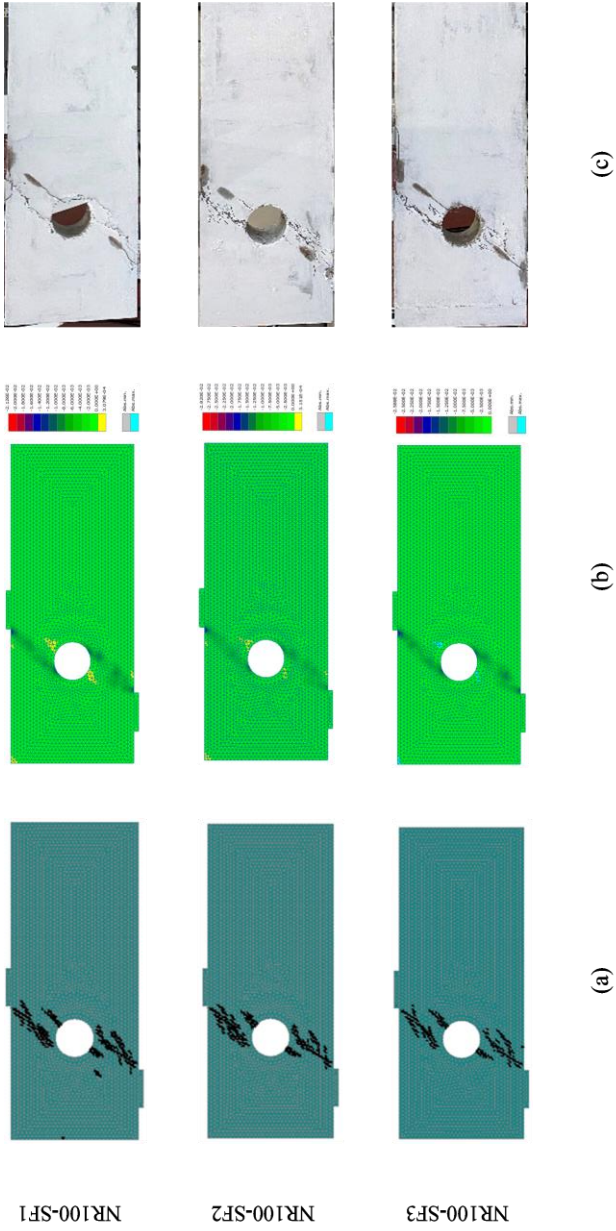
Figure 2.63: Crack patterns and principal strains; (a) Numerical crack patterns, (b) minimum principal strains, (c) Experimental crack patterns (continued)

The stirrup strain responses predicated numerically of the deep beam models NR0-SF0-S and NR100-SF0-S are presented in Figure 2.64 (a) and Figure 2.64 (b), respectively. All predicted stirrup strains were below the yielding value indicating that failure was controlled by concrete due to the presence of the openings. Although experimental stirrup strain data at locations of most of the monitoring points were not available, the few stirrup strain data obtained from the experimental tests showed no yielding of stirrups. The full-depth vertical stirrups located at the left and right sides of the opening in NR0-SF0-S and NR100-SF0-S exhibited minimal strains as shown in Figure 2.64 (a) and Figure 2.64 (b), respectively. These reduced strains occurred because the major shear cracks were developed in the upper and lower chords rather than at the sides of the opening. Upper and lower chord stirrup strains indicate that shear cracks occurred in NR0-SF0-S at a load value of approximately 170 kN. Following cracking, there was no significant difference in the rate of increase of the horizontal and vertical stirrup strains in the upper and lower chords. The strains in the vertical and horizontal stirrups at peak load were insignificantly different. The stirrups in the lower chord tended, however, to exhibit slightly higher strains at peak load than those exhibited by the stirrups in the upper chord. Upper and lower chord stirrup strains of model NR100-SF0-S, shown in Figure 2.64 (b), indicate the initiation of shear cracks at a load value of approximately 130 kN. Figure 2.65 shows the horizontal and vertical stirrup strain responses in the upper chord for models NR0-SF0-S and NR100-SF0-S. It can be seen that the deep beam model NR100-SF0-S made with RCAs exhibited shear cracks at a lower load than that of NR0-SF0-S made with NAs. Following shear cracking, the stirrup strains of NR100-SF0-S increased at a slightly higher rate than that of model NR0-SF0-S. The reduced shear cracking load and the increased stirrup strains of model NR100-SF0-S compared to those of model

NR0-SF0-S indicated less contribution of RCAs to the shear resistance than NAs.

(a)   (b)
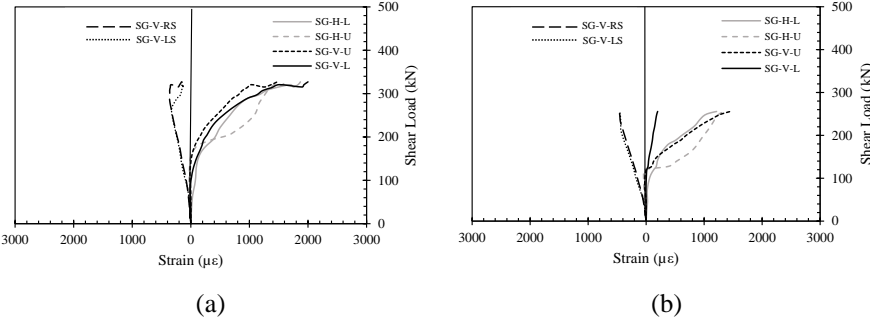
Figure 2.64: Numerical stirrup strain response of group N: (a) NR0-SF0-S; (b) NR100-SF0-S

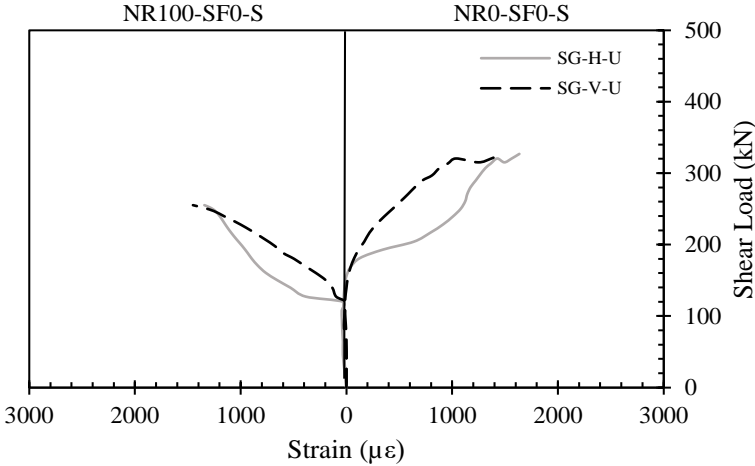Figure 2.65: Horizontal and vertical stirrup strain responses in the upper chord of models NR0-SF0-S and NR100-SF0-S

2.3.3.2.4 Tensile Steel Strains

The numerical and experimental tensile steel strain responses of the deep beam models containing openings are presented in Figure 2.66. The monitoring point of SG1 was located at a distance 85 mm away from the face

of the support plate, whereas that of SG4 was under the load point. Other monitoring points, SG2 and SG3, were located in between SG1 and SG4 at a spacing of 80 mm. The numerical and experimental steel strain responses showed a similar trend. The steel strains predicted numerically in all models at different locations within the shear span were insignificantly different, verifying the deep beam action. This behavior was verified experimentally despite being less evident in the steel strain data measured experimentally in beam NR100-SF0. The strains recorded numerically at SG1, which was close to the support, were slightly lower than those recorded at other locations. The tensile steel reinforcement did not reach the yielding strain in any of the models, which has been verified experimentally, except at one location (SG2) in beam NR100-SF3.
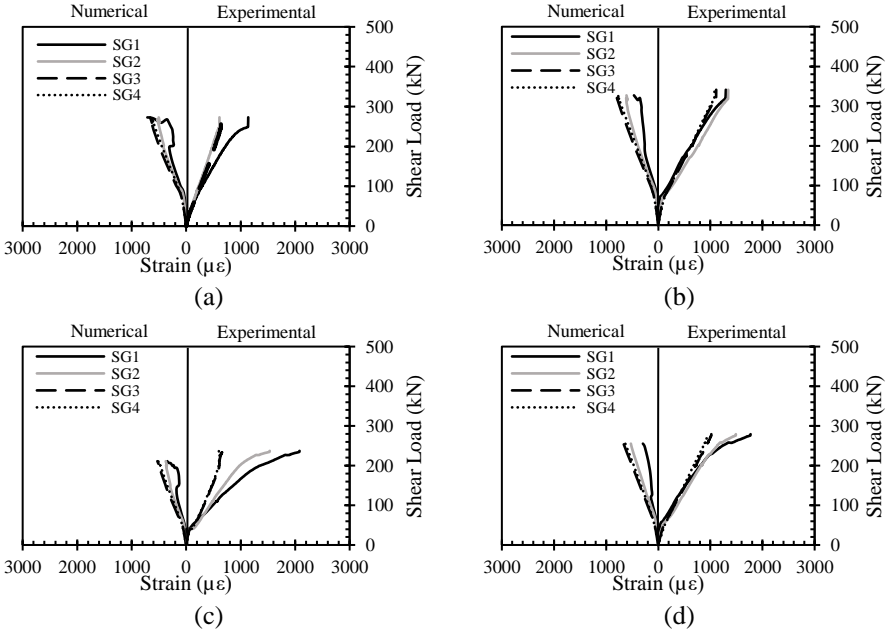

Figure 2.66: Numerical and experimental tensile steel strain responses: (a) NR0-SF0; (b) NR0-SF0-S; (c) NR100-SF0; (d) NR100-SF0-S; : (e) NR100-SF1; (f) NR100-SF2; (g) NR100-SF3
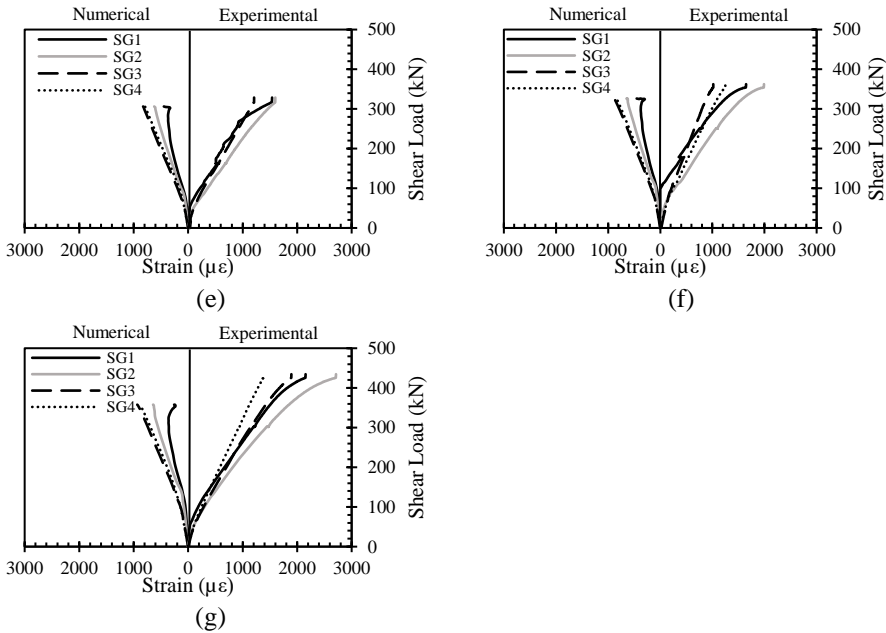
Figure 2.66: Numerical and experimental tensile steel strain responses: (a) NR0-SF0; (b) NR0-SF0-S; (c) NR100-SF0; (d) NR100-SF0-S; : (e) NR100-SF1; (f) NR100-SF2; (g) NR100-SF3 (continued)

2.3.4 Parametric Study and Discussion

It was not possible to test solid RC deep beams with *a/h* of 0.8 due to the limited capacity of the laboratory facility at UAEU. The models developed and verified in the current study are considered a valid alternative to laboratory testing. As such, additional seven solid deep models with *a/h* of 0.8 were developed. The performance of these models was predicted numerically and compared to that of other models presented earlier with and without openings.

2.3.4.1 Effect of Shear Span-to-Depth Ratio

Figure 2.67 presents the shear load-deflection responses of RCA-based solid deep beam models with different *a/h* ratios. The models with *a/h* of 0.8 were significantly stiffer than their counterparts with *a/h* of 1.6. Figure 2.67 (a) shows that at *a/h* of 0.8, the use of steel fibers with v_f of 1% (model

R100-SF1) was sufficient to restore the stiffness of the model with RCAs and minimum steel stirrups (model R100-SF0-S). However, at *a/h* of 1.6, the use of steel fibers at v_f of 2% (model SR100-SF2) was necessary to restore the stiffness of the counterpart model with RCAs and minimum steel stirrups (model SR100-SF0-S), as shown in Figure 2.67 (b). At both *a/h* values, the stiffness of the models with v_f of 3% coincided with that of the model with NAs and conventional steel stirrups. Figure 2.68 shows the effect of *a/h* on the shear capacity of the RCA-based deep beam models. The shear capacity of the deep beam models with steel fibers increased almost linearly with an increase in the steel fiber volume fraction. Obviously, the shear capacity of the deep beam models with *a/h* of 0.8 was higher than that of their counterparts with *a/h* of 1.6. For the deep beam models without steel fibers, the increase in the shear capacity due to the decrease in the *a/h* from 1.6 to 0.8 ranged from 31 to 66% with an average of 51%, whereases for those with steel fibers, the increase in shear capacity ranged from 42 to 88% with an average of 67%.
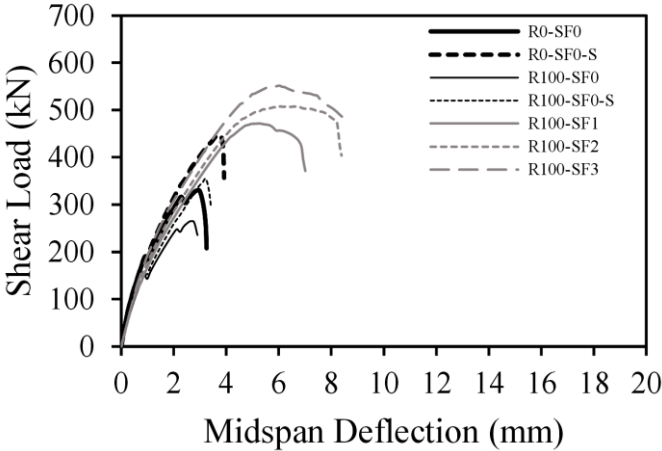
(a)

Figure 2.67: Shear load-deflection responses: (a) Solid models with *a/h* 0.8; (b) Solid models with *a/h* 1.6
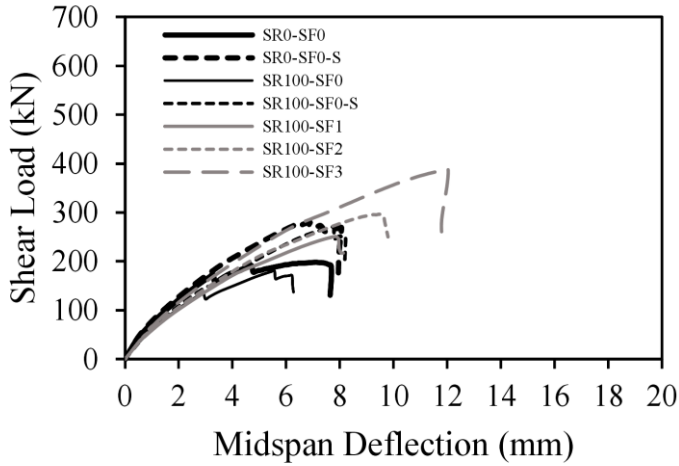
(b)

Figure 2.67: Shear load-deflection responses: (a) Solid models with *a/h* 0.8; (b) Solid models with *a/h* 1.6 (continued)
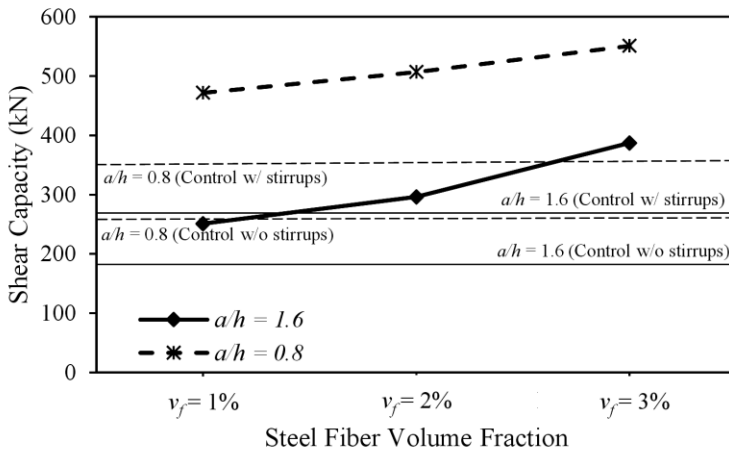

Figure 2.68: Effect of *a/h* on shear capacity

Figure 2.69 illustrates the effect of the inclusion of minimum steel stirrups on the shear strength gain of the beam models with different types of aggregates at different *a/h* ratios. The shear strength gains exhibited by the models with NAs and those of their counterparts with RCAs were

insignificantly different, regardless of *a/h*. Figure 2.70 shows the effect of steel fibers on the shear strength gain of the deep beam models with RCAs at different *a/h* ratios. The strength gains caused by the steel stirrups are also included in Figure 2.70 to serve as a benchmark. The shear strength gain was calculated relative to the shear capacity of the corresponding control model made with RCAs without steel stirrups nor steel fibers. At *a/h* of 1.6, the addition of steel fibers at v_f of 1, 2, and 3% resulted in respective shear strength gains of 39, 64, and 114%. For the models with *a/h* of 0.8, the addition of steel fibers at v_f of 1, 2 and 3% resulted in shear strength gains of 78, 91, and 108%, respectively. At v_f of 1 and 2%, the shear strength gain was higher for the models with the lower *a/h* of 0.8. The presence of steel fibers reduced the severity of cracks within the shear span, improved the tension stiffening effect, and hence, increased the strut capacity. The shear capacity (*V*) of RC deep beams is sensitive to the strut capacity (F_s) and its angle of inclination in the shear span (θ) through the relationship $V = F_s\sin\theta$. The impact of increasing the strut capacity on the shear strength is more pronounced for struts with a greater angle of inclination θ. This relationship could explain why the shear strength gain caused by steel fibers was higher at the lower *a/h* of 0.8. The effect of *a/h* on the shear strength gain caused by steel fibers diminished at the higher v_f of 3%. It seems that, at v_f of 3%, the increase in the shear capacity was too high to show an effect for the strut angle of inclination. From Figure 2.70, it can be seen that at *a/h* of 0.8, the use of v_f of 1% was sufficient to provide a shear strength gain higher than that provided by the minimum steel stirrups. At *a/h* of 1.6, it was necessary to use v_f of 2% to substitute the minimum steel stirrups.
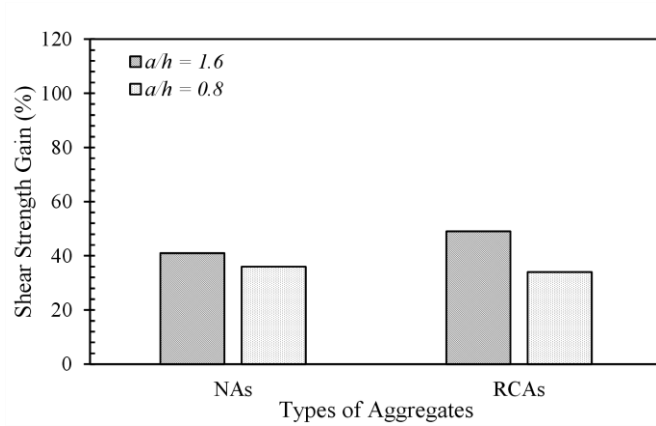
Figure 2.69: Shear strength gain of models with minimum stirrups at different *a/h* ratios
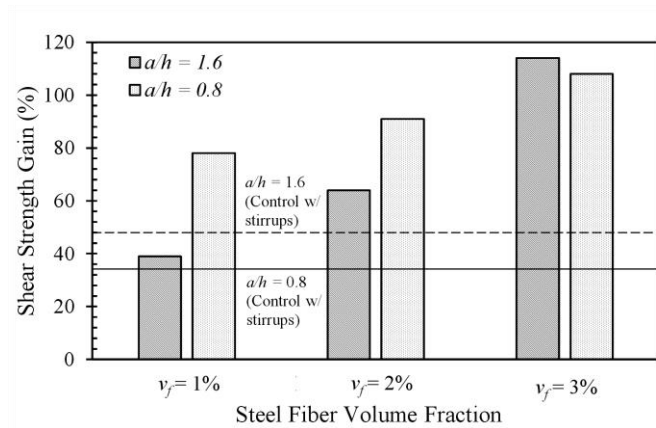
Figure 2.70: Shear strength gain of models with RCAs and steel fibers at different *a/h* ratios

2.3.4.2 Effect of Web Openings

Figure 2.71 (a) and Figure 2.71 (b) present the shear load-deflection responses of the deep beam models having *a/h* of 0.8 without and with web openings, respectively. The deep beam models with the web opening exhibited a reduced stiffness and significant reduction in the shear capacity relative to those of their counterparts without opening. At both *a/h* values, the

inclusion of steel fibers at v_f of 1% was sufficient to restore the stiffness of the corresponding counterpart model with RCAs and minimum steel stirrups. This behavior is manifested in the responses of counterpart models R100-SF1 and R100-SF0-S in Figure 2.71 (a) and those of models SR100-SF1 and SR100-SF0-S in Figure 2.71 (b).

Figure 2.72 shows the effect of the web opening on the shear capacity of the RCA-based deep models at different steel fiber volume fractions. The shear capacity of the models with and without openings increased almost linearly with an increase in v_f. For the models without steel fibers, the reduction in shear capacity due to the presence of the web opening ranged from 17 to 28%, with an average of 23%. For the models with steel fibers, the reduction in shear capacity caused by the web opening ranged from 35 to 36%, with an average of 35%. It is worth mentioning that the shear capacity of the deep beam model having v_f of 3% and the web opening was equal to that of the solid beam model with steel stirrups.
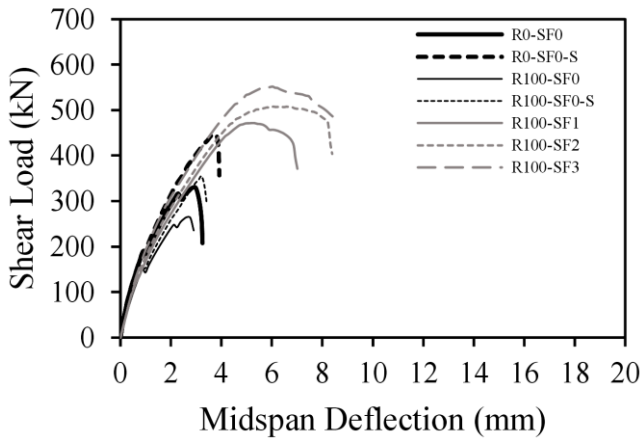
(a)

Figure 2.71: Shear load-deflection responses: (a) Solid models; (b) Models with web openings
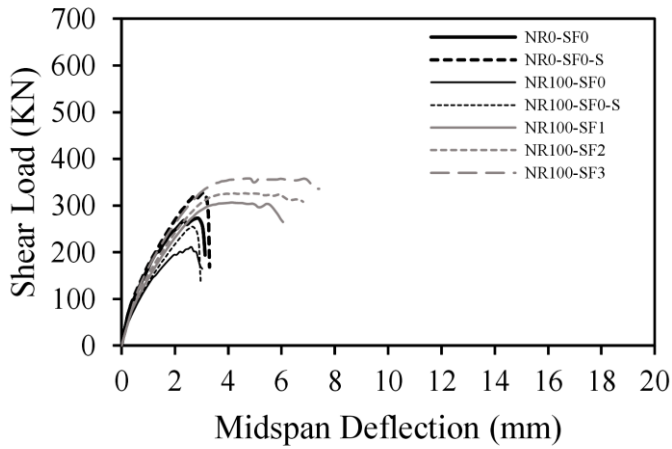
(b)

Figure 2.71: Shear load-deflection responses: (a) Solid models; (b) Models with web openings (continued)
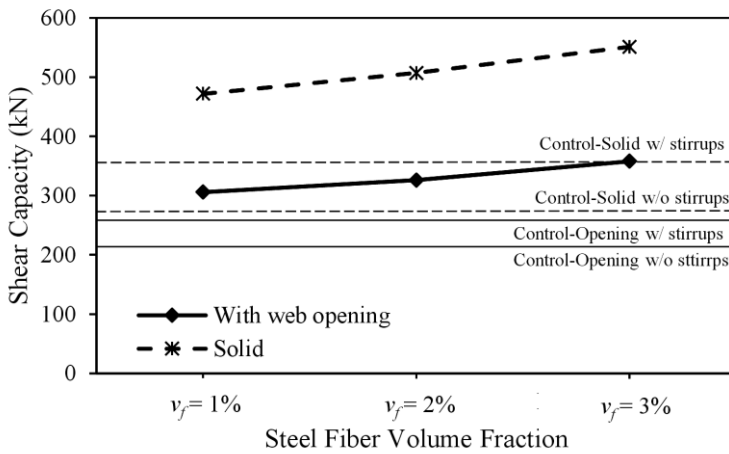
Figure 2.72: Effect of web opening on shear capacity on the shear capacity of RCA-based models

Figure 2.73 illustrates the effect of the minimum steel stirrups on the shear strength gain of the deep beam models having a/h of 0.8 with and

without openings. The inclusion of minimum steel stirrups was less effective in improving the shear capacity of the models with web openings, irrespective of the type of aggregates. This occurred because of the failure mode of these models that was controlled by properties of concrete since no yielding of stirrups took place. Figure 2.74 shows the shear strength gain caused by the addition of steel fibers to RCA deep beams having *a/h* of 0.8 with and without web openings. The strength gains caused by the steel stirrups are also provided in Figure 2.74 as a benchmark. The strength gain was calculated relative to the shear capacity of the corresponding control models made with RCAs without steel stirrups nor steel fibers. The shear strength gain caused by steel fibers for the deep beam models with the web opening was in the range of 45 to 70%, whereases their solid counterparts exhibited a shear strength gain of 78 to 108%. Nevertheless, for the models with and without openings, the addition of steel fibers at v_f of 1% was sufficient to achieve a shear strength gain higher than that provided by the minimum conventional shear reinforcement.
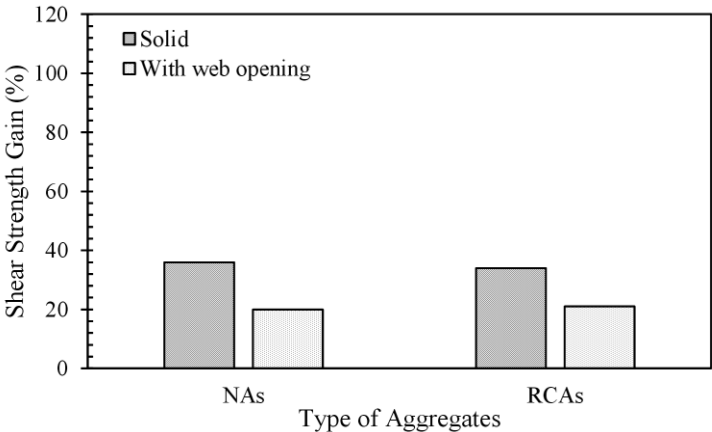
Figure 2.73: Shear strength gain of models with minimum stirrups with and without openings
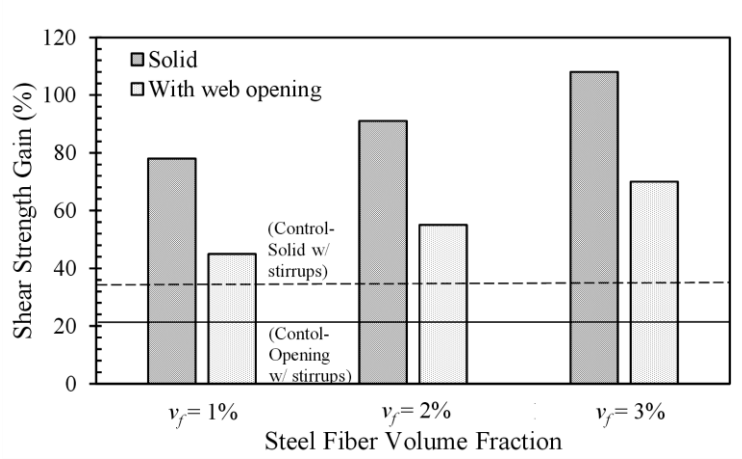
Figure 2.74: Shear strength gain of RCA steel fiber-reinforced models with and without openings

Chapter 3

Chapter 3: Conclusion and Future Perspectives

3.1 Overview

The research work provided new knowledge on the behavior of concrete made with steel fibers and recycled aggregates through experimental testing and numerical simulation. New characterization test data were produced. New tensile softening laws necessary for numerical simulation of large-scale concrete elements were developed. Numerical simulation models for large-scale deep beams made with recycled aggregates and steel fibers were generated. The characterization test data along with the developed constitutive laws were used as input data in the analysis. Large-scale deep beam tests were conducted to validate the numerical models. A comparative analysis between numerical and experimental results verified the accuracy and validity of the deep beam simulation models. Main conclusions of the work along with limitations and recommendations for future studies are presented in this chapter.

3.2 Conclusions Related to Material Characterization

Different fresh and hardened properties of concrete mixtures were examined in this study. Based on material characterization test results, the following conclusions can be drawn:

- The use of 30, 70, and 100% RCAs reduced the slump by 10, 22, and 37%, respectively. Concrete mixes with a 100% RCA replacement and steel fibers v_f of 1, 2, and 3%, exhibited 43, 87, and 100% slump reductions, respectively.

- The use of RCAs in concrete mixtures at replacement percentages of 30, 70, and 100% reduced the cylinder compressive strength of the concrete (f'_c) by 15, 29, and 32%, respectively. The addition of steel

fibers at v_f of 3% to the mixes with 30, 70, and 100% RCAs increased f'_c by 11, 19, and 13%, respectively.

- The elastic moduli of concrete made with RCA replacement percentages of 30, 70, and 100% were 19, 42, and 46% lower than that of the benchmark specimen made with NAs, respectively. The addition of steel fibers slightly increased the elastic modulus.

- The splitting tensile strength of concrete made with 30% RCAs did not reduce compared to that of the NA-based counterpart. The RCA replacement percentages of 70 and 100% resulted in 10 and 21% reductions in the splitting tensile strength, respectively, compared to that of the control NA-based specimen. The addition of steel fibers at v_f of 3% to the mix made with 100% RCAs increased the splitting tensile strength by 85%, compared to that of the counterpart plain mix.

- The uniaxial tensile strength of concrete made with 30, 70 and 100% RCAs decreased by 14, 23, and 18%, respectively, relative to that of the control mix made with NAs. The addition of steel fibers did not always increase the uniaxial tensile strength of the RCA-based specimens. However, the post-peak tensile strength was significantly improved with the addition of steel fibers.

- The modulus of rupture, f_r, decreased by up to 51% when 100% RCAs was used. The addition of steel fibers v_f of 2% and 3% significantly increased f_r to a level even higher than that of the benchmark specimen made with NAs.

- The flexural toughness and the post-cracking behavior of RCA-based mixes with steel fibers were significantly improved.

- The flexural strength at limit of proportionality, f_L, decreased with an increase in RCA replacement percentage. Plain concrete mixes had no residual flexural strengths. The addition of steel fibers increased

the flexural strength at the limit of proportionality and the residual flexural strengths of the RCA-based specimens.

- The fracture energy, G_F, of the RCA-based specimens obtained from the three-point test of notched prisms, significantly increased G_F with the addition of steel fibers.

- The water absorption of concrete increased by 65% with the substitution of NAs by 100% RCAs. The addition of steel fibers at v_f of 3% reduced the water absorption of RCA-based concrete mixes by an average of 22% compared to their plain counterparts.

- The UPV values decreased by up to 54% with an increase in the RCA replacement percentages to 100%. The addition of steel fibers at v_f of 1, 2, and 3% to concrete mixtures made with 100%, resulted in 23, 38, and 59% respective increases in the value of UPV.

- The mass loss due to abrasion increased with an increase in the RCA replacement percentages. The addition of steel fibers at v_f of 1, 2 and 3% to the mixes with 100% RCAs resulted in respective reductions of 27, 40 and 47% in the abrasion mass loss compared to that of their plain RCA-based counterpart.

- The bulk resistivity reduced by 30, 36, and 40% with the RCA replacement percentage of 30, 70, and 100%, respectively, compared with that of the NA-based concrete specimen.

- Tensile softening constitutive laws of concrete made with RCAs and steel fibers were developed from the four-point bending test results using an inverse FE analysis. The tensile softening constitutive laws developed in the current study were used as input data in the numerical simulation models of the large-scale RC deep beams.

3.3 Conclusions Related to Shear Behavior of Steel Fiber-Reinforced RCA Deep Beams

This part of the research work examined the shear behavior of RC deep beams with and without openings made with RCAs and steel fibers. The main conclusions of this part of the work are summarized hereafter.

- Solid RC deep beam specimens with neither traditional shear reinforcement nor steel fibers failed either by crushing of concrete at the top part of the diagonal concrete strut or in a shear-compression mode of failure. The specimens with traditional shear reinforcement without steel fibers exhibited a band of multiple cracks within the shear span, then eventually failed due to crushing of the concrete along the diagonal concrete strut. The specimens with steel fibers failed due to fracture of concrete across the major diagonal crack developed in the shear span accompanied by crushing of the diagonal strut.

- Deep beams with web openings without conventional steel stirrups or steel fibers failed due to formation of two independent diagonal splitting cracks in the chords above and below the openings (frame-type mode failure). Specimens with conventional steel stirrups or steel fibers failed by crushing of the concrete struts in the upper and lower chords of the openings.

- The shear cracking load and shear capacity of solid RC deep beams were reduced by 25 and 5% in the absence of traditional shear reinforcement due to the full replacement of NAs by RCAs. The RCA-based deep beams with traditional shear reinforcement exhibited 12 and 2% reductions in the shear cracking load and shear capacity, respectively, relative to those of a benchmark specimen made with NAs.

- Reinforced concrete deep beams with web openings made with a 100% RCAs exhibited 13 to 18% reductions in the shear capacity relative to those of their counterparts made with NAs. The use of RCAs rather than NAs in RC deep beams with web openings increased the beam deflection at service and ultimate loads.

- The inclusion of steel fibers in the RCA-based solid deep beams resulted in a remarkable increase in their shear cracking load to a level even higher than that of the control NA-based containing traditional shear reinforcement. The addition of steel fibers also improved the shear capacity of the RCA-based beams. The RCA-based beams with v_f of 1, 2, and 3% exhibited respective shear capacity gains of 22, 40, and 107%, relative to that of the control RCA-based counterpart without fibers.

- The inclusion of steel fibers in the RCA deep beams with web openings at volume fractions of 1, 2, and 3% resulted in 39, 53, and 84% respective increases in the shear capacity relative to that of the control RCA-based beam without steel stirrups nor steel fibers.

- The shear capacities of the RCA-based beams having v_f of 1 and 2% were approximately 80 and 90% of that of their RCA-based counterpart with traditional shear reinforcement. The deep beam specimen with v_f of 3% exhibited a shear capacity even higher than those of the RCA- and NA-based counterparts containing traditional shear reinforcement.

- The use of 1% steel fiber volume fraction in the deep beam specimen with openings made with a 100% RCAs without steel stirrups was sufficient to restore 96% of the original shear capacity of the NA-based beam having conventional steel stirrups.

- The shear capacities of the RC deep beams obtained from the tests were compared with predictions of published analytical models. The

predicted-to-measured shear capacity was in the range of 0.76 to 1.27 for the solid RC deep beams and 0.71 to 1.49 for the beams with web openings.

3.4 Conclusions Related to Numerical Modeling

Numerical deep beam models were developed and validated through a comparative analysis with experimental results. A parametric study was conducted to investigate the effect of a/h and presence of a web opening on the shear response of RC deep beam models at different steel fiber volume fractions. Main conclusions of the work are summarized hereafter.

- The developed numerical deep beam models predicted the shear behavior of the tested RC deep beams with good accuracy. The numerical results of the solid RC deep beam models indicated that the shear capacity increased almost linearly with an increase in the steel fiber volume fraction. At a/h of 1.6, the addition of steel fibers at v_f of 1, 2 and 3% increased the shear capacity by of 39, 64, and 114%, respectively. At a/h of 0.8, the respective shear strength gains were 78, 91, and 108%. At a/h of 0.8, a steel fiber volume fraction of $v_f = 1\%$ was sufficient to substitute the minimum steel stirrups, whereases at a/h of 1.6, it was necessary to use v_f of 2% to substitute the steel stirrups.

- The addition of steel fibers was more effective in improving the shear capacity of the solid deep beam models rather than those with the web opening at the same a/h of 0.8. The shear strength gain caused by the addition of steel fibers for the deep beam models with the web opening was in the range of 45 to 70%, whereases their solid counterparts exhibited a shear strength of 78 to 108%.

- For the deep beam models without steel fibers, the reduction in shear capacity due to the presence of the web opening ranged from 17 to

28%, with an average of 23%. For the deep beam models with steel fibers, a more pronounced reduction in the shear capacity of approximately 35% was reported because of the web opening.

- The addition of steel fibers to the deep beam models with the web opening at v_f of 1% was sufficient to achieve a shear strength gain higher than that provided by the minimum steel stirrups. The shear capacity of the deep beam model with the web opening and v_f of 3% was equal to that of a similar solid deep beam model with steel stirrups

3.5 Limitations

Replacement of NAs by RCAs would preserve natural resources, reduce the cost, and diminish the environmental impacts associated with the storage of construction and demolition waste. The use of steel fibers in RCA-based concrete structures as a substitution to traditional shear reinforcement could compensate for the initial cost of the steel fibers, eliminate congestion of steel, and reduce the risk of defects and cracks. This research provided an insight into the material characterization of steel fiber-reinforced RCA concrete and the shear behavior of RC deep beams with and without web openings made with RCAs. The limitations of this research are summarized hereafter.

- The experimental results of the present investigation are limited to properties of the materials used, dimensions and geometry of the tested specimens, and reinforcement details. However, the FE models developed and validated in this study can be used as a numerical platform for performance prediction of steel fiber-reinforced RCA deep beams with a wider range of parameters.
- Steel fibers are vulnerable to corrosion in harsh environmental conditions. Therefore, typical preventive measures should be adopted

in practical setting to protect the steel fibers and steel reinforcement from corrosion.

- Despite the substantial environmental benefits that can be obtained by using RCAs in the construction industry as an alternative to NAs, they are not commonly accepted by the engineering community or code provisions to produce structural concrete elements due to the uncertainty in properties of RCAs. Varying the source and time of acquiring the RCAs would affect properties of the so-produced concrete. As such, preliminary trial mixes and characterizations tests should be conducted in practical setting to evaluate fresh and hardened properties of concrete with RCAs and steel fibers prior to adopting a particular mix design in construction projects. Material characterization test results of such trial mixes are necessary for practitioners to design and simulate the behavior of concrete structures made with RCAs and steel fibers.

3.6 Future Research

The following are recommendations for future studies:

- Investigate the environmental and economic impact of replacing NAs by RCAs to produce sustainable concrete with different steel fiber volume fractions and cement replacement materials (e.g. fly ash, slag, silica fume, and microsilica). The use of such cement replacement materials would reduce the consumption of cement and emission of CO_2.

- Perform parametric studies using the validated numerical FE models as a numerical platform to investigate the effect of a wider range of parameters and acquire data difficult to measure in the laboratory such as studying the effect of different opening sizes, shapes, and locations, different *a/h* ratios, and different material properties.

- Employ life cycle cost analysis and assessment techniques using well-defined quantifiable measures to obtain an improved understanding of the interrelations between the structural performance, environmental benefits, and associated costs of RC structures made with RCAs and steel fibers.

- Study the durability of RC structures made with RCAs and steel fibers under harsh environmental conditions.

- Examine the chemical composition of the steel fibers, homogeneity of steel fiber distribution within the concrete mixture, bridging effect of steel fibers, and intensity of concrete porosity through scanning electron microscopy (SEM) analysis.

- Investigate the effectiveness of using non-metallic fibers in enhancing the fresh and hardened RCA-based concrete properties and study the structural behavior of concrete made with RCAs and non-metallic fibers.

References

ACI 318 (2014). Building Code Requirements for Structural Concrete. American Concrete Institute (ACI), Farmington Hills, MI, USA.

ACI Committee 544.6R (2015). Report on Design and Construction of Steel Fiber-Reinforced Concrete Elevated Slabs. American Concrete Institute (ACI), Farmington Hills, MI, USA.

ACI Committee E-701 (2016). Aggregates for Concrete, American Concrete Institute (ACI), Farmington Hills, MI, USA.

ACI Committee 211.1 (2009). Standard Practice for Selecting Proportions for Normal, Heavyweight, and Mass Concrete. American Concrete Institute (ACI), Farmington Hills, MI, USA.

ACI Committee 222R-1 (2010). Protection of Metals in Concrete Against Corrosion. American Concrete Institute (ACI), Farmington Hills, MI, USA.

ACI Committee 363 (1992). State of the Art Report on High-Strength Concrete. American Concrete Institute (ACI), Farmington Hills, MI, USA.

ASTM C1609 (2013). Standard Test Method for Flexural Performance of Fiber-Reinforced Concrete. West Conshohocken, PA: ASTM International.

ASTM A820 (2011). Standard Specification for Steel Fibers for Fiber-Reinforced Concrete. West Conshohocken, PA: ASTM International.

ASTM C33 (2016). Standard Specification for Concrete Aggregates. West Conshohocken, PA: ASTM International.

ASTM C88 (2013). Standard Test Method for Soundness of Aggregates by Use of Sodium Sulfate or Magnesium Sulfate. West Conshohocken, PA: ASTM International.

ASTM C143 (2015). Standard Test Method for Slump of Hydraulic-Cement Concrete. West Conshohocken, PA: ASTM International.

ASTM C138 (2017). Standard Test Method for Density (Unit Weight), Yield, and Air Content (Gravimetric) of Concrete. West Conshohocken, PA: ASTM International.

ASTM C131 (2014). Standard Test Method for Resistance to Degradation of Small-Size Coarse Aggregate by Abrasion and Impact in the Los Angeles Machine. West Conshohocken, PA: ASTM International.

ASTM C642 (2013). Standard Test Method for Density, Absorption, and Voids in Hardened Concrete. West Conshohocken, PA: ASTM International.

ASTM C192 (2015). Standard Practice for Making and Curing Concrete Test Specimens in the Laboratory. West Conshohocken, PA: ASTM International.

ASTM C1170 (2014). Standard Test Method for Determining Consistency and Density of Roller-Compacted Concrete Using a Vibrating Table. West Conshohocken, PA: ASTM International.

ASTM C642 (2013). Standard Test Method for Density, Absorption, and Voids in Hardened Concrete. West Conshohocken, PA: ASTM International.

ASTM C1585 (2013). Standard Test Method for Measurement of Rate of Absorption of Water by Hydraulic-Cement Concretes. West Conshohocken, PA: ASTM International.

ASTM C597 (2016). Standard Test Method for Pulse Velocity Through Concrete. West Conshohocken, PA: ASTM International.

ASTM C1747 (2013). Standard Test Method for Determining Potential Resistance to Degradation of Pervious Concrete by Impact and Abrasion. West Conshohocken, PA: ASTM International.

ASTM C1760 (2012). Standard Test Method for Bulk Electrical Conductivity of Hardened Concrete. West Conshohocken, PA: ASTM International.

ASTM C39 (2015). Standard Test Method for Compressive Strength of Cylindrical Concrete Specimens. West Conshohocken, PA: ASTM International.

ASTM C469 (2014). Standard Test Method for Static Modulus of Elasticity and Poisson's Ratio of Concrete in Compression. West Conshohocken, PA: ASTM International.

ASTM C496 (2017). Standard Test Method for Splitting Tensile Strength of Cylindrical Concrete Specimens. West Conshohocken, PA: ASTM International.

ATENA Computer Software, Červenka Consulting s.r.o., Prague, Czech Republic.

Afroughsabet, V., Biolzi, L., & Ozbakkaloglu, T. (2017). Influence of double hooked-end steel fibers and slag on mechanical and durability properties of high performance recycled aggregate concrete. Composite Structures, 181, 273–284. https://doi.org/10.1016/j.compstruct.2017.08.086.

Awchat, G. D. (2021). Cost-Benefit Analysis of Using Recycled Coarse Aggregate In Plain and Fiber Reinforced Concrete. Advances in Science and Technology. Research Journal, 15(3), 233–242. https://doi.org/10.12913/22998624/139205.

Alzard, M. H., El-Hassan, H., & El-Maaddawy, T. (2021). Environmental and Economic Life Cycle Assessment of Recycled Aggregates Concrete in the United Arab Emirates. Sustainability, 13(18), 10348. https://doi.org/10.3390/su131810348.

Aly, S. A., Ibrahim, M. A., & Khttab, M. M. (2015). Shear Behavior of Reinforced Concrete Beams Casted with Recycled Coarse Aggregate. Euro. J. Adv. Engg. Tech., 2(9):59-71.

Arezoumandi, M., Smith, A., Volz, J.S., & Khayat, K.H. (2014). An experimental study on shear strength of reinforced concrete beams with 100% recycled concrete aggregate. Construction and Building Materials, vol. C, no. 53, pp. 612–620, doi: 10.1016/j.conbuildmat.2013.12.019.

Al Mahmoud, F., Boissiere, R., Mercier, C., & Khelil, A. (2020). Shear behavior of reinforced concrete beams made from recycled coarse and fine aggregates. Structures, vol. 25, pp. 660–669, doi: 10.1016/j.istruc.2020.03.015.

Ashour, S. A., Hasanain, G. S., & Wafa, F. F. (1992). Shear Behavior of High-Strength Fiber Reinforced Concrete Beams. Structural Journal, 89(2), 176–184. https://doi.org/10.14359/2946.

Amin, A., & Foster, S.J. (2016). Shear strength of steel fibre reinforced concrete beams with stirrups. Engineering Structures, vol. 111, pp. 323–332, doi: 10.1016/j.engstruct.2015.12.026.

Al-Sarraf, D. S. Z., & Diab, D. A. S. (2011). Effect of Steel Fiber on The Behavior of Deep Beams with and without Web Opening. Eng. & Tech. Journal, Vol. 29, No. 1.

Ahmed, S.H., & Shah, S.P. (1985). Structural Properties of High Strength Concrete and its Implications for Precast Prestressed Concrete, PCI Journal 30(6), 97-123.

British Standard (2009). Testing hardened concrete - Compressive strength of test specimens, BS EN 12390-3, British Standard, London, UK.

BSI - BS 1881-203 (2022). Testing Concrete Part 203: Recommendations for Measurement of Velocity of Ultrasonic Pulses in Concrete | Engineering360. https://standards.globalspec.com/std/996041/BS%201881-203.

Bencardino, F., Rizzuti, L., Spadea, G., & Swamy, R. (2008). Stress-Strain Behavior of Steel Fiber-Reinforced Concrete in Compression. Journal of Materials in Civil Engineering. https://doi.org/10.1061/(ASCE)0899-1561(2008)20:3(255).

Barros, A. O. (2001). Fracture Energy of Steel Fiber-Reinforced Concrete. Mechanics of Composite Materials and Structures. JSCJ. 2001/01/01;8(1):29-45.

Bencardino, F., Rizzuti, L., Spadea, G., & Swamy, R. N. (2010). Experimental evaluation of fiber reinforced concrete fracture properties. Composites Part B: Engineering, 41(1), 17–24. https://doi.org/10.1016/j.compositesb.2009.09.002.

Braga Maia, A., Silvestre, J., & Brito, J. (2017). Compared environmental and economic impact from cradle to gate of concrete with natural and recycled coarse aggregates. Journal of Cleaner Production, 162. https://doi.org/10.1016/j.jclepro.2017.06.057.

Bre (2015). Environmental Product Declaration; BREG EN EPD No.: 000065, Saint-Gobain Isover, UK.

Bekaert, Dramix 3D 65/35 Report (2012). Bekaert, Belgium.

Çakır, Ö. (2014). Experimental analysis of properties of recycled coarse aggregate (RCA) concrete with mineral additives. Constr Build Mater 68 17-25.

Campione, G., & Minafò, G. (2012). Behaviour of concrete deep beams with openings and low shear span-to-depth ratio. Engineering Structures, 41, 294–306. https://doi.org/10.1016/j.engstruct.2012.03.055.

Chaboki, H. R., Ghalehnovi, M., Karimipour, A., de Brito, J., & Khatibinia, M. (2019). RETRACTED: Shear behaviour of concrete beams with recycled aggregate and steel fibres. Construction and Building Materials, 204, 809–827. https://doi.org/10.1016/j.conbuildmat.2019.01.130.

CEB-FIP (1990). Evaluation of the Time Dependent Behavior of Concrete, Fib, Lausanne, Switzerland.

Carneiro, J.A., Lima, P.R.L., & Leite, M.B. (2014). Toledo Filho, Compressive stress–strain behavior of steel fiber reinforced-recycled aggregate concrete, Cem Concr Compos 46 (2014) 65-72.

Corinaldesi, V. (2010). Mechanical and elastic behaviour of concretes made of recycled-concrete coarse aggregates, Constr Build Mater 24(9) 1616-1620.

Cucchiara, C., La Mendola, L., & Papia, M. (2004). Effectiveness of stirrups and steel fibres as shear reinforcement. Cement and Concrete Composites, vol. 26(7), pp. 777-786.

Cunha, V. M. (2010). Steel fibre reinforced self-compacting concrete (from micromechanics to composite behavior). Ph.D. thesis, Univ. of Minho, Braga, Portugal.

Ceb-fip model code (1993). Thomas Telford Publishing. https://doi.org/10.1680/ceb-fipmc1990.35430.

Debieb, F., Courard, L., Kenai, S., & Degeimbre, R. (2010). Mechanical and durability properties of concrete using contaminated recycled aggregates. Cement and Concrete Composites, 32(6), 421–426. https://doi.org/10.1016/j.cemconcomp.2010.03.004.

Dinh, H.H., Parra-Montesinos, G., & Wight, J. (2010). Shear Behavior of Steel Fiber-Reinforced Concrete Beams without Stirrup Reinforcement. ACI Structural Journal, doi: 10.14359/51663913.

Dilli, M., Atahan, H., & Şengül, C. (2015). A comparison of strength and elastic properties between conventional and lightweight structural concretes designed with expanded clay aggregates. Construction and Building Materials, 101, 260–267. https://doi.org/10.1016/j.conbuildmat.2015.10.080.

Do-Dai, T., Tran, D. T., & Nguyen-Minh, L. (2021). Effect of fiber amount and stirrup ratio on shear resistance of steel fiber reinforced concrete deep beams. Journal of Science and Technology in Civil Engineering (STCE) - HUCE, 15(2), 1–13. https://doi.org/10.31814/stce.nuce2021-15(2)-01.

European Standard (2005). Test method for metallic fibre concrete. Measuring the flexural tensile strength (limit of proportionality (LOP), residual). Brussels, Belgium: European Committee for Standardization.

El Hakam, A.A., Mohamed, A.E., & Awad, E. (2012). Influence of self-healing, mixing method and adding silica fume on mechanical properties of RAs concrete, Constr. Build. Mater. 35 421–427.

EN 14889-1 (2006). Fibres for concrete - Part 1: Steel fibres - Definitions, specifications and conformity.

El Maaddawy, T., & Sherif, S. (2009). FRP composites for shear strengthening of reinforced concrete deep beams with openings. Composite Structures, 89(1), 60–69. https://doi.org/10.1016/j.compstruct.2008.06.022.

Elmatty, M. A., Elsayed, M., Serag, A., & Mohamed, W. (2020). Behavior Of Recycled Concrete Beams with Openings in Shear Region: Experimental and Numerical Study. IOSR Journal of Mechanical and Civil Engineering (IOSR-JMCE) e-ISSN: 2278-1684, p-ISSN: 2320-334X, Volume 17, Issue 2 Ser. I, PP 01-10.

Etxeberria, M., Vázquez, E., Marí, A., & Barra, M. (2007). Influence of amount of recycled coarse aggregates and production process on properties of recycled aggregate concrete. Cement and Concrete Research, 37(5), 735–742. https://doi.org/10.1016/j.cemconres.2007.02.002.

Evangelista, L., & de Brito, J. (2010). Durability performance of concrete made with fine recycled concrete aggregates. Cement and Concrete

Composites, 32(1), 9–14. https://doi.org/10.1016/j.cemconcomp.2009.09.005.

Fathifazl, G., Razaqpur, A.G., Isgor, O.B., Abbas, A., Fournier, B., & Foo, S. (2009). Shear strength of reinforced recycled concrete beams without stirrups. Magazine of Concrete Research, vol. 61, no. 7, pp. 477–490, doi: 10.1680/macr.2008.61.7.477.

Fédération internationale du béton (2010). fib Model Code for Concrete Structures 2010. Lausanne, Switzerland: Ernst & Sohn.

Fonseca, N., De Brito, J., & Evangelista, L. (2011). The influence of curing conditions on the mechanical performance of concrete made with recycled concrete waste, Cem. Concr. Compos. 33 (6), p. 637–643.

Garcia, S., Pereira, A., & Pierott, R. (2021). Shear Strength of Sand-Lightweight Concrete Deep Beams with Steel Fibers. Structural Journal, 118(2), 203–214. https://doi.org/10.14359/51729347.

Gao, D., Zhang, L., & Nokken, M. (2017). Compressive behavior of steel fiber reinforced recycled coarse aggregate concrete designed with equivalent cubic compressive strength, Constr Build Mater 141, p. 235-244.

Gao D, & Zhang L. (2018). Flexural performance and evaluation method of steel fiber reinforced recycled coarse aggregate concrete. Constr Build Mater. 2018/01/20/; 159:126-136.

Gao, D., Zhang, L., Zhao, J., & You, P. (2020). Durability of steel fibre-reinforced recycled coarse aggregate concrete. Construction and Building Materials, 232, 117119. https://doi.org/10.1016/j.conbuildmat.2019.117119.

Gonzalez-Fonteboa, B., & Martinez-Abella, F. (2007). Shear strength of recycled concrete beams. Construction and Building Materials, vol. 21, no. 4, Accessed: Jun. 06, 2021. [Online]. Available: https://trid.trb.org/view/797793.

Guo, M., Grondin, F., & Loukili, A. (2020). Numerical analysis of the failure of recycled aggregate concrete by considering the random composition of old attached mortar. Journal of Building Engineering, 28, 101040. https://doi.org/10.1016/j.jobe.2019.101040.

Hu, O. E., Tan, K. H., & Liu, X. H. (2007). Behaviour and strut-and-tie predictions of high-strength concrete deep beams with trapezoidal web openings. Magazine of Concrete Research, 59(7), 529–541. https://doi.org/10.1680/macr.2007.59.7.529.

Hossain, M.S., Lane, D.S., & Schmidt, B.N. (2007). Use of the Micro-Deval Test for Assessing the Durability of Virginia Aggregates, in: V.T.R. Council (Ed.) Virginia Transportation Research Council, Charlottesville, Virginia, p. 33.

Ignjatovic, I.S., Marinkovic, S.B., & Tošic, N. (2017). Shear Behaviour of Recycled Aggregate Concrete Beams with and Without Shear Reinforcement. Engineering Structures, vol. 141, no. 0, doi: https://trid.trb.org/view/1464996.

International standard ISO 13270 (2013). Steel fibers for concrete – Definitions and Specifications.

Juárez, C., Valdez, P., Durán, A., & Sobolev, K. (2007). The diagonal tension behavior of fiber reinforced concrete beams. Cement and Concrete Composites, 29(5), 402–408. https://doi.org/10.1016/j.cemconcomp.2006.12.009.

Kachouh, N., El-Hassan, H., & El-Maaddawy, T. (2019). Effect of steel fibers on the performance of concrete made with recycled concrete aggregates and dune sand. Construction and Building Materials, 213, 348–359. https://doi.org/10.1016/j.conbuildmat.2019.04.087.

Kachouh, N., El-Hassan, H., & El-Maaddawy, T. (2021). Influence of steel fibers on the flexural performance of concrete incorporating recycled concrete aggregates and dune sand. J. Sustain. Cem. Based Mater., 10, 165–192, https://doi.org/10.1080/21650373.2020.1809546.

Kachouh, N., El-Maaddawy, T., & El-Hassan, H. (2020). Numerical Modelling of Steel Fiber Recycled Aggregate Concrete Deep Beams. In 5th World Congress on Civil, Structural, and Environmental Engineering (CSEE'20). Avestia, Virtual Conference.

Kang, T. H.-K., Kim, W., Kwak, Y.-K., & Hong, S.-G. (2011). Shear Testing of Steel Fiber-Reinforced Lightweight Concrete Beams without Web Reinforcement. Structural Journal, 108(5), 553–561. https://doi.org/10.14359/51683212.

Kwak, Y. K., Eberhard, M. O., Kim, W. S., & Kim, J. (2002). Shear Strength of Steel Fiber-Reinforced Concrete Beams without Stirrups. Structural Journal, 99(4), 530–538. https://doi.org/10.14359/12122.

Kong, F. K., & Sharp, G. R. (1977). Structural idealization for deep beams with web openings. Magazine of Concrete Research, 29(99), 81–91. https://doi.org/10.1680/macr.1977.29.99.81.

Koushkbaghi, M., Kazemi, M. J., Mosavi, H., & Mohseni, E. (2019). Acid resistance and durability properties of steel fiber-reinforced concrete incorporating rice husk ash and recycled aggregate. Construction and Building Materials, 202, 266–275. https://doi.org/10.1016/j.conbuildmat.2018.12.224.

Khergamwala, P.C. (2016). Experimental Study on Shear Behavior of Reinforced Recycled Aggregate Concrete Beams. International Journal of Civil Engineering and Technology (IJCIET), vol. 7, pp. 128–139, doi: /paper/Experimental-Study-on-Shear-Behavior-of-Reinforced-Khergamwala/21d55e56cf0ff211d0d31ff310e771f133473f08 (accessed Jun. 06, 2021).

Kwan, W.H., Ramli, M., Kam, K.J., & Sulieman, M.Z. (2012). Influence of the amount of recycled coarse aggregate in concrete design and durability properties, Constr. Build. Mater. 26 (1), p. 565–573.

Kou, S.C., & Poon, C.S. (2013). Long-term mechanical and durability properties of RAC prepared with the incorporation of fly ash, Cem. Concr. Compos. 37, p. 12–19.

Madar Emirates for Buildings Materials. (2022). Available online: https://www.madar.com.

Ma, K., Qi, T., Liu, H., & Wang, H. (2018). Shear Behavior of Hybrid Fiber Reinforced Concrete Deep Beams. Materials (Basel, Switzerland), 11(10), E2023. https://doi.org/10.3390/ma11102023.

Mansur, M., & Alwist, W. (1984). Reinforced fibre concrete deep beams with web openings. Int. J. Cem. Compos. Lightweight Concr., 6, 263–71.

Marco, d.P., Matteo, C., & Daniele, D. (2013). Fibre-reinforced concrete in fib Model Code 2010: principles, models and test validation, Structural Concrete 14(4), p. 342-361.

Malešev, M., Radonjanin, V., & Marinković, S. (2010). Recycled Concrete as Aggregate for Structural Concrete Production, Sustainability 2(5), p. 1204.

Manzi, S., Mazzotti, C., & Bignozzi, M. C. (2013). Short and long-term behavior of structural concrete with recycled concrete aggregate. Cement and Concrete Composites, 37, 312–318. https://doi.org/10.1016/j.cemconcomp.2013.01.003.

Meddah, M. S., & Bencheikh, M. (2009). Properties of concrete reinforced with different kinds of industrial waste fibre materials. Construction and Building Materials. https://doi.org/10.1016/J.CONBUILDMAT.2009.06.017.

Meyer, C. (2009). The greening of the concrete industry. Cement and Concrete Composites, 31(8), 601–605. https://doi.org/10.1016/j.cemconcomp.2008.12.010.

Mendis, P. (2003). Design of high-strength concrete members: state-of-the-art. Progress in Structural Engineering and Materials 5(1), p. 1-15.

Nixon, P.J. (1978). Recycled concrete as an aggregate for concrete—a review, Matér. Constr. 11 (5), p. 371–378.

Nilson, A., Darwin, D., & Dolan, C. (2009). Design of Concrete Structures (14th edition). McGraw-Hill Education.

Narayanan, R., & Darwish, I. Y. S. (1987). Use of Steel Fibers as Shear Reinforcement. Structural Journal, 84(3), 216–227. https://doi.org/10.14359/2654.

Polat, G., Arditi, D., Ballard, G., & Mungen, U. (2006). Economics of on-site vs. Off-site fabrication of rebar. Construction Management & Economics, 24, 1185–1198. https://doi.org/10.1080/01446190500529432.

Perumal, R. (2015). Correlation of Compressive Strength and Other Engineering Properties of High-Performance Steel Fiber–Reinforced Concrete. Journal of Materials in Civil Engineering, 27, 5533.0001050. https://doi.org/10.1061/(ASCE)MT.1943-5533.0001050.

Radonjanin, V., Malešev, M., Marinković, S., & Al Malty, A. E. S. (2013). Green recycled aggregate concrete. Construction and Building

Materials, 47, 1503–1511. https://doi.org/10.1016/j.conbuildmat.2013.06.076.

Rahal, K.N., & Alrefaei, Y.T. (2017). Shear strength of longitudinally reinforced recycled aggregate concrete beams. Engineering Structures, vol. 145, pp. 273–282, doi: 10.1016/j.engstruct.2017.05.028.

Rahal, K.N., & Alrefaei, Y.T. (2018). Shear strength of recycled aggregate concrete beams containing stirrups. Construction and Building Materials, vol. 191, pp. 866–876, doi: 10.1016/j.conbuildmat.2018.10.023.

Ray, S.P., & Reddy, C.S. (1979). Strength of reinforced concrete deep beams with and without opening is the web. Indian Concr. J., 54, 242–246.

Ramadoss, P., & Nagamani, K. (2008). Tensile Strength and Durability Characteristics of High-Performance Fiber Reinforced Concrete. Arabian Journal for Science & Engineering (Springer Science & Business Media B.V., 33(2B), 307–319.

Rao, A., Jha, K. N., & Misra, S. (2007). Use of aggregates from recycled construction and demolition waste in concrete. Resources, Conservation and Recycling, 50(1), 71–81. https://doi.org/10.1016/j.resconrec.2006.05.010.

RILEM TC 162 (2001). Test and design methods for steel fibre reinforced concrete: Uniaxial tension test for steel fibre reinforced concrete. Mater Struct.,34(235), p. 3-6.

RILEM (2002). Test and design methods for steel fibre reinforced concrete. RILEM Publications SARL.

RILEM (2001). RILEM Recommendations for the Testing and Use of Constructions Materials. RILEM Publications SARL.

Shaikh, F. U. A., & Nguyen, H. L. (2013). Properties of concrete containing recycled construction and demolition wastes as coarse aggregates. Journal of Sustainable Cement-Based Materials, 2(3–4), 204–217. https://doi.org/10.1080/21650373.2013.833861.

Sanal, I. (2018). Performance of Macrosynthetic and Steel Fiber–Reinforced Concretes Emphasizing Mineral Admixture Addition. Journal of Materials in Civil Engineering, 30. https://doi.org/10.1061/(ASCE)MT.1943-5533.0002292.

Sahoo, D.R., & Sharma, A. (2014). Effect of Steel Fiber Content on Behavior on Concrete Beams with and without Shear Stirrups. ACI Structural Journal, vol. 111, pp. 1157–1166, doi: 10.14359/51686821.

Shi, X., Park, P., Rew, Y., Huang, K., & Sim, C. (2020). Constitutive behaviors of steel fiber reinforced concrete under uniaxial compression and tension. Construction and Building Materials, 233, 117316. https://doi.org/10.1016/j.conbuildmat.2019.117316.

Salem, R. M., & Burdette, E. G. (1998). Role of Chemical and Mineral Admixtures on Physical Properties and Frost-Resistance of Recycled Aggregate Concrete. ACI Materials Journal, 95(5). https://trid.trb.org/view/542151.

Shanmugam, N., & Swaddiwudhipong, S. (1988). Strength of fibre reinforced concrete deep beams containing openings. Cem. Concr. Compos., 10, 53–60.

Sharma, S., Arora, V. V., Kumar, S., Daniel, Y. N., & Sharma, A. (2018). Durability Study of High-Strength Steel Fiber-Reinforced Concrete. ACI Materials Journal, 115(2), 219–225. http://dx.doi.org/10.14359/51701122.

Sahoo, D. R., Flores, C., & Chao, S.-H. (2012). Behavior of Steel Fiber-Reinforced Concrete Deep Beams with Large Opening. Aci Structural Journal, 109, 193–204.

Shi, C., Li, Y., Zhang, J., Li, W., Chong, L., & Xie, Z. (2016). Performance enhancement of recycled concrete aggregate – A review. Journal of Cleaner Production, 112, 466–472. https://doi.org/10.1016/j.jclepro.2015.08.057.

Shi, X., Park, P., Rew, Y., Huang, K., & Sim, C. (2020). Constitutive behaviors of steel fiber reinforced concrete under uniaxial compression and tension. Construction and Building Materials, 233, 117316. https://doi.org/10.1016/j.conbuildmat.2019.117316.

Senaratne, S., Gerace, D., Mirza, O., Tam, V.W.Y., & Kang, W.H. (2016). The costs and benefits of combining recycled aggregate with steel fibres as a sustainable, structural material. J. Clean. Prod., 112, p. 2318–2327.

Sinopro Industrial Products (2022). Available online: https://sinopro.ae.

Stevens, A., Blanchard, J., Booth, E., Corr, B., Konopicky, J., & Newey, J. (1984). The design of deep beams in reinforced concrete. Construction Industry and Information Association (CIRIA) Guide 2.

Tabsh, S.W., & Abdelfatah, A.S. (2009). Influence of recycled concrete aggregates on strength properties of concrete, Constr Build Mater 23(2), p. 1163-1167.

Tam, V.W.Y., Mirza, O., Senaratne, S., Kang, W.H., & Kotrayothar, D. (2013). Shrinkage development of recycled aggregate concrete and future directions of using steel fibers as a reliable and cost-effective option. In Proceedings of the 38th Australasian Universities Building Education Association Conference 2013, Auckland, New Zealand.

Thomas, C., Setién, J., Polanco, J. A., Alaejos, P., & Sánchez de Juan, M. (2013). Durability of recycled aggregate concrete. Construction and Building Materials, 40, 1054–1065. https://doi.org/10.1016/j.conbuildmat.2012.11.106.

Topçu, İ. B., & Şengel, S. (2004). Properties of concretes produced with waste concrete aggregate. Cement and Concrete Research, 34(8), 1307–1312. https://doi.org/10.1016/j.cemconres.2003.12.019.

Wagih, A. M., El-Karmoty, H. Z., Ebid, M., & Okba, S. H. (2013). Recycled construction and demolition concrete waste as aggregate for structural concrete. HBRC Journal, 9(3), 193–200. https://doi.org/10.1016/j.hbrcj.2013.08.007.

Wardeh, G., & Ghorbel, E. (2019). Shear strength of reinforced concrete beams with recycled aggregates. Advances in Structural Engineering, vol. 22(8), pp. 1938-1951, https://journals.sagepub.com/doi/abs/10.1177/1369433219829815.

Yang, K.-H., & Ashour, A. (2008). Effectiveness of web reinforcement around openings in continuous concrete deep beams. ACI Structural Journal, 105, 414–424.

Yang, K.-H., Eun, H.-C., & Chung, H.-S. (2006). The influence of web openings on the structural behavior of reinforced high-strength concrete deep beams. Engineering Structures, 28, 1825–1834. https://doi.org/10.1016/j.engstruct.2006.03.021.

Xiao, J., Li, J., & Zhang, Ch. (2005). Mechanical properties of recycled aggregate concrete under uniaxial loading. Cement and Concrete

Research, 35(6), 1187–1194. https://doi.org/10.1016/j.cemconres.2004.09.020.

Xie, J. h, Yong-chang, G., Li-sha, L., & Zhi-hong, X. (2015). Compressive and flexural behaviours of a new steel-fibre-reinforced recycled aggregate concrete with crumb rubber. Construction and Building Materials, 79. https://doi.org/10.1016/j.conbuildmat.2015.01.036.

Xu, B., & Shi, H. S. (2009). Correlations among mechanical properties of steel fiber reinforced concrete. Construction and Building Materials - CONSTR BUILD MATER, 23, 3468–3474. https://doi.org/10.1016/j.conbuildmat.2009.08.017.

Yehia, S., Helal, K., Abusharkh, A., Zaher, A., & Istaitiyeh, H. (2015). Strength and Durability Evaluation of Recycled Aggregate Concrete. International Journal of Concrete Structures and Materials, 9(2), 219–239. https://doi.org/10.1007/s40069-015-0100-0.

Younis, K., Pilakoutas, K., Guadagnini, M., & Angelakopoulos, H. (2014). Feasibility of Using Recycled Steel Fibres to Enhance the Behaviour of Recycled Aggregate Concrete.

Zewair, M. S., Hamoodi, A. Z., & Ojaimi, M. F. (2021). Effect of types of fibres on the shear behaviour of deep beam with opening. Periodicals of Engineering and Natural Sciences, 9(2), 1086–1095. https://doi.org/10.21533/pen.v9i2.1929.

List of Other Publications

Kachouh, N., El-Hassan, H., & El-Maaddawy, T. (2019). The use of steel fibers to enhance the performance of concrete made with recycled aggregate. Fifth International Conference on Sustainable Construction Materials and Technologies (SCMT5). doi: 10.18552/2019/IDSCMT5012.

Kachouh, N., El-Maaddawy, T., & El-Hassan, H. (2020). Numerical Modelling of Steel Fiber Recycled Aggregate Concrete Deep Beams. Fifth World Congress on Civil, Structural, and Environmental Engineering (CSEE'20). Paper No. ICSECT 119. doi: 10.11159/icsect20.119.

Kachouh, N., El-Hassan, H., & El-Maaddawy, T. (2021). Mechanical Properties of Recycled Coarse Aggregate Concrete Reinforced with Steel Fibers. The Eleventh International Structural Engineering and Construction ConferenceAt: Cairo, Egypt. MAT-12 doi: 10.14455/ISEC.2021.8(1).

Kachouh, N., El-Maaddawy, T., El-Hassan, H., & El-Ariss, B. (2022). Shear Strength of Steel Fiber-Reinforced Recycled Aggregates Concrete Deep Beams. Seventh International Conference on Structural Engineering and Concrete Technology (ICSECT'22). Paper No. 132.

Kachouh, N., El-Maaddawy, T., El-Hassan, H., & El-Ariss, B. (2022). Numerical Modeling of Concrete Deep Beams Made with Recycled Aggregates and Steel Fibers. Buildings, 12(5):529. https://doi.org/10.3390/buildings12050529.

UAE UNIVERSITY DOCTORATE DISSERTATION NO. 2022:8

Recycled concrete aggregates (RCAs) obtained from construction and demolition waste can be reused in the building industry rather than being stored in landfills or used as road base or fill. However, the use of RCAs has been limited to non-structural applications owing to inferior mechanical and durability properties of RCA concrete. The inclusion of steel fibers has a potential to improve the properties of concrete made of RCAs. This investigation provided the engineering community a cutting-edge material characterization of steel fiber-reinforced RCA concrete and an insight into the structural performance of reinforced concrete deep beams with and without web openings, made with RCAs and steel fibers at different volume fractions.

Nancy Kachouh received her PhD from the Department of Civil and Environmental Engineering, College of Engineering at UAE University, UAE. She received her MSc from the College of Civil and Environmental Engineering, American University of Beirut, Lebanon.